PEOPLE'S DEMOCRATIC REPUBLIC OF ALGERIA

Ministry of Higher Education and Scientific Research

University of Amar Telidji - Laghouat

Faculty of Technology
Doctorate in science
Specialty: Energetic Mechanics

HADJAISSA AISSA

THEME

Study of the dynamic behavior of sand grains under the effect of the wind

Étude du comportement dynamique des grains du sable sous l'effet du vent

JURY:

Pr. YOUSFI AHMED	*Chair*	*Professor*	*U.A.T.Laghouat*
Pr. BENCHATTI AHMED	*Examiner*	*Professor*	*U.A.T.Laghouat*
Pr. AOUISSI MOKHTAR	*Examiner*	*Professor*	*U.A.T.Laghouat*
Pr. Kherris SAHRAOUI	*Examiner*	*Professer*	*U.Y.E. Tissemsilt*
Dr. BENCHATTI TOUFIK	*Examiner*	*Doctor*	*E.N.S.Laghouat*
Pr. MEDJELLED AHMED	*Supervisor*	*Professor*	*U.A.T.Laghouat*
Dr. BOUALI BELKACEM	*Co-Supervisor*	*Doctor*	*U.A.T.Laghouat*

2022-2023

الملخص

تم في السابق دراسة و تحليل تركيز الجسيمات الصلبة عدديًا باستخدام نموذج الخليط في تدفقات متعددة الحالات. تطبيقات متعددة لهذا النموذج في تدفقات المتضمنة حالات صلبة و سائلة اثبتت موثوقيتها. في حالة نقل الرمال عن طريق الهواء، تكون كثافة الحالة الصلبة والمتمثلة بحبات الرمل منخفضة جدا (من درجة 10^{-5} إلى 10^{-4}). يمكن تقريب معادلة زخم الخليط ومعادلة الاستمرارية كتدفق أحادي الحالة لغاز غير قابل للضغط، حيث تكون سرعة الانزلاق للطور المشتت (u_{slip}) نسبية بالنسبة إلى الطور المستمر. تم حساب سرعة الانزلاق بناءً على التوازن بين جسيمات حبات الرمل وقوى السحب بسبب الاختلاف في الكثافة. تمت المحاكاة على أساس نظرية الخليط و بالمقارنة مع نتائج الاختبارات السابقة. تم عرض السرعات وتركيز حبات الرمل و كذلك الطاقة الحركية. تؤكد النتائج أن تركيز الجسيمات يتناقص بشكل كبير مع الارتفاع وفق معادلة أسية. يمكن وصف معامل الانتشار لجزيئات الرمل (D_{md}) مع الارتفاع كتوزيع غوس ، والذي بدوره يتأثر بحجم الجسيمات المنقولة وطاقتها الحركية. أحجام الجسيمات الأصغر لها معامل انتشار أكبر من تلك ذات الأحجام الأكبر. وفقًا لنسبة رقم شميدت ، فإنه يمثل العلاقة بين معدلات انتقال الزخم المضطرب والنقل الكتلي المضطرب ، والتي يمكن أن تفسر تأثير الطاقة الحركية للرياح على الانتشار المضطرب للرمل. يتوافق تطبيق طريقة الخليط جيدًا مع أعمال تجريبية سابقة، ويمكن تطبيق هذه الطريقة لدراسة خصائص الاضطراب في نقل الرمال عن طريق الهواء.

الكلمات المفتاحية : نقل الرمل عن طريق الهواء ، نفق الرياح ، تركيز الرمال ، نموذج الخليط ، معامل الانتشار المشتت

Abstract:

The particle concentration is analyzed numerically with a mixture model in multiphase flows. Multiple applications of this model in liquid-particle flows ensure its reliability. In the Aeolian sand transport, the density of the dispersed phase is small (in the order of 10^{-5} to 10^{-4}). The mixture momentum equation and the continuity equation can be approximated using the single phase for an incompressible gas where the dispersed phase slip velocity (u_{slip}) is relative to the continuous phase. The slip velocity was calculated based on the balancing between the body and drag forces due to the density difference. The simulation results based on the mixture theory were determined in comparison to previous test results. The velocity profiles and particle concentration were presented. The results confirm that particle concentration decreases exponentially with altitude. The variation of the diffusion coefficient of sand particles (D_{md}) with height direction can be traced as a Gaussian distribution, which is influenced by the transported particle size and its kinetic energy. The smaller particle sizes have a larger diffusion coefficient than those with the larger ones. According to the ratio of Schmidt number, it describes the relationship between the rates of turbulent momentum transport and turbulent mass transport, which can explain the effect of the wind kinetic energy on the sand turbulent diffusion profiles. The mixture approach application is in good agreement with previous wind tunnel works. This approach can be applied to study the turbulence properties in the Aeolian sand transport.

Keywords : Aeolian sand transport, wind tunnel, sand concentration, mixture model, dispersed diffusion coefficient

---

Résumé :

La concentration des particules est analysée numériquement avec un modèle de mélange dans des écoulements multiphasiques. multiples applications de ce modèle dans les écoulements liquide-particules assurent sa fiabilité. Dans le transport éolien du sable, la densité de la phase dispersée est faible (de l'ordre de 10^{-5} à 10^{-4}). L'équation de quantité de mouvement du mélange et l'équation de continuité peuvent être approximées en utilisant la phase unique pour un gaz incompressible où la vitesse de glissement de la phase dispersée (uslip) est relative à la phase continue. La vitesse de glissement a été calculée sur la base de l'équilibrage entre les forces du corps et de traînée due à la différence de densité. Les résultats de la simulation basés sur la théorie des mélanges ont été déterminés par rapport aux résultats des tests précédents. Les profils de vitesse et la concentration de particules ont été présentés. Les résultats confirment que la concentration de particules diminue de façon exponentielle avec l'altitude. La variation du coefficient de diffusion des particules de sable (Dmd) avec la direction de la hauteur peut être tracée comme une distribution gaussienne, qui est influencée par la taille des particules transportées et son énergie cinétique. Les particules les plus petites tailles ont un coefficient de diffusion plus grand que celles avec les plus grandes. Selon le rapport du nombre de Schmidt, il décrit la relation entre les taux de transport de quantité de mouvement turbulent et transport de masse turbulent, ce qui peut expliquer l'effet de l'énergie cinétique du vent sur les profils de diffusion turbulente du sable. L'application de l'approche de mélange est en bon accord avec les travaux antérieurs en soufflerie. Cette approche peut être appliquée pour étudier les propriétés de turbulence dans le transport éolien du sable.

Mots-clés : Transport éolien du sable, soufflerie, concentration de sable, modèle de mélange, coefficient de diffusion dispersée

Notations :

U : Velocity of mixture flow (m/s)

ρ : Density of Mixture flow (kg/m^3)

μ_T : Mixture turbulent viscosity (Pa.s)

P : Pressure of mixture flow (Pa)

D_{md} : Turbulent dispersion coefficient (m^2/s)

C_d : Mass fraction of the dispersed phase (kg/kg)

u_{slip} : The relative velocity between the two phases (m/s)

τ_{Gm} : Sum of the turbulent and viscous stresses ($kg/(m \cdot s^2)$)

g : The gravitational acceleration (m/s^2)

$\emptyset_c$: The volume fractions of the continuous phase (m^3/m^3)

$\emptyset_d$: The volume fractions of the dispersed phase (m^3/m^3)

u_c : The velocity vector of the continuous phase (m/s)

u_d : The velocity vector of the dispersed phase (m/s)

ρ_c : The density of the continuous phase (kg/m^3)

ρ_d : The density of the dispersed phase (kg/m^3)

m_{dc} : Rate of mass transport from the dispersed to the continuous phase($kg/(m^3.s)$)

σ_T : Turbulent particle Schmidt number

$Q_{.d}$: the total amount of radiative and convective heat transmission to the particle or droplet

d_0 : the starting drop diameter

Ds : the percentage of particle mass

U_h : the mean wind speed at the top of the saltation layer

F_f : the fluid forces

xp : the droplet location

z_0 : the roughness length

n : Conservation of the number density ($1/m^3$)

k : The kinetic energy of turbulence (m^2/s^2)

ε : The dissipation energy of turbulence (m^2/s^2)

a : drag force

b : buoyancy force

A : the maximum projected area of the grain

τ_0 : the surface shear stress

A : spherical particles with dimension d

W : the grain's weight,

ρ_s : the density of the submerged grain

C_L : the coefficient of lift

F_L : the lift force

V : the volume of the computational cell

V_d : average droplet volume along trajectory j in the cell

N_p : the number of particles in the cluster p

v, x : the particle's velocity and location at time t

D_v : the vapor's molecular diffusion coefficient

S_h : the droplet's Sherwood number

vg : the gas's kinematic viscosity

N : the volume's total number of particles,

m_k : the mass of particle k

d : the dispersed phase's volume proportion,

vi : the mass average velocity of the dispersed phase

v'i : the velocity's divergence from the average

pc , $c_{,ij}$: the continuous phase's average compressive and shear stresses

Li : Basset force are included in the force

k : the ratio of drag to Stokes drag

C : represents the particle motion's fluctuating speed

Acknowledgments

I would like first to express my deep gratitude and appreciation to my doctoral supervisors ***Pr. Ahmed MDJELLED*** *and* ***Dr.Belkacem BOUALI*** *for giving me such a great scientific journey, for providing patient guidance, encouragement and support along the years of this degree. They, by their skills and talent, have inspired me to accomplish the goals of this thesis.*

I express my sincere thanks to ***Pr. Ahmed Yousfi****, Professor at the University Amar Télidji of Laghouat, for having accepted to chair the Jury of this dissertation.*

I would also like to say a big thank you to the members of the jury: ***Pr. KHERISS Sahraoui*** *Professor at the University of Tismsilet.* ***Dr. Toufik Benchatti*** *Lecturer at the E.N.S.Laghouat, and* ***Pr. Ahmed Benchatti*** *Lecturer at the University of Amar Télidji of Laghouat* ***, Pr. Mokhtar Aouissi.*** *Lecturer at the University of Amar Télidji of Laghouat who have Accepted, without any reserve, to evaluate this thesis to its true value, and to share with me their remarks surely relevant, which, with a little hindsight, will undoubtedly contribute to the improvement of this work. THANKS!*

Table of Contents

Table of Contents

General Introduction:

Aeolian sand transport plays an essential role as a geomorphological process for soil forms on Earth and other planets such as Mars, Titan and Venus "(Greeley and Iversen, 1985)",in which the wind entrains soil particles and carries them away from their source. It is a complicated process in which many factors (e.g. sand transport, rate wind speed, morphology and particle size distribution) not only act directly, but also interact with each other and vary both spatially and temporally"(Wang and Zhang, 2019)". Also leads to some extreme environmental phenomena such as desertification, dust storms and soil erosion "(Kang and Zhao, 2015)". Experimental and numerical works have been conducted to predict and understand the process of windblown sand transport. Many Aeolian equations are available for predicting the transport of loose grains along a surface of sand without obstacles "(van Rijn and Strypsteen, 2019)". The total sand flow, the concentration of sand particles, and the wind profile in the saltation layer were measured using the wind tunnels and in the field "(Kang and Liu, 2009)" "(Rasmussen and Mikkelsen, 1998)" "(White and Mounla, 1991)" "(Neuman and Maljaars, 1997)" "(Rasmussen and Iversen, 1996)" "(Dong and Liu, 2003)".

Aeolian wind tunnel configuration aims to simulate the mechanism and estimate the transport rate of sand particles in different sizes under the influence of wind flow "(Rasmussen and Valance, 2015)". In the very early phase of Aeolian sand transport, aerodynamic entrainment of grains plays an important role in salting dynamics, and more small grains than large grains can be transported by wind flow. As more and more grains of sand are carried away, the wind flow changes significantly "(Zongyan and Fengjun, 2020)". The particle concentration in the windblown clouds has major attention in modeling and studying the Aeolian sand research such as the formation of dune fields "(Dong and Wang, 2004)" "(Liu and Dong, 2004)" "(Dong and Qian, 2006)" "(Wang and Zhang, 2006)". The volume fraction of sand particles is a factor that reflects the particle concentration degrees in physical configurations during the movement of windblown sand. In the experiments of "(Creyssels and Dupont, 2009)" using the PIV technology (Particle Images Velocimetry), it was found that the profile of particle density decreases exponentially with altitude "(Mostafa and Mongia, 1988)".

Similarly, analytical and numerical studies have been conducted to try to understand and predict the saltation dynamic variables "(Valance and Rømer, 2015)". Relying on the basic physics approaches, the averaging methods can be divided into three main groups for formulating the multiphase flow"(Sauermann and Kroy, 2001)" "(Jenkins and Cantat, 2010)" "(Ishii, 1975)" "(Mannine and Taivassalo, 1996)": Euler averaging, Lagrangian averaging, and Boltzmann averaging.
In Euler's approach, the particles are considered as a continuum phase. Several models based on Euler's approach have been developed "(Valance and Rømer, 2015)" "(Lämmel and Rings, 2012)" "(Pähtz and Kok, 2012)". "(Jenkins and Cantat, 2012)" Obtained a local relation between the particle shear rate and the shear stress in the dispersed phase, which is influenced by averaging the equations governing the trajectories of individual particles at each trajectory

height. A local constitutive law with the balance equations based on the continuum model was used to evaluate the particles' horizontal and vertical momentum “(Lu and Gidaspow, 2003)”. “(Yang and Changsong, 2020)” have simulated the sand transport by the wind inside the atmospheric boundary layer using the coupling Eulerian model and the granular pseudo-fluidic optimization. For the dispersed phase, the sand particles are considered as a form of continuous pseudo-fluid. The approach of the kinetic theory of granular flow (KTGF) was introduced to describe the transport of saltation sand clouds.

The simulation of sand velocity profiles and mass flow rates are consistent with reported experiments “(Mathiesen and Solberg, 2000)”. “(Yintang and Yi, 2008)” Worked on the Eulerian model, which considers the dispersed phase as a continuous fluid (the quasi-fluid) to simulate the transport of sand across a flat surface. The eddy viscosity model is applied to calculate average variation quantities in the continuous phase. The Tchen theory is used to predict the turbulence quantities for the dispersed phases “(Tchen, 1947)”. The model was verified by comparing the findings with both wind tunnel experimental data and an analytical solution. However, Euler's approach is suitable for simulating sand-air flows for two reasons. First, it needs much less time than the discrete approaches. Second, it allows for a consistent format for collective modeling of sand particle motion and air turbulence.

Accordingly, an alternative method is available, namely the mixture model, which considers the flow as a one-component flow with a continuity and a momentum equation governing the evolution of mixture quantities (velocity and mixture density, combinations of phase properties to be defined), supplemented by an additional equation for the mass conservation of a phase. In these equations appear some additional terms related to the relative velocity between the phases, which are calculated by a closure law depending on the flow regime. Without relative velocity one has a homogeneous fluid model “(Fonty and Ferrand, 2019)”. This model is used in the classical Eulerian theory “(Bowen, 1976)” “(Johnson and Massoudi, 1991)” “(Joseph and Lundgren, 1990)” “(Yuan and Michaelides, 1992)”. In this approach, the basis of continuum mechanics for a single phase is generalized to different interpenetrable continua.

The essential supposition is that all phases are present at every point in time at every material point. The mixture model approach based on the Euler-Euler method is applied to model the multiphase flows at high Reynolds numbers, The dispersed phase can be liquid droplets, bubbles, or solid particles “(Ishii, 1995)” “(Simonin, 1990)” “(Passman and Nunziato, 1984)”.

Many applications of the mixture model have been used to model liquid-particle mixture in a few complex flow geometries“(Bakker and Fasano, 1994)” “(Creyssels and Dupont, 2009)” “(Pericleous and Drake, 1986)” “(Kim and Verlag, 1991)” “(Kocaefe and Bui, 1994)” “(Hwang and Shen, 1991)” “(Hwang, 1989)”. The particle distribution in a stirred tank was simulated by “(Creyssels and Dupont, 2009)” utilizing a mixture model to calculate the particle density. Along the axial direction, the diffusion rate of the particles was assumed and the effects on the average liquid flow due to the solid particles were not considered. “(Ishii, 1975)” implemented the mixture model and modelled the air-liquid-particle flow in a hydrocyclone classifier. Two-

axisymmetric dimensional grid configuration was used in the modelling. Both components of relative velocity radial and vertical were computed from both centripetal and gravitational accelerations. They found the limitations of this model are related to the unresolved quantities such as the behaviour of particles near solid boundaries and turbulence, and are not related to the mixture model itself when they validated their results.

However, in Aeolian sand transport research, the density of the particles is often on the order of 10^{-5} to 10^{-4}, the continuity equation of the sand-air mixture flow can be described as a single-phase continuity equation for an incompressible gas. The purpose of this thesis is to study the wind tunnel model that applies the theory of the mixture model to predict the characteristic saltation, including particle concentration, particle velocity, kinetic energy and diffusion coefficient of sand particles.

Beginning in the first chapter with an overview of the state of the art of dust storms and sand transport. In the second part, we try to understand the physical side of the sand transport phenomenon and know the modes of transport. In the third chapter we see the essential formulation using to modelate multiphase flows and especially in detail the mixture approach configuration of the computational domain, which finally summarizes the results of this work and the conclusions

Chapter 1: Sand transport and dust storms phenomena

1.1 Background

Uncontrolled, powerful, or turbulent winds combined with exposed, loose, dry surfaces result in sand and dust storms (SDS). These ailments are widespread in semiarid and arid areas. Sandstorms happen relatively close to the surface of the Earth, but smaller dust particles can be propelled miles into the air by powerful winds, where they can travel great distances and even cover continents. Governments and the worldwide community are become more concerned about SDS due to its negative effects on agriculture, infrastructure, transportation, and human health. Policy-makers need to know the answers to three key questions: (i) have dust storms gotten worse recently? (ii) how much of SDS is caused by human activity? (iii) and what can be done to stop them and protect us from their effects? Although exact figures are very difficult to determine, approximately 75% of current worldwide dust emissions are due to non-anthropogenic, natural causes. These topographical depressions in arid areas are primarily dry, old lake bottoms with scant flora. About 25% of the world's dust emissions are attributable to anthropogenic sources, which are primarily (85%) hydrological sources (ephemeral waters). For SDS mitigation methods, the predominance of natural sources and a rising threat of greater anthropogenic inputs have significant ramifications.

Chapter 1 : Sand transport and dust storms phenomena

The amount of surface winds that surpass the erosion threshold established by local surface characteristics determines the activity of a sand or dust source. Due to the wind erosive character of their surface materials, which is exacerbated by the drought and restricted vegetation as a result of the drought, inland catchments in arid regions are the majority of important dust sources. The vulnerability to dust formation in these places is increased by the removal of vegetation, decline in biodiversity, and disturbance of the sediment or soil surface (such as through the breakdown of biological crusts by vehicles). Wet or ephemeral water bodies have dried up, increasing the risk of SDS, as a result of man-made hydrological changes, which are frequently brought on by the need for water in places near natural springs.

Unsustainable land use and degraded soil, particularly in semi-arid regions, greatly increase the likelihood of increasing wind erosion, which can negatively impact agricultural yield even in the absence of SDS production. By serving as a mechanical barrier, limiting wind flow, and decreasing surface shear stress at the soil surface and by physically defending the soil surface, vegetation acts as a protective mechanism. It also increases soil stability by recycling organic matter.

Fig1.1 : In May 2010, a dust storm strikes a community in Golmud, China's Qinghai Province, close to the Gobi desert. [Source: mail.com].

SDS risk is increased by all elements resulting in unsustainable land use and decreased plant cover in sensitive locations. Major dust bowl episodes have been caused by a mix of unsustainable farming techniques and extended drought in many regions of the world. Future hazards of wind erosion and SDS are likely to be influenced by climate change, especially when drier and more frequent high wind events occur. However, the opposite is also probable. Predicting the effects of climate change and increasing anthropogenic dust emissions on the Earth system balance is challenging due to the numerous feedbacks between anthropogenic dust emissions, temperature, and both terrestrial and marine biogeochemical cycles.

Through the emission of greenhouse gases, modifications in the surface energy balances, and direct dust inputs into the atmosphere, land degradation also contributes to climate change. Simulations show that dust emissions are very sensitive to human intervention, which will have significant long-term effects on the climate and biogeochemistry. As a result, preventative measures should be taken.

1.2 Condition and trends:

SDS are identified and monitored by combining computational modeling, ground surveillance data, and satellite photography. The Northern Hemisphere is home to the biggest concentrations of high levels of dust, both naturally occurring and caused by human activity. This is particularly true of a huge dust belt that stretches from China to the west coast of North Africa to the Middle East, Central Asia, and South Asia. Although these sources have significant local effects, the southern hemisphere does not exhibit significant dust activity, with modest concentrations in central Australia, southern Africa, the Atacama in South America, and the Great Basin in North America. The paper gives a thorough explanation of the origins, patterns, and trajectories of dust for various geographical areas. The southern Sahel has more anthropogenic dust sources, which are assumed to be mostly related to agriculture and grazing operations, compared to the Sahara, which is the most significant producer of dust globally and is essentially natural. Additionally, human sources predominate in the Atlas Mountains and along the Mediterranean coast.

Mesopotamia is a significant source region in the Middle East, which displays a complex mixture of anthropogenic and natural sources. The Etosha and Makagadikgadi Basins in Southern Africa are two of the three major dust generators in the Southern Hemisphere. Except for a few transient lakes, the majority of dust activity in North America occurs in the vast plains

that run from southern Texas to Montana. The Atacama Desert in Chile and Peru is South America's greatest natural source, whereas Argentine Pantagonia is the region with the most human-made sources. The Indian subcontinent's northern region is a significant producer of dust, largely because of ephemeral bodies of water generated by land usage that range in size from huge rivers to tiny lakes. On the border between Iran, Pakistan, and Afghanistan, dust storms are prevalent. The greatest natural springs in East Asia are located in basins in China, including the Taklamakan Desert.

According to simulations, a combination of land use and climate change over the past century has resulted in an increase in yearly worldwide dust emissions of 25% to 50%. Over the past few decades, SDS has become more common and severe in certain places while declining in others. Over the previous three decades, there don't seem to have been any significant changes in dust activity over North Africa, the Middle East, or South America, but there have been significant changes over the US Plateau, Central Asia, and Australia.

There is evidence to suggest that better land management helps certain places reduce SDS. According to climate change forecasts, the majority of Mediterranean Europe and Africa, the northern Sahara, central and western Asia, the US southwest, and southern Australia are among the locations that are already dusty and are predicted to grow drier. Since 1950, precipitation has increased in northern hemisphere mid-latitude land regions, which may help slow the mid-latitude belt's desertification. East Africa and East Asia are dusty regions that are predicted to grow wetter, but Sahel-Sudan, the Gangetic Basin, and the Lake Eyre region cannot be projected due to substantial model uncertainty.

1.3 Impacts

Both good and bad things might happen when there are dust accumulations in the environment. Dust has an impact on the climate system, perhaps changing the Earth's radiative balance and tropical cyclones, which might result in droughts getting worse. On the other hand, because it serves as a droplet nucleus, dust can boost precipitation. Dust improves primary production by supplying nutrients to the seabed, ecosystems on land, and surface oceans. This is done in part by lowering the phosphorus limit on nitrogen fixation and by iron fixation, which encourages phytoplankton growth. In turn, the primary production has an impact on the global carbon cycle. The Amazon rainforest receives fertilization by saharan dust, which supplies an input of phosphorus equal to the hydrological loss from the basin. Similar to this, dust from Central Asia

provides nutrients to Hawaiian rainforests. On the other side, dust from Asia and Africa can harm the coral reefs in the United States.

Numerous health issues are brought on by dust, which is particularly harmful in dry and semi-arid areas. Breathing small particles can cause or exacerbate conditions including silicosis (pulmonary fibrosis), asthma, bronchitis, and emphysema (damage to the air sacs in the lungs). Lung cancer, acute lower respiratory tract infections, and chronic exposure to particulate matter are all linked to early mortality from cardiovascular and respiratory conditions. Various contaminants, spores, germs, fungus, and possible allergies are all found in particulate matter. Eye infections, skin irritation, meningococcal meningitis, Valley fever, illnesses linked to toxic algal blooms, and fatalities and injuries linked to transportation accidents are additional frequent issues. Meningitis outbreaks and the amount of dust carried in from the Sahara are strongly correlated in the Sahel nations. SDS have broad economic repercussions, both now and in the future. In addition to the aforementioned negative effects on the environment and human health, there are also immediate expenses associated with crop loss, animal loss, infrastructure loss (such as buildings, electricity, and communications), disruption of transportation and communications, accidents on the road and in the air, and the price of removing sand and dust. Chronic health issues, deteriorated soil quality, soil degradation from pollutant deposition, and interference with global climate control are some of the longer-term effects. The financial costs of a single SDS incident might be in the hundreds of millions of dollars.

1.4 The importance of sand and dust storms

Wind erosion, which causes sediment particles to become loose from the ground surface, is what causes sand and dust storms (SDS), which occur in the lower atmosphere. Sandstorms happen relatively near to the surface of the Earth, but smaller dust particles may be propelled kilometers into the air by powerful winds, where they travel great distances. These episodes typically take place in semi-arid and dry regions with little plant cover because bare terrain is most vulnerable to sediment entrainment. Dust storms may sweep across land and water thousands of kilometers from their points of origin, dumping debris far from those locations. Aeolian deposition rates can be comparable to river and aeolian erosion, and dust storm trajectories are a natural component of ecosystems in dry and semi-arid areas (Goudie and Middleton 2006).

Chapter 1 : Sand transport and dust storms phenomena

According to Knippertz et al. (2014), SDS have both good and negative impacts on the environment. The many interactions are complicated and yet not fully understood. Dust has an impact on human, terrestrial, biological, marine, and atmospheric processes and systems (Washington and Wiggs 2011). For instance, dust is crucial to the biogeochemical processes that keep forests and seas alive on Earth (Goudie 2009). Dust has an impact on the climate system by influencing the strength of tropical cyclones and storms (Evan et al. 2006) and the Earth's radiative balance, which can cause droughts to get worse (Han et al. 2008; Highwood and Ryder 2014). As a droplet nucleus, dust, on the other hand, can promote precipitation (Nenes et al. 2014). Health issues are exacerbated or caused by airborne dust (WHO 2013). Lung cancer, acute lower respiratory tract infections, and chronic exposure to particulate matter are all linked to early mortality from cardiovascular and respiratory conditions. Inhaling particulate matter exposes people to toxic mixtures of pollutants, spores, germs, fungus, and possible allergies in addition to deadly fine mineral particles (Kellogg et al. 2004; Smith et al. 2011). Traffic accidents and aviation dangers are also more common as a result of poor vision, sand movement, and debris brought on by SDS. SDS has a number of economic ramifications in addition to those affecting human health. Infrastructures related to supply chains, transportation, and communications are among them (Goudie and Middleton 2006). SDS may cause the disappearance of productive topsoil, which might directly harm crops and kill livestock, raising the cost of food production and threatening the sustainability of production (Middleton and Sternberg 2013; Sivakumar 2005).

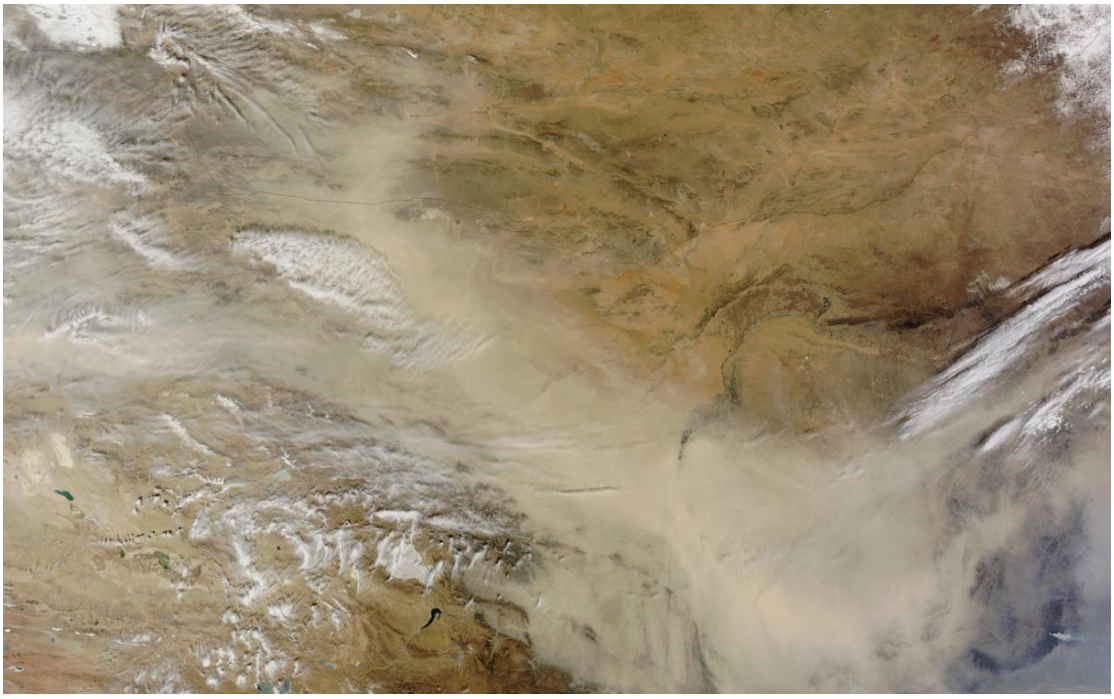

Fig1.2 : On March 9, 2013, dust storms were seen reaching along the China-Mongolia border. Millions of individuals were impacted by the large territories that the dust storms covered. [Source: NASA pictures courtesy of LANCE MODiS and Jeff Schmaltz]

Due of their global occurrence and transboundary character, SDS have a broad geographic extent (Figure 1.2). They have important local, regional, and global ramifications for attaining sustainable development, necessitating coordinated actions at each of these levels. Are dust storms getting worse (more frequent and severe) in recent decades? are two key questions that are crucial to have the answers to for policy-making. How much of SDS is a result of human activity? What steps can be taken to stop them and shield us from their negative effects? This evaluation seeks to clarify these difficulties by compiling the most recent scientific data. However, it must be made apparent right away that the majority (75%) of current emissions come from natural and not from anthropogenic sources (Goudie and Middleton 2006; Ginoux et al. 2012).

In reality, geographical depressions in drylands remote from populous regions are the world's biggest generators of dust (Muhs et al. 2014). Additionally, the frequency of dust storms has historically been significantly higher than it is now (Thomas 2011), and the quantity of dust emissions attributed to human activity is highly unknown. It's also crucial to remember that throughout the last few decades, there hasn't been a continuous global trend of rising SDS incidence and severity; rather, SDS appears to have grown in some places while declining in others (Goudie and Middleton 2006).

Since the 1950s, there have been an exponentially greater number of scholarly papers on SDS (Figure 1.3), which reflects the growing concern this issue has generated on a worldwide scale. In example, the necessity of include dust in climate change models has been more widely acknowledged (Washington and Wiggs 2011).

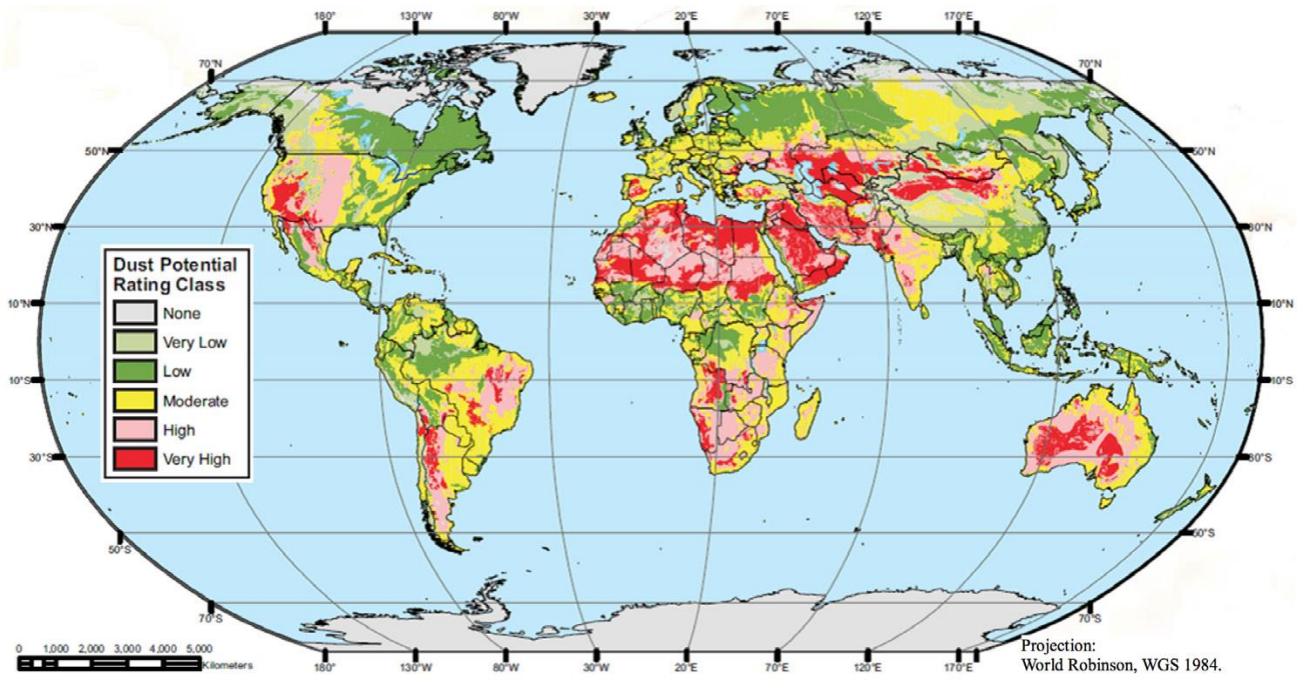

Figure 1.3: Global Dust Potential Map. [Source: DTF (2013)].

1.5 Processes Related to Sand and Dust Storms

The World Meteorological Organization (WMO) defines dust storms technically as surface winds that lift significant volumes of dust into the air and reduce visibility below 1000 meters (McTainsh and Pitblado 1987). As opposed to dust or aerosols from other sources, such as cosmic dust, sea salt, volcanic dust, or smoke particles, we only refer to mineral dust from the ground surface in this section. Different definitions of mineral dust particle size are used here, but as a general rule, the <1.63 micron range is utilized, which generally correlates to the size fractions of clay (<2 microns) and silt (2.63 microns) in soils and sediments. The majority of particles that travel more than 100 kilometers from their source are typically less than 20 microns in diameter, consistent with settling rate theories (Gillette 1979).

Although there is a chance that particles could coagulate during deposition, there is an anomaly in that giant sand-sized dust particles even larger than 63 microns (i.e. grains of sand) have been discovered thousands of kilometers from their source. Due to the continuum of particle sizes present in each storm, there is no clear distinction between sand and dust storms.

The WMO also defines other terms, such as dust vortices, which are whirling columns of dust that move with the wind, and dust bubbles, which occur when vision is lowered to eye level but

not less than 1000 m. Particle motion can be produced by wind transport or deflation through the processes of creep, salting, and levitation. Particles with a diameter more than 500 microns creep across the surface of the ground. When the wind transports particles that are between 63 and 500 microns in size and are typically less than 1.5 meters above the ground, this is known as saltation. Particles less than 63 microns in diameter are referred to as being suspended when they are transported over a long distance (Pye 1987; Figure 2.1). A type of sandblasting is a process in which salting particles bombard soil aggregates, resulting in aggregate fragmentation and the release of fine particles, which are then entrained (Marticorena 2014; Shao 2008).

1.6 Sand and dust storms Causes

A number of interconnected direct (proximal) and indirect (distal) causes acting at various scales result in sand and dust storms. Strong feedback mechanisms exist both within and between scales. The mitigation of SDS is significantly impacted by these interconnections. It is important to differentiate between human and natural sources of SDS, which together account for the majority of the world's dust emissions. However, human strain on natural ecosystems is growing (MA 2005a), which may increase their significance as source regions in the future. A common driver in both natural and anthropogenic systems is human-caused climate change.

1.6.1 Direct forces in biological systems

Sandstorms and dust emissions are primarily caused by wind in all systems. distinct geographical areas experience distinct synoptic climatic conditions that result in winds (Section 2.2; Knippertz 2014). According to a review of trends in terrestrial near-surface wind speeds conducted globally (McVicar et al. 2012), wind speed has decreased globally over the past few decades. Decreases have been noted in both hemispheres' tropics and mid-latitudes, but increases have been noted at high-latitudes (i.e., latitudes >70°). At low latitudes, lower wind speeds are anticipated to lessen the danger of SDS. The proportion of surface winds that surpass the erosion threshold established by the local surface parameters determines the activity of a dust source (Marticorena et al. 2014).

Due to the wind-erodible character of their surface materials and geomorphic processes, inland drainage basins or depressions in dry regions represent the majority of important dust generators (Bullard et al. 2011). Examples include the Bodélé Depression in the South Central Sahara, the

West Sahara in Mali and Mauritania, and the Taklamakan Desert in the Tarim Basin in China (Washington and Wiggs 2011). These are discussed in more length in Section 3. The Bodélé Depression produces the majority of its dust through extensive exposures of a friable, low density diatomite deposit (Washington and Wiggs 2011).

While the Taklaman Desert, on the other hand, is distinguished by its smooth surfaces and dry, sandy soils that also have low erosion thresholds, according to Marticonena (2014). Bullard et al. (2011) identified seven geomorphic categories that are often present in arid and semi-arid areas, differ in terms of surface traits determining their susceptibility to aeolian erosion, and are easily distinguishable using remotely sensed data. High danger of dust release exists in ephemeral lakes and dry lakes with unconsolidated sediments. If not replaced by external sediments, the selective removal of small particles over an extended period of time may deplete erodible material. Ephemeral water bodies are frequently significant generators of dust because of the renewal of sediments.

Significant dust emissions only happen in unarmed, high relief deposits after sporadic rains introduce new material to the system. Unincised, low relief deposits can provide substantial emissions and allow for the replenishing of sediments. Low relief sand deposits are known as sand sheets. The size and classification of the sediments make them vulnerable to wind erosion, however in many situations, vegetation, coarse sands, or shallow water tables prevent wind erosion (Bullard et al. 2011). A wind-worked deposit with characteristic relief are aeolian sand dunes. Sand dunes' contribution to dust emissions varies by type, amount of activity, and palaeoenvironmental history.

Although dynamic, young, or tiny sand dunes with a relatively quick turnover of sand are unlikely to be important or persistent dust producers because they contain little fine material, large, more stable, or older dunes may store fines inside the dune structure (Bullard et al. 2011). On the other side, older dunes will be more likely to emit dust if disturbed. However, mobile dunes can be dangerous to human welfare when they are close to infrastructure because of sand storms and sand migration. Dune instability may result from any decline in plant cover, including those caused by excessive harvesting, agriculture, grazing, burning, or even drought (Middleton 2011). A depositional landform with an aeolian origin that is predominantly made up of sediments the size of silt is called loess. 2011 (Thomas).

When there is less vegetation or disturbance, loess can become a substantial source of dust (Bullard et al. 2011). The degree of connectedness with nearby landforms also influences the possibility for dust emissions in addition to geomorphic type since it impacts salt and sediment

supply. Figure 2.3 depicts the distribution of aeolian deposits over the world, including movable dunes and loess deposits. In the area of ephemeral lakes and playas, human interference with the hydrological cycle has the potential to hasten desiccation, lower water tables, decrease soil moisture, and diminish plant cover, exposing sediments to wind erosion (Gill 1996). Examples are provided in the section that follows. In summary, human interference in or near places with high vulnerability to dust emission poses the biggest direct harm to natural systems.

Dust production will be more likely to occur in these regions if vegetation is removed, biodiversity is lost, and the sediment or soil surface is disturbed (for example, by destroying biological crusts or exposing erodible underlying sediments). SDS risk is further increased by human-caused hydrological modifications that cause moist or transient water bodies to dry out. Therefore, it is advised to protect natural ecosystems that might act as sources of dust.

1.6.2 Indirect influences on ecological systems

Although there is still substantial ambiguity regarding the impact of human activity on SDS, it is quite probable that perturbation of natural systems brought about by human pressure, notably through human-induced climate change, will rise in the upcoming decades. With the aim of sustainable use using cutting-edge technology and creative water-saving techniques to promote areas like renewable energy, irrigated agriculture, desert cities, and eco-tourism, there has been an increase in interest in reversing the harmful effects of drivers in desert ecosystems (UNEP 2006; 2015b). Effects of climate change may extend beyond higher emissions of dust.

For instance, research indicates that as a result of the global warming of the twenty-first century, sand dune fields across southern Africa are expected to be reactivated (the sand will become increasingly exposed and shift). Demand for water resources for irrigation or in ephemeral lakes and playas frequently causes hydrology to be disturbed. Another factor in playa desiccation is the construction of roadways and communication lines that obstruct or redirect drainage water input (Gill 1996). In the western US, particularly in California, parched playas as a result of human activity were shown to occur most frequently (Gill 1996). Desiccation of the Aral Sea is one such example.

1.7 Overall picture

The Northern Hemisphere (Figure 1.4) is home to the biggest concentrations of high aerosol

levels, both from natural and anthropogenic causes. This concentration is mostly found in a broad dust belt that stretches from China to the west coast of North Africa, to the Middle East, Central and South Asia, and the Middle East. There is very little significant dust activity outside of this area. Although SDS occurrences are significant in terms of their local consequences, the southern hemisphere in particular does not demonstrate significant dust activity. Lower amounts can be found in the North American Great Basin, the Atacama Desert in South America, central Australia, southern Africa's Botswana, and Namibia.

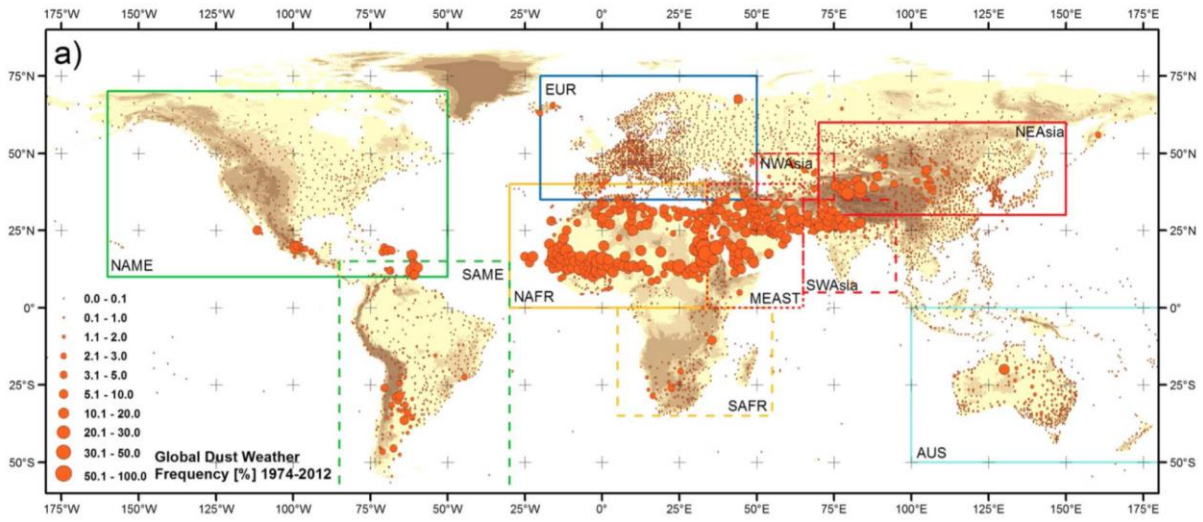

Fig1.4 : The synoptic current weather records for the period of January 1974 to December 2012 were used to determine the global pattern of dust frequency. Shao et al. (2013) as the source.

Most desert dust is emitted from natural sources with little influence from humans (Prospero et al. 2002), and the relative contributions from global dust sources that are significantly influenced by human activities have a large uncertainty, ranging from less than 10% to 50% of global emissions, but are most likely around 25%. Deposition rates associated with some of the main dust lanes indicate high rates along the Niger River in Mali. According to MODiS Deep Blue data, ephemeral water bodies and other hydrological dust sources account for 31% of worldwide emissions, 15% of which are natural and 85% of which are human (Ginoux et al. 2012). According to Ginoux et al. (2012), partly vegetated surfaces account for around 20% of emissions, primarily agricultural land and scrubland in the desert.

In topographical depressions in dry areas, thick alluvial deposits created by periodic floods during the Quaternary and into the Holocene represent the majority of the principal producers of dust (Prospero et al. 2002). The alluvium layer is deep enough in some of these depressions to support dust emission without further filling, but in others, flooding frequently creates fresh

sediment deposits, which subsequently serve as potential sources. According to Ginoux et al. (2012), ephemeral lakes and riverbeds (such as wadis) are frequently active producers of dust.

1.7.1 The Northern Africa, the Sahara, and Southern Europe

According to Goudie and Middleton (2006), the Sahara is the primary producer of dust in the globe, contributing half of the Aeolian desert material dumped into the seas. Recent research (Figure 1.5) reveals that the Sahara is the most significant natural source (sites 6 to 11), whereas the southern Sahel's sources are primarily anthropogenic (sites 1 to 5). This could be explained by the fact that agricultural and grazing activities are confined to relatively localized areas around point water sources in regions with an annual rainfall of 200–250 mm, and the majority of these activities occur in wetter areas south of the 200–250 mm Isohyets (Prospero et al 2002). Sites 20 to 23 in the Atlas Mountains and Site 19 near the Mediterranean coast are examples of sources that are primarily human-made. The Sahel's dust emissions are influenced by land usage. Playas and ephemeral lakes were reactivated by overgrazing and farming in Senegal (site 1) and from Lake Faguibine in Mali (blue spot at site 3 on the border with Mauritania), according to measurements from the 1950s (Gill 1996).

Analysis of centuries' worth of dust deposition in the estuary of the Senegal River revealed a dramatic rise in deposition following the introduction of commercial agriculture in the Sahel around 200 years ago (Mulitza et al. 2010).

Livestock disturbance of surface crusts has been linked to dust storms arising from alluvial sediments of the interior Niger River delta (site 3) near Mopti in Mali (Nickling and Gillies 1993). Natural sources are the major sources outside of the Sahel (Prospero et al. 2002). These include large depressions (Bodl, site 7 and Qattarah, site 17), large basins with sand lakes (Erg of Bilma, site 8; Erg el Djouf, site 10; Grand Erg Occidental, site 13; Grand Erg Oriental, site 14; and Libyan desert, site 15), ephemeral lakes (Sebkhet te-n-Dgmcha, site 11; Chott el Jerd, site 19; Chott Melrhir, site 20; and lakes in the Tiris Zemmour region, site 12), and the Nile river basin (site 16).

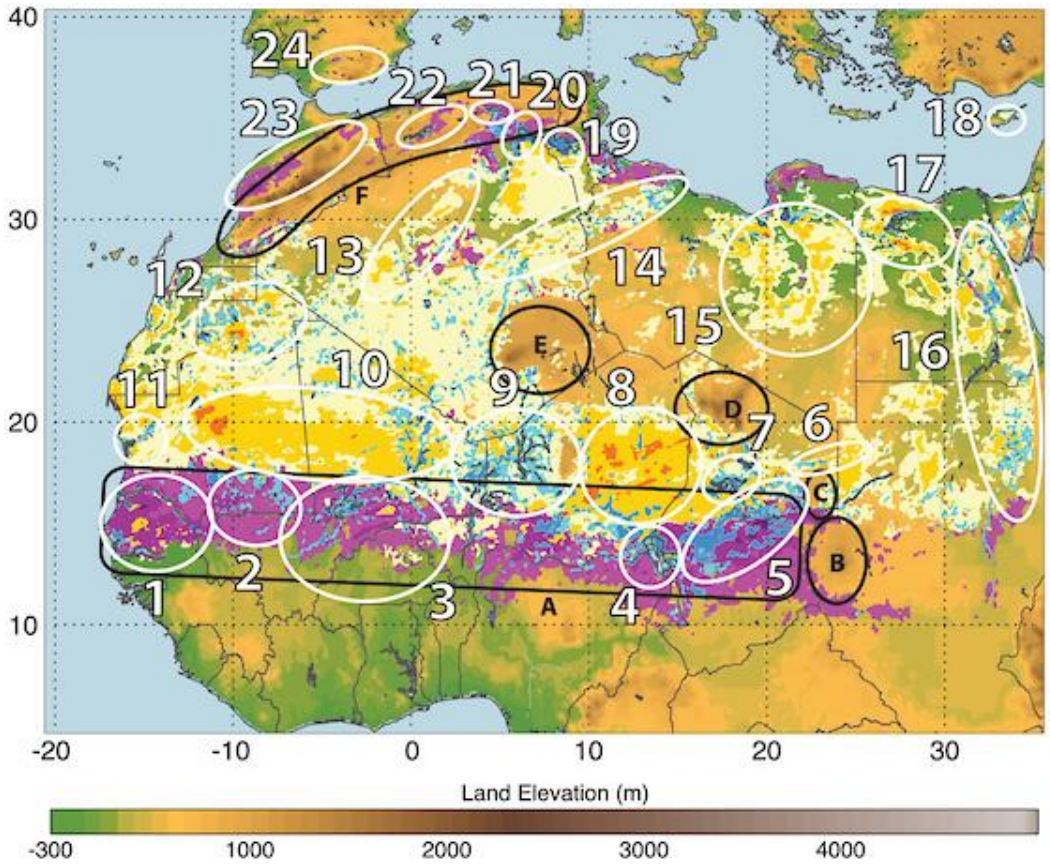

Fig1.5 : Distribution of the proportion of days per year in West and North Africa and Southern Europe with Dust Optical Depth > 0.2. Natural land use is coloured in yellow to red, human land use (greater than 30%) is shaded in magneta, and the frequencies related to hydrologic sources are shaded in blue. There are five different frequencies: 10%, 20%, 40%, 60%, and 100%. Dark green dominates the topography at 300 meters, followed by brown at 1000–4000 meters and finally grey at high elevations of up to 8000 meters. The following numbers correspond to the white circled source areas:
1, Senegal River Basin; 2, Aoukar depression; 3, upper Niger River Basin; 4, Lake Chad; 5,river drainage basin of the Ennedi and Ouaddaï highlands; 6, Mourdi depression; 7, Bodélé depression; 8, Grand Erg of Bilma; 9, river drainage basin of the Aïir; 10, Erg El Djouf; 11, Sebkhet te-n-Dgâmcha; 12, Tiris Zemmour region; 13, Grand Erg Occidental; 14, Grand Erg Oriental; 15, Libyan Desert; 16, Nile River Basin; 17, Qattarah depression; 18, Mesaoria plain in Cyprus; 19, Chott el Jerïd; 20, Chott Melrhir; 21, Chott el Hodma; 22, Chott ech Chergui; 23, Morocco coastal plains; and 24, Andalusia in Spain. Some geographic features are contoured in black and are labeled as follows: A, the Sahel; B, the Ouaddaï Highlands; C, Ennedi; D, Tibesti; E, Ahaggar; and F, Atlas Mountains. Source: Ginoux *et al.* (2012).

According to Goudie and Middleton (2006), four key pathways are frequently used to carry saharan dust. There are supplies going southwest to Ghana, the Ivory Coast, and the Gulf of Guinea. Dust travels in a westward direction to the Canary Islands, North America, and South America across the North Atlantic. Dust travels northward across the Mediterranean, reaching

Scandinavia and the Baltics as well as southern Europe. Dust travels through an eastern route that passes via the Mediterranean, the Middle East, the Himalayas, East Asia, and Japan. The main stream of dust migration, which accounts for 30 to 50% of emissions, is westward, with longer-lasting plumes moving dust further. For instance, it typically takes 5 to 7 days to travel to the Caribbean, where 20 million tons of Saharan dust are dumped each year.

Every year, between 80 and 120 million tons are brought to Europe and mainly dumped as precipitation. The majority of the North African deposit lies in the eastern Mediterranean. Since the late 1950s, longer and more frequent dust outbreaks have been recorded in the Sahel, which have been linked to drought spells (Middleton 1985; Goudie and Middleton 1992; NTchayi et al. 1997) and may be a sign of climate change. According to Clark et al. (2004), the deflationary power of the wind also appears to have grown between 1970 and 1985. Data demonstrating a rise in Saharan dust deposition in several depositional sites in Europe and Barbados (Goudie and Middleton 2012) support the trends.

1.8 Climate and dust

Condition and trends According to Singh et al. (2008), dust influences climate through involvement in the biogeochemical cycles (mentioned above), primarily through impacts on marine bloom and sea surface temperatures, as well as through direct processes due to dust chemical reactivity and physical effects. Dust can change the strength of cyclones and tropical storms (Evan et al. 2006). According to Highwood and Ryder (2014), dust pollution can change the Earth's radiative balance by altering both the amount of incoming shortwave radiation and the amount of outgoing longwave radiation. Depending on a variety of factors, the overall impact of air dust can be either warming or cooling (Arimoto 2001; Miller et al. 2014). Drought intensity may be influenced by modifications to the Earth's radiative balance.

According to studies by DeMott et al. (2003), Mahowald and Kiehl (2003), and Creamean et al. (2013), desert dust can interact with liquid or ice clouds to alter their optical characteristics and lifetimes. Dust has an impact on how clouds form and behave, and dust nuclei can either reduce precipitation by generating more and smaller water droplets or increase it by acting as the nuclei for ice particles (Nenes et al. 2014; Toon 2003). By altering convective activity as a result of shifting temperature gradients, dust can also indirectly impact precipitation (Maley 1982).

Mineral dust buildup on glaciers may decrease their surface albedo and hasten their melting (Oerlemans et al. 2009). According to Martin et al. (2003), mineral dust has an impact on

tropospheric ozone by lowering the photolysis rates that lead to ozone generation by up to 50% and by providing reactive surfaces that help with the processing of trace gases.

1.9 Land processes, SDS, and wind erosion

According to Blanco and Lal (2010) and Goudie and Middleton (2006), wind erosion is a significant factor in the deterioration of the land, especially in dry and semi-arid areas. Even without creating SDS, wind erosion can impact the ecosystem. Finer soil particles, which are the most effective soil component at retaining nutrients and organic matter, are preferentially removed by wind erosion, which degrades their chemical, physical, and biological properties, reduces soil productivity, and impairs their ability to provide other ecosystem services, like regulating the climate. According to Ravi et al. (2011), the eroded debris can mechanically harm crops and natural flora by abrasion, and blown sand can cover young plants.

According to Squires (2016), the accumulation of dust particles on plant surfaces can hinder photosynthesis, and according to Burkhardt (2010), plants that can withstand drought also operate as desiccants. Pollutants and plant pathogens can also be found in eroded materials (Goossens 2003). According to reports, SDS cause cattle fatalities. Sand buildup can result in significant ongoing maintenance expenses along fence lines and in drainage ditches in agricultural regions. In many places across the world, even frequently far from the margins of deserts, dust deposition has contributed to the creation of soil. The effect of aeolian processes on the production of loess soils (loose silt), which are common in North and South America, Central Asia, and China, is the most dramatic example.

Fig1.6 : A recently constructed road is traversed by sand dunes (Photo credit: David Thomas).

According to Goudie and Middleton (2006), aeolian processes have also led to the development of rocky pavements and duricrusts, salinization and soil alkalinity through the buildup of soluble salt, and a reduction in soil acidity through the addition of carbonates. While soil organic matter may be exposed to increased decomposition due to wind erosion, soil organic carbon may be protected from decomposition by being deposited in deep sediments (Jacobs and Mason 2005). Last but not least, there is a substantial degree of uncertainty over how future land use and management changes, as well as climate change, may affect SDS and dust emissions, with significant regional differences.

Point to possible significant but extremely unclear environmental problems when combined with the ambiguity regarding the effects of dust on the environment. In fact, modeling studies show that dust emissions are very sensitive to human activity, with significant effects on future temperature and biogeochemistry (Mahowald et al. 2010). Due to this sensitivity and the significant potential environmental effect, precautionary approaches should be followed and steps should be done to reduce dust emissions from man-made sources.

Chapter 2: Physics of Aeolian sand transport processes

2.1 Aeolian Sand Research : Nature and Importance

The term "Aeolian" refers to processes that involve wind action, such as erosion, transport, or deposition brought on by air movement across the Earth's surface. The term comes from the Greek deity of winds named Aeolus. A liquid is described as a material that cannot withstand shear stress without deforming indefinitely. Air is one of two significant liquids, along with water, that are principally responsible for carrying sediments over the Earth's surface. Air and water have very distinct physical characteristics, and the two liquids' modes of transporting sediment also differ greatly. Cohesive forces keep the individual molecules of liquid water together, providing the body of water volume but no structure.

Non-cohesive molecules that are constantly moving at random and have a propensity to scatter when not contained make up air as a gas. The density of air at 18 degrees Celsius and sea level (1.3 kgm-3) is nearly 800 times less than that of water (1000 kgm-3) hence is considerably simpler to compress than water. Additionally, water has a viscosity of 1.0610-3 N s m-2, whereas air has a viscosity of 1.8105 N s m-2. As a result, compared to an air flow moving at the same speed, a water flow may entrain and suspend significantly bigger sediment particles.

Aeolian dunes and waves often include grains that are in the sand-size range, which is classified as 0.063 mm2 mm by the Udden Wentworth grain size scale. This size of grain is mostly carried

in the air by saltation (impact) or surface creep (rolling). Smaller silt and clay particles can be dispersed over broad areas because they are carried in suspension. With the exception of when the grains are combined into pellets the size of sand, such small particles do not often create aeolian ripples or dunes. The three primary aeolian process groups that cause erosion, transport, and sedimentation are as follows:

There are various different types of erosion processes, such as (a) the direct wind drag-induced shedding of loose sediments, (b) the effect of grains in the wind stream on loose sediments, and (c) the abrasion of hard surfaces by particles entrained in the flow. Individual grains can migrate by aeolian processes like as creep, saltation, or suspension as well as bed-form migration. Additionally, there are two types of sedimentation processes: those that influence individual grains and those that stabilize bed forms. The creation of ascending ripple layers is an example of how sedimentation and layer migration can occur concurrently, blurring the boundary between transport and deposition processes (Hunter 1977a).

The three basic types of aeolian deposits are loess covers, sand plates, and dunes. Simply put, an aeolian sand dune is a mound or ridge made of loose sand that has been deposited by the wind. Less than one meter to many kilometers in length are considered dunes. They can be found together in dune areas or separately. Due to their geographic distribution, dunes may be divided into four basic types: inland or continental dunes, coastal dunes, riverbank dunes, and lakeside dunes. Wind-blown sand accumulations known as "sand plates" have a level or gently undulating surface and little to no dune morphology.

In some places of Western Europe, the phrase "cover sand" has both morphological and stratigraphic connotations. It refers to late Pleistocene (mostly Weichselian) sand-plate deposits that cover broad regions with a thickness that is more or less consistent, creating a relief that varies no more than 5 m and has dip angles that are primarily less than 6 (Koster 1982). According to Koster (1982) and Castel et al. (1989), shifting sands is the term used in Europe to characterize later (Holocene) sand plate or dune deposits created by partial reworking of Pleistocene cover sands.

A pre-existing land surface is covered in layers of wind-blown dust that are predominantly made up of mud-sized particles, or loess. The surface of a loess deposit might be almost flat, gently undulating, or extensively dissected depending on the underlying topography (for a summary of loess qualities, see Pye (1987)). Eolian sediments. They can result from either fluvial reworking and redeposition of aeolian sediments during floods or from partial aeolian reworking of the upper surface of an exposed river deposit (Glennie 1970, Mader 1982, Good

& Bryant 1985, Langford 1989). According to Cailleux 1978, Ballantyne & Whittington 1987, Koster & Dijkmans 1988, niveo-aeolian deposits are combinations of wind-blown sediments (often sand) and snow that are typically found in polar areas and in certain temperate regions, especially at higher elevations.

2.2 Previous Work

Numerous fields of natural science, earth science, life science, and developmental studies, including agriculture, do study on aeolian sand (Fig. 1.2). While there is a lot of overlap, engineers have a tendency to concentrate on the mechanics of sand transport and practical ways to stabilize shifting sands, whereas geomorphologists and geologists have a tendency to concentrate primarily on the classification and morphometric analysis of dune shapes, measurements of aeolian processes, and the interpretation of sedimentary and interior property structures. By the late 19th century, most geologists believed that sediment transport by water or glaciers was far more important than that of wind.

Ehrenberg (1847), who described the airborne dust carried from Africa to Europe, Blake (1855), who was among the first to recognize the extensive evolution of wind erosion patterns in deserts, and von Richthofen (1882), who recognized the primary Aeolian origin of the vast loess deposits covering much of northern China, all contributed to the early understanding of the effects of aeolian processes. However, most geologists of the 19th century believed that water was a much more important mechanism of delivering silt than wind.Uddenc, for instance, stated that "wind erosion becomes geologically important only in certain localities, and the conditions favouring it are a dry climate and a topography of abrupt and broken reliefs" (1894, p. 320).

However, he also believed that the job done by the winds in the atmosphere "appears hardly to have received its fair share of attention" (Udden 1894, p. 318). As a result, he later conducted some of the earliest in-depth sedimentological investigations of windblown sand and dust (Udden 1896, 1898, 1914).

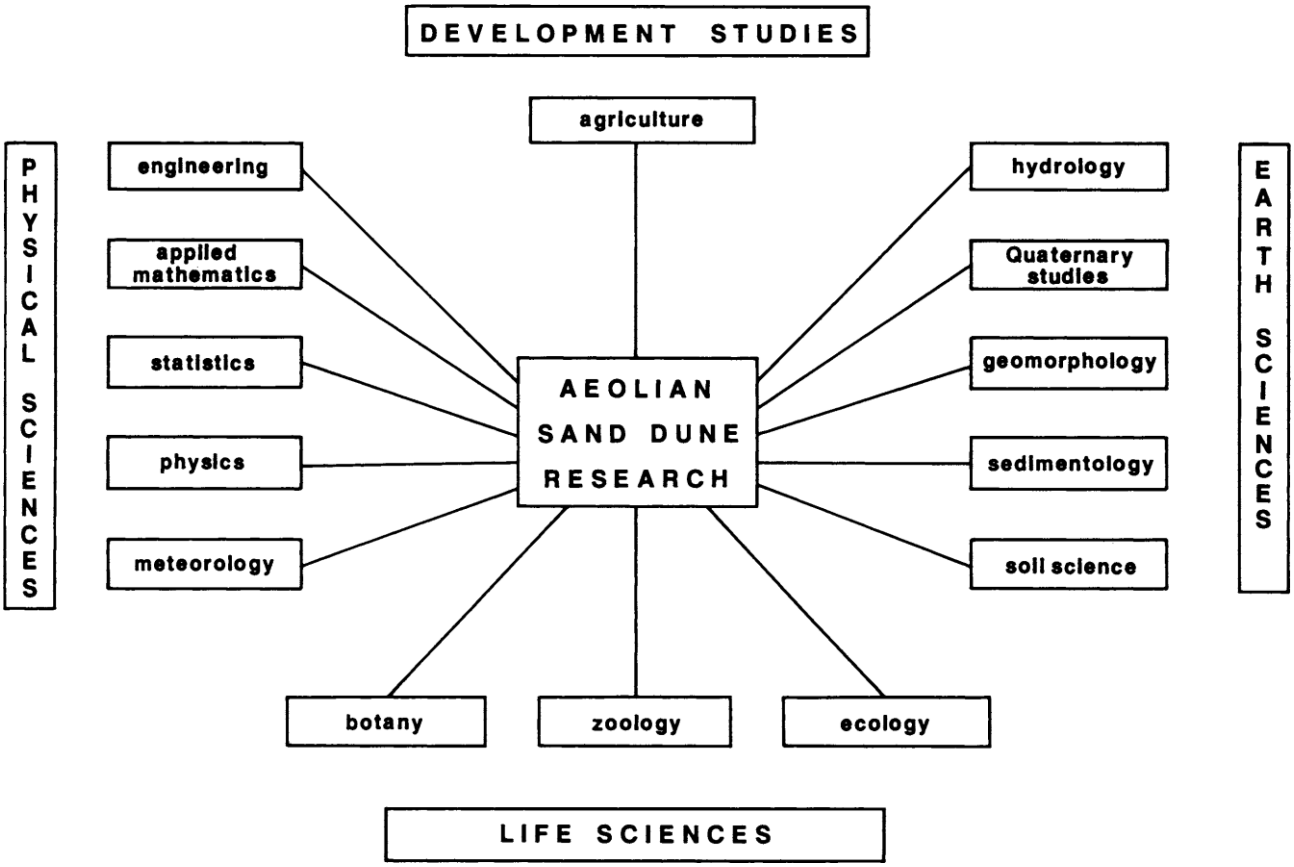

Fig. 2.1 : multidisciplinary of sand Aeolian research

Aeolian processes and sediments attracted slightly more attention in the early 20th century. In this time, several books and articles on the development of inland and coastal sand dunes were published (Sokolow 1894, Cornish 1897, 1900, 1914, Beadnell 1910, Case 1914, Hogbom 1923, Townsend 1925, Cressey 1928, Aufrre 1931, Enquist 1932, Dieren 1934), as well as wind erosion of soils in the Midwestern United States became a concern (Free 1911). To understand the mechanics of aeolian transport and dune formation, however, most of this early study was descriptive, and it was not until the mid-1930s that significant headway was achieved.

R.A. Bagnold, an engineer and soldier who made multiple missions in the Libyan Desert in the early 1930s (Bagnold 1931, 1933, 1935a), is by far the author of the most significant single contribution in this field. Then, in Bagnold 1935b, 1936, 1937a, and 1937b, he conducted a number of fundamental experimental experiments on the transport of sand by wind. Bagnold was able to use and expand on many of the fundamental fluid mechanics ideas developed by Kramn (1934, 1935), Prandtl (1935), and Shields (1936) as a result of his schooling. The Physics of Blown Sand and Desert Dunes, which Bagnold described in 1941, offered a crucial

theoretical framework that has informed all subsequent research on aeolian sand movement and dune development.

2.3 Mechanics of Aeolian Sand Transport

2.3.1 Wind Forces Acting on Static Grains

Two different types of forces are applied to a grain of sand by wind passing over it while it is sitting on a horizontal surface: (a) a drag force that acts horizontally in the direction of the flow, and (b) a buoyancy force that acts vertically upward. Inertial forces, the most significant of which is grain weight, which directly opposes the lift force, counteract these aerodynamic forces. Cohesive forces, or the forces of attraction between adjacent grains, and adhesive forces operating between grains and other surfaces must also be considered in the case of fine grains. The latter is caused by the grain experiencing overpressure on its windward side and underpressure on its leeward side The viscous stress operating tangentially to the grain surface is what causes the skin's resistance to friction. The grain's overall drag force (Fd) is given by

$$F_d \propto \tau_0 A \propto \rho u*^2 A \qquad \textbf{(2.1)}$$

where A is the maximum projected area of the grain, u is the friction velocity, and τ_0 is the surface shear stress. A = $d^2/4$ for spherical particles with dimension d. Consequently, the sphere's drag force is given by

$$F_d = \beta \rho u*^2 \left(\pi d^2/4\right) \qquad \textbf{(2.2)}$$

where β is a coefficient that varies depending on the height at which the drag force acts, the ratio of the momentary velocities of turbulent fluctuations to the average wind velocity, and the amount of drag per unit area experienced by the grain as a result of its position in relation to other grains on the bed (Bagnold 1941, p. 86).

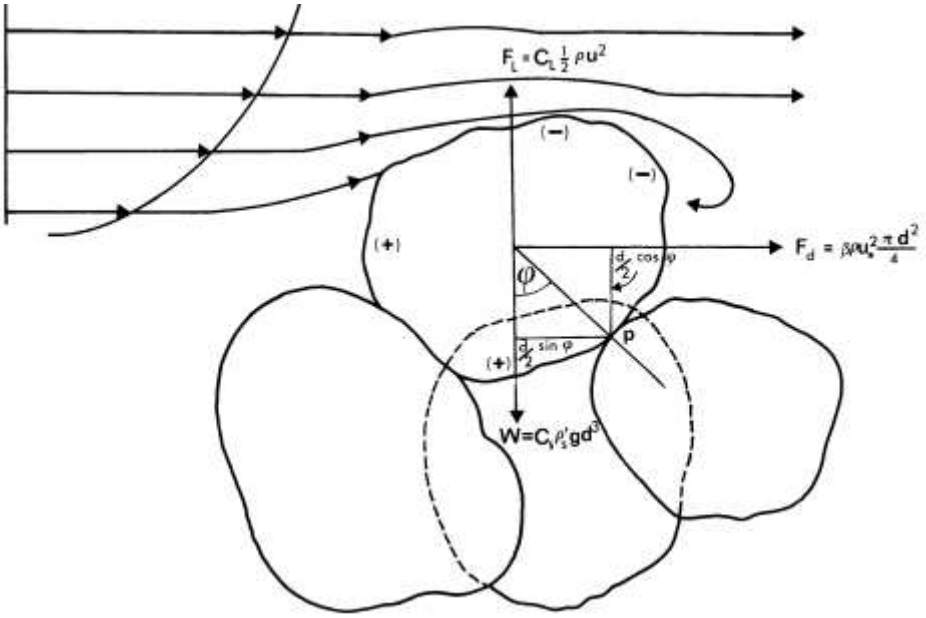

Fig2.1 : Diagrammatic representation of the wind's effects on a static sand particle. The wind profile and its associated streamlines may be seen on the upper left; (+) denotes relatively high pressure, while (-) denotes relatively low pressure on the grain surface. The two moments (d/2)sin and (d/2)cos are computed around the pivot point p. To understand the three forces affecting the grain,

On the grounds that it is irrelevant, the lift force has been left out of various theoretical and experimental considerations (Shields 1936, White 1940, Bagnold 1941, p. 32, Kalinske 1947). However, the Bernoulli effect and subsequent aerodynamic thrust are accompanied by a lift force (Jeffreys 1929) (Eq. 2.26). During wind tunnel tests, several writers have noticed that sand grains virtually vertically rise off the bed (Chepil 1945a; White et al. 1976).

Fig2.2 : A pair of instantaneous PIV photos at 0.66 m/s for the 0.23 mm sand particle are shown as an example [Liqiang Kang, Guodan Zhao 2014s].

The strong wind velocity gradient close to the bed is what causes the lift force. When a grain is at rest on the bed, the flow velocity on its underside is zero, while it is positive on its upper side. As a result, the static pressure is high beneath the grain and significantly lower above it. If the force from the static pressure differential is greater than the inertial force caused by the grain's weight, W, which is determined by, the grain will be lifted off the bed.

$$W = C_s \rho_s' g d^3 \qquad \textbf{(2.3)}$$

where Cs is a form coefficient such that Cs d^3 is the grain's volume (for a sphere, Cs = 0.524), and ρs is the density of the submerged grain (ρs = ρs-ρ, ρs being the grain density and the fluid density). A short-term lift force strong enough to lift grains off the surface may be produced by the huge instantaneous fluctuations in flow velocity and pressure that occur during turbulent flow, according to experiments (Einstein & El-Samni 1949; Bisal & Nielsen 1962). Einstein and El-Samni (1949) determined the average lift force as the difference in pressure between the top and bottom of a hemisphere to be

$$F_L = \Delta pA = \left(C_L \rho U^2 A\right)/2 \qquad \textbf{(2.4)}$$

CL is the coefficient of lift, FL is the lift force, and p is the pressure differential between the top and bottom of the hemisphere. [Einstein & El-Samni (1949)'s CL value was changed by Chepil (1958b) to CL = 0.0624], and U is the fluid velocity as measured at 0.35 grain diameters from the hypothetical surface that is denoted by the roughness length (z0). Additionally, Chepil (1958b) discovered that, within the specified range of Reynolds numbers, the ratio FL/FD is constant for any size of roughness element and friction velocity:

$$F_L = cF_d \qquad \textbf{(2.5)}$$

When the wind speed falls within the range needed to move soil particles, and the coefficient c is equal to 0.85 for nearly spherical grains. In a different experiment, spheres with a diameter of 0.3 cm and 5.1 cm sitting on the ground had an average value of c of 0.74 (Chepil 1961). The drag force was consistently shown to be larger than the lift force in various trials. Chepil

also noted that the relevance of the lift force increased with surface roughness (and grain size), friction velocity, and friction angle.

The results may not necessarily be extrapolated since the particle Reynolds numbers in the studies conducted by Chepil and Einstein & El Samni are much higher than those typical of aeolian sand grains. The rolling motion of the grains during aeolian sand movement may produce extra lift force, which would speed up the airflow passing over the grains (Chepil 1945a). Small- and medium-scale vortices can also produce significant lift forces (Greeley et al. 1981).

2.3.2 Impact Threshold

Bagnold (1937a) made the initial observation that introducing sand grains into the airflow at the upwind end of a wind tunnel causes other grains on the bed to move, and that this movement may be sustained at wind speeds lower than the fluid threshold velocity. Bagnold (1941) referred to this lower threshold velocity as the impact threshold velocity. The fluid and impact thresholds' velocity differences (Fig. 2.3) are caused by the kinetic energy of the moving grains. Sand grains bigger than 0.1 mm travel primarily by a sequence of leaps (saltation), where the force of one grain striking another adds energy to the wind drag. the impact threshold for grains bigger than 0.25mm may be determined.

Chepil (1945b) discovered that the coefficient A for impact threshold had a value of 0.085 for grains bigger than 0.1 mm.

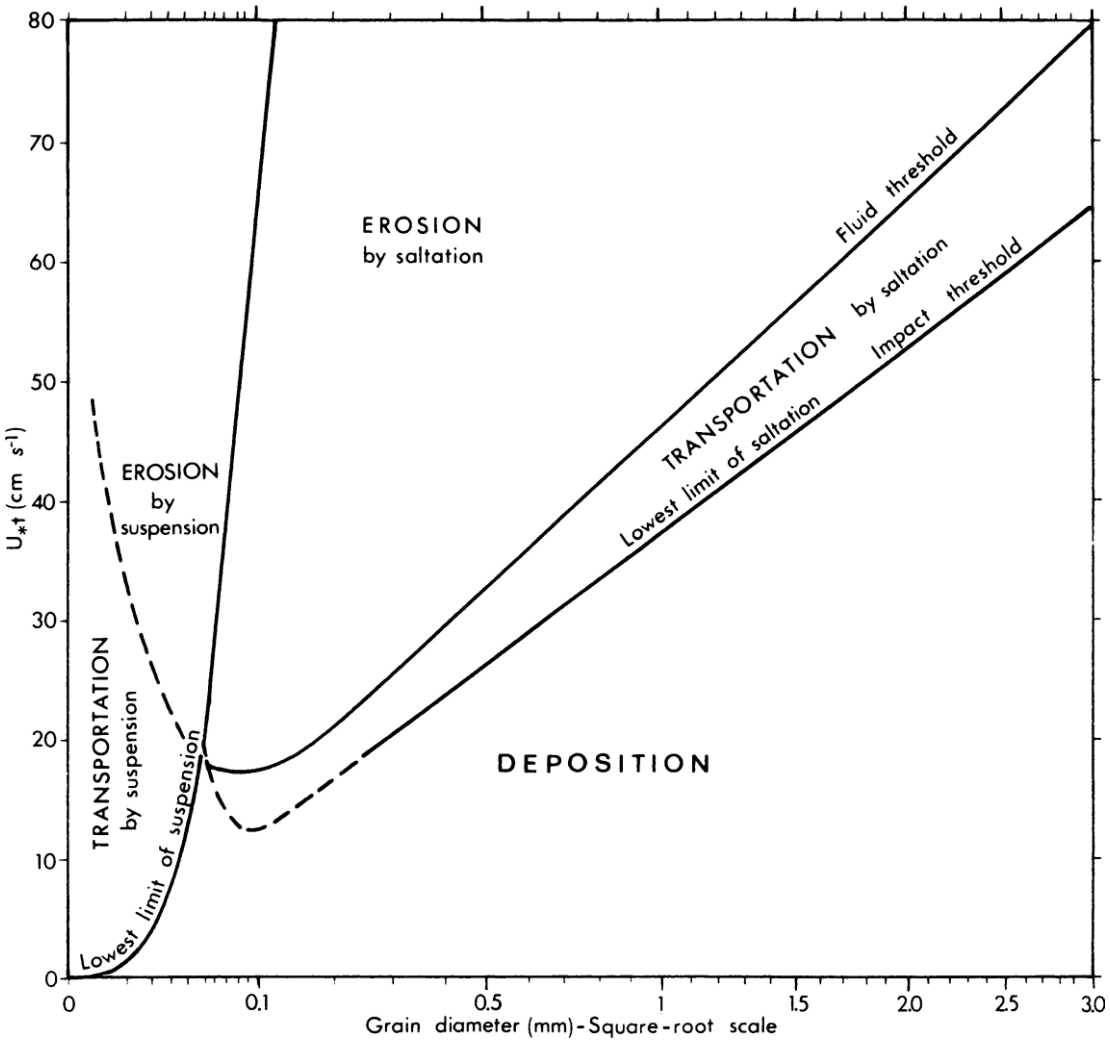

Fig2.3 : The relationship between the fluid threshold velocity and the impact threshold velocity. The differences in the mechanisms of transportation of saltation and suspension as well as between erosion, transportation, and deposition are also demonstrated. (Data from Chepil 1945b and Bagnold 1941, p. 88, in part)

Because their settling velocities are lower than the vertical component of turbulent airflow, grains smaller than 0.06 mm are mostly conveyed in suspension. The fluid and impact threshold curves blend in the size range of 0.06-0.1mm, and grains smaller than 0.06mm do not have substantial effects with other grains on the bed. However, it should be emphasized that ballistic collisions of saltating grains bigger than 0.1 mm frequently lead to the entrainment of sediments made up of grains smaller than 0.06 mm (Gillette et al. 1974).

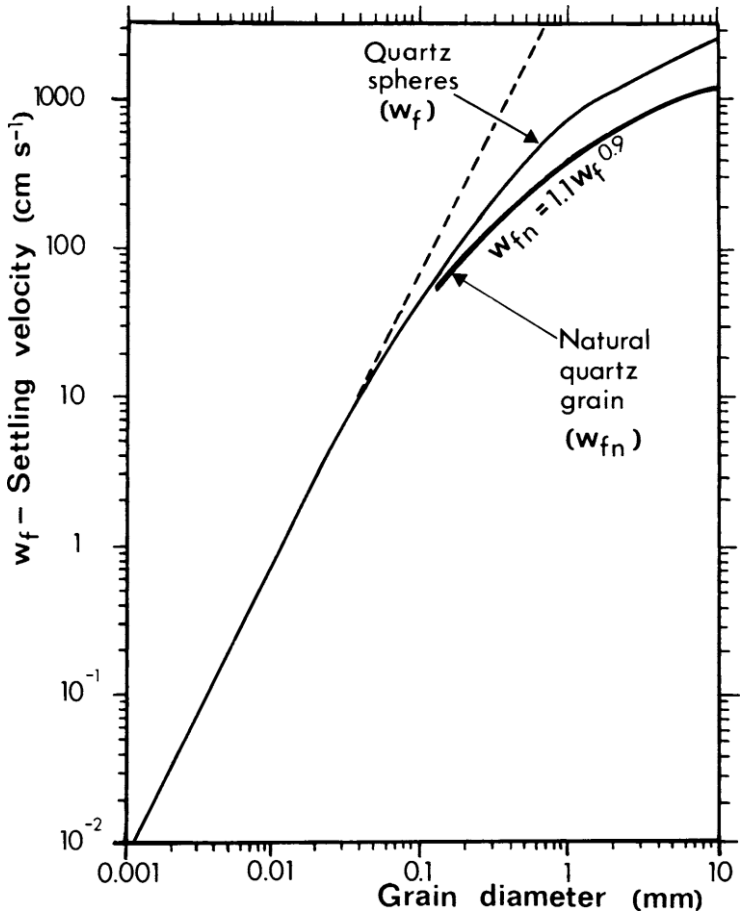

Fig2.4 : observed settling velocities (wfn) of natural quartz grains in air (after Cui et al. 1983) and calculated settling velocities (wf) of quartz spheres (after von Engelhardt 1977). For particles bigger than 0.04 mm, the Stokes' law divergence is shown by the dotted line.

The threshold velocity curve was initially utilized by Hjulstrom in 1935 and 1939 to identify zones where erosion, transportation, and deposition by flowing water predominate. The impact threshold curve may be thought of as the lowest transportation velocity curve.

2.4 Particle Transport by the Wind

2.4.1 Aeolian Transportation Modes

Wind speed and grain size determine several particle transport modalities. Bed load refers to grains that migrate extremely closely to the bed. This mode consists of surface traction, in which grains roll or slide down the surface as a result of direct fluid drag, and saltation, in which grains advance via a series of leaps. Because the grains do not lose touch with the surface, the surface traction load is also sometimes referred to as the contact load. Surface creep (e.g., Greeley & Iversen 1985, p. 293) and reptation are other words used to describe the forward movement of

grains that do not lose contact with the bed or do so only for extremely brief durations.a term derived from the Latin *reptare* to crawl (Haff, cited by Anderson 1987b).

Suspension is a second important form of transport in which particles are lifted off the flow's surface and transported over long distances without making contact with the bed. When the vertical fluctuation velocity component of the flow is greater than the grain's settling velocity (wf), turbulent airflow can hold a grain suspended. The observed settling velocities of natural quartz grains in air and the estimated settling speeds of various-sized quartz spheres.

The distribution of the vertical fluctuating velocity components near the ground is normally distributed in a neutrally stratified atmosphere, where buoyancy effects resulting from thermal differences are unimportant (Sutton 1934; von Kármán 1937); the mean is zero, and the standard deviation is equal to Au, where Au is a constant. As $w^{2}/u_{1.0}$, the average value of A lies within the range of 0.7 and 1.4, with a roughly 1.0 mean value (Lumley & Panofsky 1964, p. 134; Bagnold 1973; Pasquill 1974, p. 77). The susceptibility of a grain to be transported in suspension can be determined by the ratio of wf/u (Francis 1973; Tsoar & Pye 1987).

The boundary at which wf/u = 1 is drawn is arbitrary. The transition between the bed load and the hanging load is gradual rather than abrupt (Nickling 1983). When the vertical velocity components linked to turbulence have little to no impact on particle trajectories, pure bed load transfer occurs. When wf/u 1, this occurs.

When the particle settling velocity is extremely low in comparison to the friction velocity (wf/u 1), pure suspension occurs. Particles move in modified saltation (Hunt & Nalpanis 1985; Nalpanis 1985) when wf/u takes a value close to 1, showing random paths across the flow transition between saltation and suspension. Figure 4.10 displays the theoretically calculated arbitrary border between pure and modified saltation. It roughly relates to wf/u = 1.25, which was identified by Bagnold (1973) as the threshold at which a solid particle is susceptible to suspension.

According to Gillette et al. (1974), wf/u 0.7 might be considered as the maximum value for a pure suspension. The difference between bed load and suspended load, and the distance that particles are transported by the wind, has sedimentological relevance. While particles smaller than 0.1mm, which are transported in suspension, are carried farther and are eventually deposited as loess (Fig. 4.10), and grains larger than 0.3mm move primarily by rolling, they tend to concentrate in residual sand sheets and saltate most easily during typical wind storms, the grains 0.1-0.3mm in diameter that saltate most easily form sand dunes.

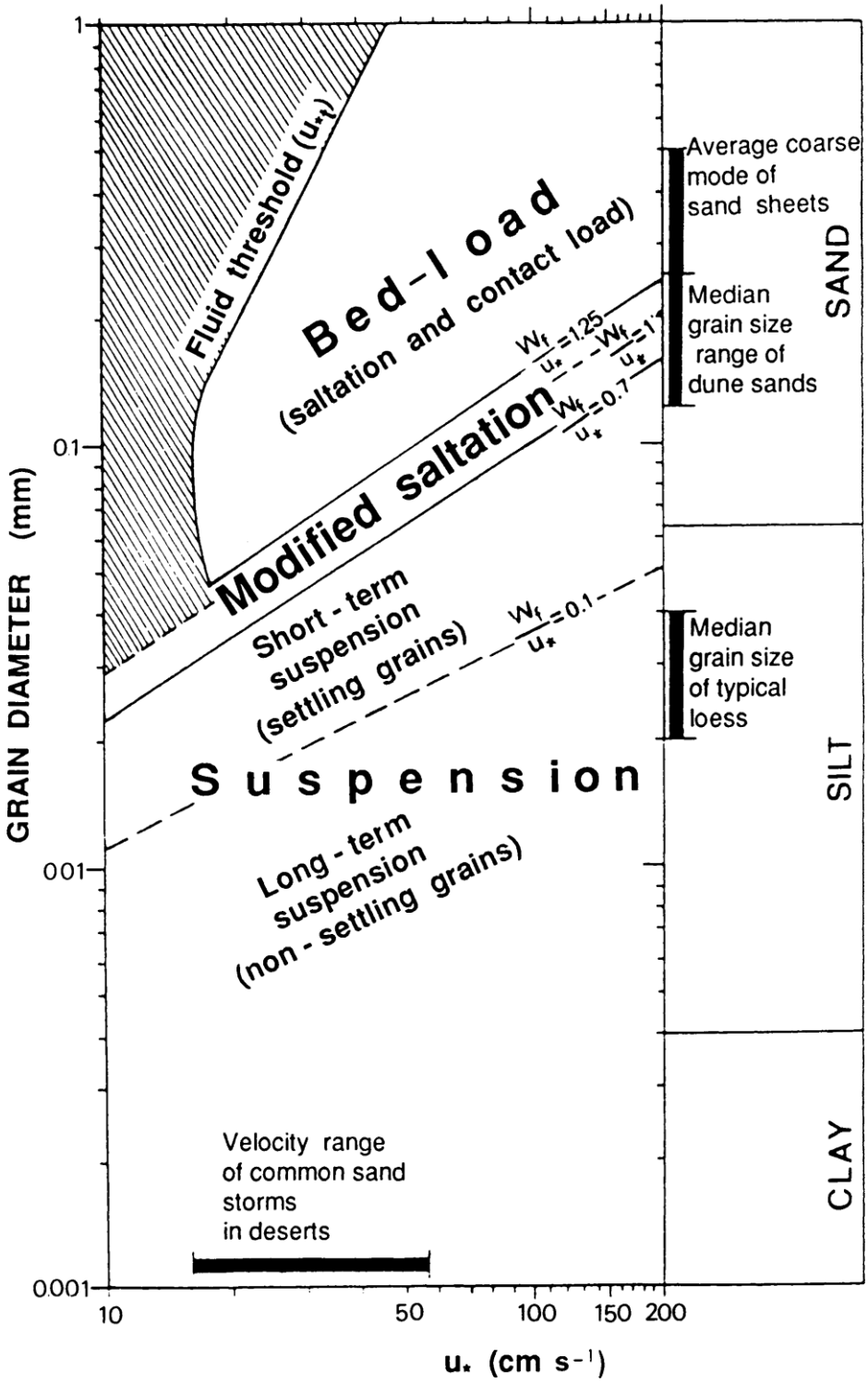

Fig2.5 : transport methods for quartz spheres at various wind shear rates. (Following Tsoar & Pye 1987)

Although aeolian sediments consisting of combinations of these sizes are present in some transitional situations, wind activity is rather successful in separating coarse sand, medium-fine sand, and silt fractions. Since aeolian sediment transport is a stochastic process in which the trajectories of individual grains are affected to varying degrees by random turbulent fluctuations

of the wind and also by considerable natural variability in the nature of grain bed collisions, perfect separation of different sized particles does not occur (Ungar & Haff 1987, Anderson 1987a).

2.4.2 Wind Velocity Profile During Saltation

Sand grains pick up momentum from the wind as they accelerate from rest, modifying the velocity profile close to the ground. depicts the wind profile measurements made by Bagnold (1936) over a homogeneous wet sand surface and again after the sand dried up and became mobile. While wind velocity gradients observed during active sand movement converge at a higher focal point, z, 0.2–0.4 cm above the surface, those measured during stable sand movement converge at a point (z0), just above the ground surface. Many subsequent researchers (Chepil & Milne 1941, Chepil 1945b, Horikawa & Shen 1960, Belly 1964, Hsu 1973, 1974, Vugts & Cannemeijer 1981a, 1981b, Ungar & Haff 1987) have corroborated this impact of shifting sand on the near-bed wind velocity profile.

Bagnold's wind measurements revealed distinct kinks up to a height of 3 cm that correspond to departures from the logarithmic velocity profile law. With increasing friction velocity, the kink's breadth and height grow (also see Zingg 1953a, Gerety & Slingerland 1983). These kinks, according to Bagnold (1941, p. 63), correspond to the mean saltation height of equally sized grains. Since various sizes have distinct typical trajectories, the kink in the velocity curves is difficult to observe for sands with non-uniform particle size. Belly 1964, Walker 1981, Gerety & Slingerland 1983, Ungar & Haff indicate positive departures from the logarithmic velocity profile, whereas others in the measured wind velocity profiles show negative deviations (Bagnold 1936, Horikawa & Shen 1960, Kawamura 1964).
According to Bagnold's (1936) data, at a height of 1 cm, there is a negative kink (lower than predicted velocities), while at a height of less than 0.5 cm, there is a positive deviation (higher velocities). Bagnold proposed that the positive deviations represent the wind being sped up by the accelerating grains shortly before they strike the bed, while the negative deviations roughly correlate to the saltation trajectory height.

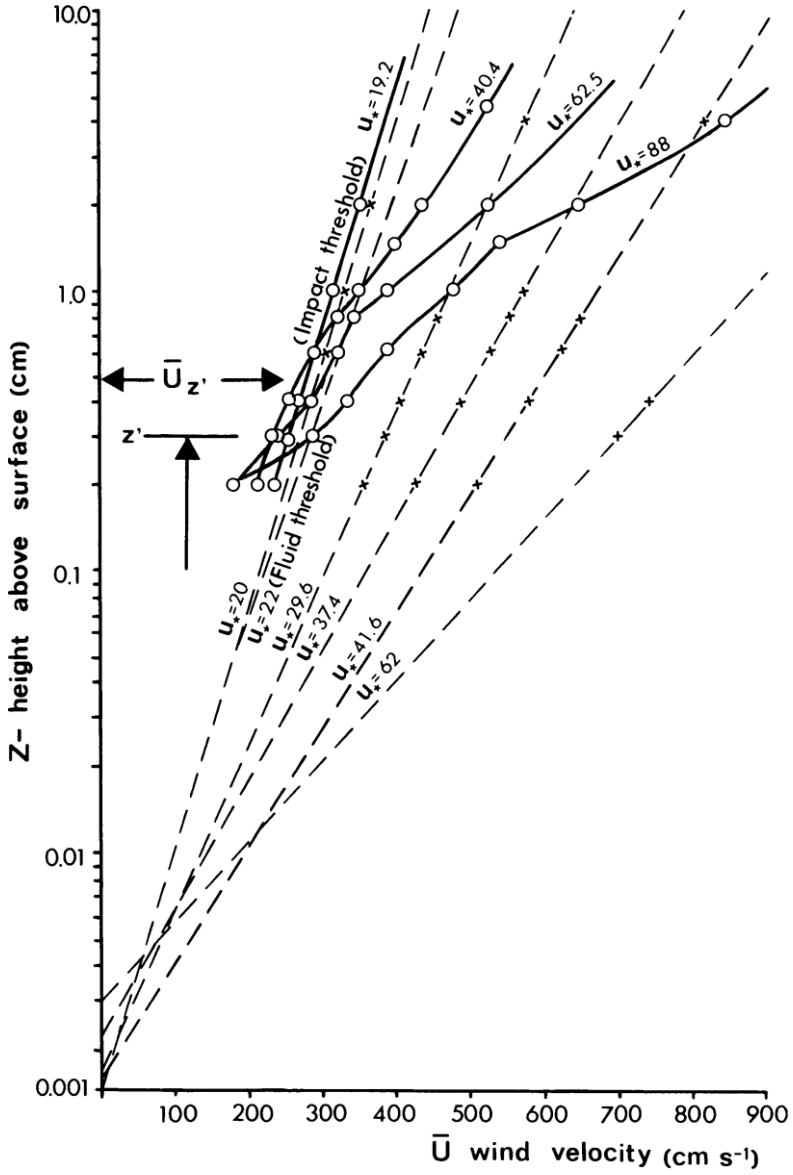

Fig2.6 : Bagnold (1936) measured wind velocity profiles over a homogenous 0.25 mm sand layer with (solid lines) and without (dashed lines) sand movement.

Bagnold (1936) was able to rewrite the logarithmic wind velocity equation for flow over stable surfaces .in a form suited to sand surfaces on which saltation is occurring by ignoring the kinks and fitting straight lines to the velocity profile data via the focal point:

$$\bar{U}(1/k)u*\ln(z/z') + \bar{u}_{z'} \qquad \textbf{(2.6)}$$

where z is the focus point's average height and uz is both the threshold velocity at that height and the mean wind speed at that height. For a particular grain size, it was discovered that these two factors remained constant independent of changes in wind speed. Except for the greatest sand size employed, Zingg (1953a) discovered that the focus point is linked to particle diameter

(d). by Like Bagnold, he discovered that when wind velocity profiles over shifting sand surfaces are plotted with a logarithmic height scale, they do not form a straight line.

$$z' = 10d$$

(2.7)

$$\bar{u}_{z'} = 8889d$$

Close agreement was found when measured drag and computed drag were compared using data from the wind tunnel's measurement of pressure drop (Fig. 4.18, Eq. (4.25)) and straight velocity profile lines (Bagnold 1936).

As u rises, the wind velocity below z actually decreases (Bagnold 1941, p. 60). Chepil & Woodruff (1963) theorized that this was caused by a larger concentration of saltating grains at higher levels of u. This explanation supports Bagnold's (1941, p. 32, 1973) claim that the impact of saltating grains that have been accelerated by wind, rather than direct airflow, is what transfers the entire applied shear stress to grains sitting on the surface. Accordingly, the consistent velocity (uz), which is reached when the sand flow reaches a steady condition, is the speed below the fluid threshold velocity (Bagnold 1973).

By fitting logarithmic law regression lines to velocity data above a presumed focal height, which is thought to reflect a fixed roughness, Gerety (1984, 1985) questioned the accuracy of calculating u for mobile sand surfaces. Gerety examined the experimental wind velocity profile data from numerous studies and came to the conclusion that there are two distinct flow zones: an inner two-phase flow zone near the bed that is 2-3 cm thick, contains a high concentration of saltating grains, and in which the wind profile differs from that predicted by the logarithmic equation and an outer, essentially grain-free zone that abides by the logarithmic law.
The transition (kink) between the two halves of the velocity profiles is frequently gradual. Gerety further emphasized that there is no clearly defined single focal height and that the wind velocity gradients near the bed are not very steep in the data collected by herself, Zingg (1953a), and Chiu (1972). Eq. (4.24) may be expressed as if the saltation layer were an aerodynamic roughness to the flow.

$$U = (1/k)u*\ln(z/h) + \bar{U}_h \qquad \textbf{(2.8)}$$

where U_h is the mean wind speed at the top of the saltation layer and h is the height of the saltation layer, proportional to $u^2/2g$ and independent of particle size. The logarithmic velocity profile can be expressed as follows (Owen 1964):

$$\bar{U}/u* = (1/k)\ln\left(2gz/u*^2\right) + D' \qquad \textbf{(2.9)}$$

Where D is a factor that controls the saltation layer's height's ratio U /u ($2gz/u^2 = 1$). In order to determine D = 9.7, Owen (1964) plotted data for uniform sand (from Bagnold (1936) and Chepil (1945a, 1945b)) and non-uniform soil (from Zingg (1953a). There appears to be a trend for the mean wind velocity to become constant in the saltation layer, where $2gz/u^2$ =0.25. Although it appears to function as a roughness height, the parameter $u^2/2g$ is not a reliable predictor of the height of the saltation layer. Given the vast variety of grain sizes and trajectory heights seen in natural sand, it is difficult to characterize (Gerety, 1984).

2.5 Techniques for Aeolian Research

Only a few of the more significant methods adopted by geomorphologists and sedimentologists may be taken into consideration here since a very wide variety of investigative procedures have been used in aeolian investigations.

2.5.1 Research in Wind Tunnels

Studies conducted in wind tunnels have the significant benefit of enabling tests to be carried out in a controlled laboratory environment. Compared to usual field scenarios, it is simpler to regulate the number of variables functioning at once, and conditions can be maintained long enough for experiments to be completed and repeated. The primary negatives are related to scale issues, however if necessary safeguards are followed, this need not diminish the usefulness of modeling work.

The majority of laboratory wind tunnel studies of aeolian processes have focused on grain-bed interactions, the nature of particle trajectories, and the threshold for particle entrainment (Bagnold 1936, 1937a, White 1985, Iversen & White 1982, Iversen et al. 1987). However,

laboratory wind tunnels have also been used to study airflow over model dunes, the impact of obstructions on sand deposition, and the production of micro-dunes under simulated Yenusian atmospheric conditions (Greeley et al. 1974b, Tsoar 1983b, Tsoar et al. 1985, Greeley et al. 1984).

There have been two different kinds of lab wind tunnels employed. The first is an open-circuit tunnel, which typically consists of three components: a diffuser, a test section, and an entry cone. A fan situated at the diffuser's end draws air in via the bell-shaped opening. As a result, there are less airflow disruptions inside the tunnel, which may be a major issue in tunnels using blower fans (Bagnold 1941, p. 25). The open-circuit tunnel is often kept inside a building since it is susceptible to outside winds.

Fig2.7 : Wind tunnel experiment setup [University of Lethbridge, Canada]

The second kind is a closed-circuit tunnel, which is, as its name suggests, sealed and has an air flow that circulates continually. For example, Kuenen 1960, Seppala & Lindé 1978, Greeley et al. 1984, employed this sort of tunnel mostly for aeolian abrasion studies and simulations of sediment transport at high pressures.

A variety of natural soils and sediments have been studied in open-floored wind tunnels in order to establish threshold velocities and the correlation between shear velocity and particle flux

(Chepil & Milne 1939, 1941, Malina 1941, Zingg 1951, Gillette 1978, Gillette et al. 1980, 1982, Nickling & Gillies 1989). It is crucial to make sure that the wind tunnel's circumstances are an accurate representation of those found in the real world (Cermak, 1971). Therefore, care should be made to guarantee that:

- Any model dune or barrier to the flow has the exact same geometry as the actual.
- The vertical wind velocity profile and degree of turbulence are typical of the flow conditions that occur in nature.
- The test segment is long enough to allow for homogeneous sand transport rates, and all the factors that impact sediment transport are scaled appropriately to preserve dynamic similitude.

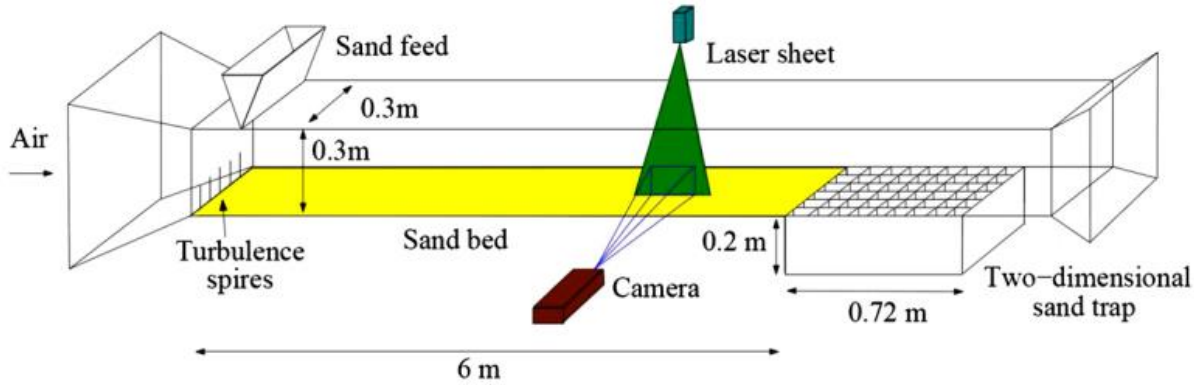

Fig2.8 : Wind tunnel used by Ho et al. For characterizing the saltation transport using Particle Image Velocimetry and sand trap system.

If the tunnel floor is roughened for a significant distance upwind of the test section, a thick boundary layer forms in the wind tunnel naturally. For this, an extremely long wind tunnel with a significant fetch in front of the test portion is necessary. With enough depth, such a naturally formed boundary layer exhibits outstanding agreement with atmospheric data (Cook 1978).

However, a substantial boundary layer may be produced in short wind tunnels by positioning a velocity profile generator upwind of the test area. According to Cowdrey (1967), this may take the form of a grid with smaller openings close to the tunnel's bottom and bigger openings farther

up the wall. As an alternative, a bent wire-mesh screen placed with its vertical edges close to the roof and its horizontal edges close to the ground will accomplish the same thing.

Using longitudinal vortex generators is another technique for artificially regulating the turbulent boundary layer's expansion (Counihan 1969). A long fetch of floor roughness and vortex generators are often used to allow a boundary layer to emerge (Cook 1978). Sand movement simulation does not need exact replication of natural boundary layer conditions, including flow field temperature stratification.

2.6 Needs for Future Research

The physics of aeolian grain transport, interactions between grains and beds, and the emergence of minute bed structures like ripples are now fairly well understood. The geographic distribution and morphological variation of dunes at the regional scale have also been extensively studied using satellite photography and other remote sensing techniques.

However, there are still a lot of questions about how dunes start, develop, and move in harmony with the wind and pattern of sediment movement across them. On various areas of large dunes, very few thorough field studies have been conducted to quantify wind speed and direction, surface shear stress, and rates of sand movement.

The micrometeorological research that has been done to date (e.g., Knott 1979, Tsoar 1978, Lettau & Lettau 1978, Livingstone 1986, Lee 1987, Mulligan 1987, Lancaster 1989b) either refers to relatively small dunes or has been constrained by a lack of suitable instrumentation at an appropriate scale on large dunes. It is thus necessary to do further in-depth research on the spatial variations in shear stress and sand transport rates, both over individual dunes and at the size of dune fields.

Clarification is also needed for the connection between instantaneous turbulent flow velocities and sediment entrainment, as well as for how high-magnitude, low-frequency winds affect dune formation. Numerical modeling approaches have been used more and more often in aeolian investigations during the past five years (Walmsley & Howard 1985; Hunt & Nalpanis 1985; Anderson 1987a, 1987b; Anderson & Hallet 1986; Anderson & Haff 1988; Fisher & Galdies 1988). The knowledge of grain transport and depositional processes across level beds and single simple dunes has already been greatly aided by these investigations. The goal for the future is

to increase the complexity of the terrain and temporal scales that may be modeled, as well as to validate models at all scales using field data.

There is currently a dearth of information on the thickness, mineral make-up, age distribution, and environmental history of the sand deposits in many of the world's main sand seas, notably those in Africa and Central Asia. Therefore, there is an urgent need for further extensive field research that includes geophysical surveys, drilling, and supporting initiatives for sediment analysis and dating. The connections between the creation of sand seas and local tectonic, geological, and climatic changes can only be properly recorded and understood in this way.

If we are to adequately predict the potential effects of greenhouse warming and other future climatic changes, we must determine the relative importance of factors that control the onset of dune activation at the regional scale, such as wind energy, rainfall, and evaporation regime.
To better understand the connections between dune development stages and variations in sea level, sediment availability, and wind and wave conditions in coastal areas, further research is needed. A mix of morpho-stratigraphic and dating research, lab and field tests, and numerical modeling is probably the most effective way to do this. We believe that through serving as a catalyst for more study.

Chapter 3: Modelling with an Eulerian approach

3.1 Overview of Multiphase Modeling

Using distinct formulations for each phase is frequently necessary when numerically simulating a multiphase flow. Let's define the continuous phase as the liquid in which these particles are typically submerged and the particulate phase as the phase made up of bubbles, particles, or droplets. The continuous fluid can be either a liquid or a gas, whereas the particles can be solid, liquid, or gas. Determine the proper numerical algorithms by classifying the nature of multiphase flow using the interaction between particle motion and its surroundings.

Dispersed and dense flows are categorized in the widest sense according to which coupling mechanism largely controls particle motion. When the influence of particle-fluid interactions predominates in the overall movement of the particles, as seen in Figure 3.1, a multiphase flow can be said to be dispersed. In general, drag forces present in particle-fluid interactions limit

the relative velocity of the particles, leading to a tendency for particle trajectories to resemblecontinuous fluid trajectories.

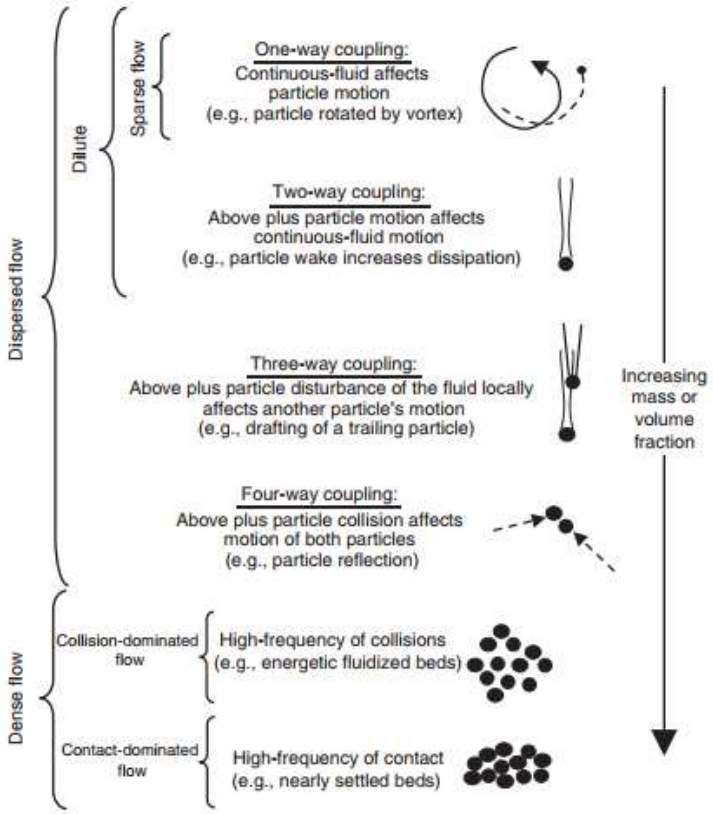

Fig3.1 : Depending on different interphase and intraphase interaction, there might be diluted, scattered, or concentrated flow conditions.

The flow can be characterized as dense when particle-particle motion predominates. Particle-particle interactions can refer to two distinct mechanisms: particle-particle collisions (where the particles can bounce, break up, or flow together by hitting each other), and particle-particle fluid dynamics interactions (where the proximity of the particle increases the forces affecting the fluid dynamics). The most common types of coupling are one-way coupling, which occurs when the motion of the dispersed phase is affected by the continuous phase but not the other way around, two-way coupling. which occurs when the dispersed phase also influences the continuous phase through interphase coupling, such as drag force, three-way coupling, which occurs when particle wakes and other continuous phase perturbations affect the motion of other particle interactions, and four-way coupling. which occurs when collisions and other particle-particle interactions

Although in some circumstances (such as granular flows), the effects of the particles on the continuous fluid are minor and frequently ignored, dense flows are typically regarded as having four-way coupling.

3.2 Modeling the Particle-Fluid field

Each single-phase zone in a multiphase flow system is bordered by a moving interface. Dispersed multiphase flows are the only ones included in this description. For stratified flows, a simpler theory can be used, although this is outside the purview of this paper. In theory, the instantaneous local variables related to each phase and the necessary boundary conditions at all phase interfaces might be used to create a multiphase flow model. In real-world situations, it is difficult to derive a solution from this statement. It can, however, be utilized as a starting point for the development of macroscopic equations that substitute a collective description of the phases for the instantaneous local descriptions of each phase.

The intuition and postulation of balancing equations served as the foundation for the first systems of equations for multiphase flows. The formulae used now are based on averaging techniques that were developed theoretically. Averaging techniques may be categorized into three primary categories, namely Euler's averaging, Lagrange's averaging, and Boltzmann's averaging (Ishii 1975), depending on the fundamental physical principles employed to design multiphase flow. Based on the variable used to create a mathematical operator or averaging, such as B. spatial, temporal, statistical, and overall averaging, these categories can be further divided into subgroups. Volume, area, or line averaging are all forms of spatial averaging that can be either local or macroscopic.

On the basis of the Boltzmann equation of the distribution function for a single particle, the kinetic theory of the gas-particle system may be thought of as the kinetic gas theory (Ahmadi & Ma 1990; Ding & Gidaspow 1990). For the gas, a molecular distribution function is specified, and for the particles, a different distribution function. The size distribution, other physical characteristics of the solid particles, and the collision processes of the solid particles with one another and with the gas molecules are difficult to describe in the theory of gas-particle systems. This method allows for the derivation of the continuity equation, momentum equation, and equation for the fluctuating kinetic energy of the solid phase.

Simple methods are used to get the constituent laws for the stress term and the energy flow term. The pseudothermal energy balance is another name for the fluctuating kinetic energy equation, and the fluctuating kinetic energy (multiplied by 2/3) is referred to as the granule

temperature. The liquid phase is treated as a continuum in the Lagrangian technique, and time averaging is done by following a specific solid particle and measuring at a certain time interval. The particle equation of motion is used to compute particle trajectories. When simulating a single particle's or a diluted suspension's dynamics, lagrangian methods are particularly well-liked. Denser flows were added to the approach (Yonemura et al. 1993).

Then, using the Monte Carlo approach, the computational particles are allowed to collide. Each computational particle represents a collection of actual particles. The particle phase is also handled as a continuum in Euler's method. The derivation of the field equations, the constitutive equations, and the boundary surface conditions make up the three main components of Euler's formulation. The conservation rules z. B. for momentum and mass are given by the field equations. By taking into account the structure of the flow field and material attributes through experimental correlations, the constitutive rules solve the system of equations. The spatial coordinate system is used to calculate the spatial, statistical, or temporal averages in Euler's averaging. Due to its strong ties to, at least in the past, Euler's method, group averaging for multiphase flows was the most popular.

In classical mixture theory, a different approach is used (Bowen 1976; Johnson et al. 1991; Joseph et al. 1990). The continuum mechanics concepts for a single phase are generalized in this method to numerous interpenetrable continua. The fundamental premise is that at any material point, all phases are present at all times. The conservation of mass and momentum is predicated on the balancing equations. The mixture theory also needs constitutive rules in order to finish the system of equations, much as other models. For multiphase flows, there is a wide variety of software.

The majority of widely used commercial flow simulation codes now include multiphase flow models. A collection of computer programs has also been created for certain multiphase flows. Nuclear power plant safety analysis and fluidized bed technology are two such fields where multiphase models have been created. Boltzmann, Lagrange, and Euler techniques have all been used to provide qualitatively plausible behavior for specific events, such as clustering and bubbling in fluidized beds (Tsuo & Gidaspow 1990; Tsuji et al. 1993; Ding & Gidaspow 1990). 1:1 scale simulations produced less encouraging results.

There are essentially three ways to simulate the particle flow field, but quantitatively good results have been obtained by fitting the termination relationship parameters to a particular process. a method for tracking specific particles or samples of particles. The Lagrangian method

is this. Another method is to use continuum-like equations to consider the particles as a cloud. Euler's strategy is as follows. Another strategy is to characterize the particle flow characteristics using particle distribution functions (PDF method).

3.3 Lagrangian Approach

Both diluted and dense flows are suitable for the Lagrangian method. Particle-fluid interaction, body forces, and particle-wall collisions govern the movement of the particles in diluted flows because the interval between particle-particle collisions is larger than the particle (or droplet) reaction time. The particle-particle interaction not only regulates the dynamics of the particles but is also impacted by the hydrodynamic and body forces as well as the particle wall interaction in a dense-phase flow because the reaction time of the particles is longer than the period between collisions. The trajectory technique (Crowe et al., 1977), a variant of the Lagrangian methodology, is simple to use when the flow is smooth and diluted. In an unstable and dense flow.

3.3.1 Trajectory Method

The easiest way to demonstrate the trajectory technique is through an illustration. Consider a nozzle that continuously squirts a liquid into the chamber.

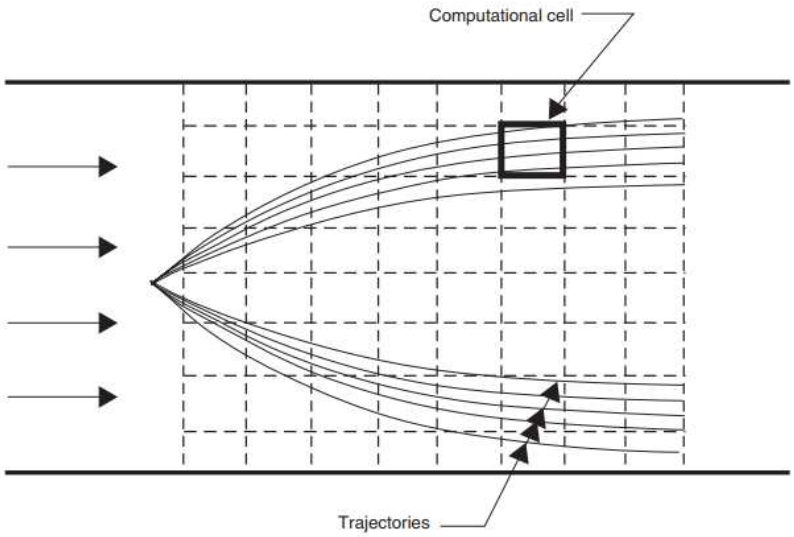

Fig3.2 : Droplet trajectories in a spray.

Assume that the flow is stationary and that the carrier flow's spatial distribution is time-invariant. As depicted, the flow field is split up into a number of computational cells. A number

of launch trajectories are created using the discretized input flow. By resolving the droplet motion equation in the flow field and knowing the initial droplet velocity and mass, the droplet velocity can be computed.

$$\frac{dv}{dt} = \frac{F_f}{m} + g \qquad \textbf{(3.1)}$$

Where g is the gravitational vector and Ff are the fluid forces (forming and frictional forces) acting on the mass-m drop. The course is derived from

$$\frac{dx_p}{dt} = v \qquad \textbf{(3.2)}$$

xp is the droplet location, where. The desired accuracy and processing efficiency will determine the integration strategy to be used. The droplet temperature curve can also be computed as follows:

$$\frac{dT_d}{dt} = \frac{1}{mc_d}(\dot{Q}_d + \dot{m}h_L) \qquad \textbf{(3.3)}$$

Where Q.d represents the total amount of radiative and convective heat transmission to the particle or droplet. This equation has to be changed if the drop's Biot number is high to account for the fact that the surface temperature is not the drop's mean temperature. Additionally, the mass transfer of the drop has to be estimated along the trajectory using the formulas. Naturally, the droplet diameter must be altered to match the droplet mass unless the application involves drying a porous particle. Assume that the nebulizer's mass flow is discretized into j paths, with M(J) serving as the mass flow for each. Next, the trajectory's j flow rate of numbers

$$\dot{n}(j) = \frac{\dot{M}(j)}{(\pi/6)\rho_d d_0^3} \qquad \textbf{(3.4)}$$

where d0 is the starting drop diameter and d is the material density of the drop. The flow rate number remains constant along each route if there is no droplet breaking apart or consolidating.

Of course, discretizing the initial circumstances in accordance with a size distribution allows for the addition of further detail. For instance, the number flow rate associated with amount Ds would be on the trajectory j if fm(Ds) is the percentage of particle mass associated with quantity Ds.

$$\dot{n}(j, D_s) = \frac{\tilde{f}_m(D_s)\dot{M}(j)}{(\pi/6)\rho_d D_s^3} \qquad \textbf{(3.5)}$$

It goes without saying that additional detail necessitates more trajectories and longer calculation times. In an axisymmetric flow, the mass flow rate on each ring must be weighted with the ring radius if the start sites are discretized into a sequence of concentric rings. The characteristics of the particle cloud may be determined in each computing cell once all trajectories have been computed. To calculate the particle number density, use:

$$n = \frac{\sum_{traj} \dot{n}\Delta t_j}{V} \qquad \textbf{(3.6)}$$

Where V is the volume of the computational cell and tj is the amount of time it takes a particle traveling along trajectory j to traverse the cell. All trajectories that intersect the cell are included in the calculation. This allows one to calculate the particle volume fraction in each computing cell.

$$\alpha_d = \frac{\sum_{traj} \dot{n}_j \bar{V}_d \Delta t_j}{V} \qquad \textbf{(3.7)}$$

The average droplet volume along trajectory j in the cell is represented by Vd. The same method may be used to determine other characteristics including temperature, particle velocity, and bulk density. Thus, when all trajectories have been computed, the cloud's characteristics may be discovered. By continuing the trajectory after the wall impact, particle or droplet wall collisions are taken into account in the computation. Different collision types result in different speeds. When a drop hits the surface, it may splatter onto it, ending the trajectory or causing it to be resumed with smaller droplets. Re-entrainment in the case of annular mist flows would be modeled by initializing droplet trajectory from the liquid layer at the wall.

3.4 Discrete Element Method

The more comprehensive discrete element technique is necessary when the flow is turbulent and dense (significant particle-particle collisions). In this method, individual particles or representative particles have their velocity and position—as well as other properties—tracked throughout time. Although tracking every particle would be ideal, it may not be computationally possible. The magnitude would be 109 particles/m3 for a gas filled with 100 m particles at a mass concentration of one. 108 particles would need to be followed through the flow field if it were one-tenth of a cubic meter. Since this is not feasible, the real particles are represented by a lesser number of computational particles.

Each computing particle would represent 104 physical particles, for instance, if 104 computational particles were chosen. It is thought of as a collection of particles in terms of computation. The particle bunch is then supposed to pass through the field at the same temperature and speed as a single particle (physical particle). Of course, by specifying packets with a specific particle size, size distribution effects may be taken into account. As a separate element, the packet is recognized. The dynamics of each individual particle must be taken into account because in some simulations, such as those of B. fluidized beds, it may not be viable to employ particle packs without compromising the details required to mimic the system.The particle motion equation now takes the following shape:

$$\frac{dv}{dt} = \frac{F_f + F_c}{m} + g \qquad \textbf{(3.8)}$$

The force that results from particle-particle (and particle-wall) interaction is designated as Fc. The challenge will determine how to define the discrete elements' beginning circumstances. A packet for droplets that appear along a runway j at a time interval tp. Therefore, Np n (j,ds) tp would be the total number of droplets in the packet, and other pieces of information would be used to estimate the beginning velocity. When simulating a fluidized bed, the starting state can be a packed bed with all the particles at rest, with the motion being started by the interstitial gas flow. By integrating the particle's equation of motion, one may determine each packet's motion over a given period of time. The particle's temperature, spin, and other characteristics can all change concurrently.

During the time step, particle collisions may take place, changing trajectories and the distribution of packets in each computing cell. By adding together all the particles in one

computation container, the characteristics of the droplet cloud at each time step may be calculated. As an illustration, consider the number density:

$$n = \frac{\sum_p N_p}{V} \qquad \textbf{(3.9)}$$

when all of the packages in the computational cell are added together. Additionally, the particle volume fraction is:

$$\alpha_{\mathrm{d}} = \frac{\sum_p N_p V_{\mathrm{d},p}}{V} \qquad \textbf{(3.10)}$$

where Np is the number of particles in the cluster p, and Vd,p is the volume of a single particle. It is simple to calculate other characteristics like bulk density and particle speed. The determination of the interstitial flow field depends on the distribution of solid phase volume fractions. Assuming that each discrete element is a single particle, Np in the aforementioned equations equals 1.

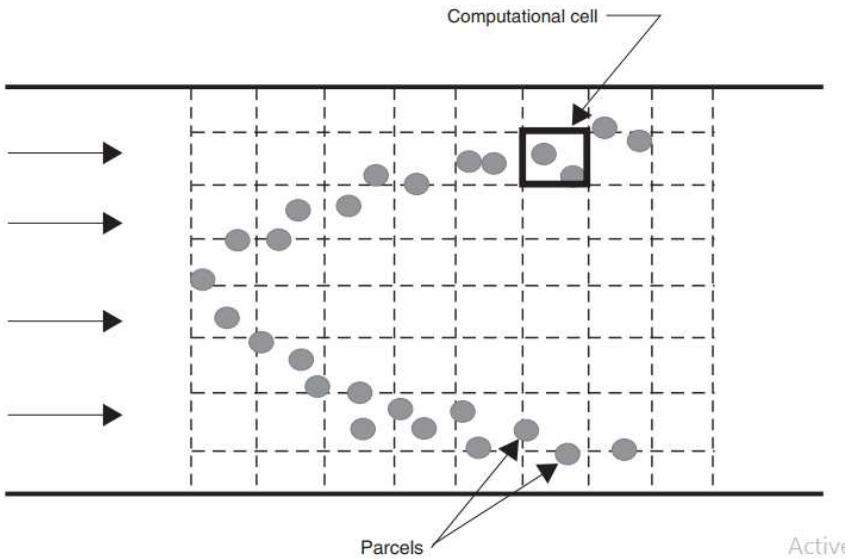

Fig3.3 : Droplet parcel distribution in a spray field

3.5 PDF Models

The study of stochastic systems' behavior has shown to be particularly beneficial when using the PDF technique. Examples of its use may be found in the kinetic theory of gases (Chapman and Cowling, 1952) and the study of Brownian motion (Chandrasekhar, 1943). More recently, Pope and others have utilized it extensively to describe turbulence as well as turbulence-related processes including combustion and air dispersion (Pope, 1991; MacInnes and Bracco, 1992). This section describes the use of PDF techniques, which may be seen as a rational method, to model the behavior of a particle-laden turbulent gas, similar to how kinetic theory models gas flows. This indicates that there is initially a fundamental equation (master equation) whose elements may be logically linked to the fundamental equations of motion of the individual particles. Second, while maintaining the natural boundary conditions at the wall (the so-called near-wall behavior), this primary equation may be employed in a strictly formal manner to derive both the continuum equations and constitutive relationships of a gaseous or dispersed phase of particles. The primary equation in kinetic theory is the well-known Maxwell-Boltzmann equation; in dispersed flows, it is referred to as the PDF equation.

There are two versions of the PDF equation in use right now. The probability density that a particle will have a specific velocity and location at a specific time is referred to as PDF in the first form, much like in kinetic theory. The kinetic method (KM) is the name given to this PDF strategy. Developed by a variety of collaborators after being started by Buyevich (1971, 1972a, 1972b), most notably Reeks (1980, 1991, 1993), Hyland et al. (1999a, 1999b), Swailes and Darbyshire (1997), Derevich and Zaichik (1988), Zaichik (1991), Pozorski and Minier (1998), and Zhou and Li (1996). The PDF technique has only been used with inert, non-reactive particles in all of these breakthroughs.

In more recent times, reactive particles that are condensing or evaporating in a turbulent gas have also been included in this strategy (Pandya and Mashayek, 2001, 2003) and polydisperse combustion sprays (Laurent and Massot, 2001). The second variant of the PDF equation, initially put out by Simonin et al. (1993), is a more comprehensive PDF that also takes into account particle location and velocity as well as the velocity of the local carrier flow as a phase space variable. It is a development of the PDF strategy employed by Haworth and Pope (1986) and is based on the generalized Langevin model (GLM) for the particle's meeting with the equation of motion of the carrier flow. Here, it is referred to as the GLM strategy.

3.5.1 PDFs Equations

Consider the motion of evaporating or condensing particles in a diluted mixture without particle collisions as an illustration of how PDFs and their equations are created. Let X(t) be a single particle's phase space vector at time t as it travels through phase space. in this instance:

$$\mathbf{X} = [m, \Theta, \mathbf{v}, \mathbf{x}] \tag{3.11}$$

where v, x are the particle's velocity and location at time t, and m is the particle's mass, temperature, and temperature. Thus, independent variables are required to define the phase space dimension. The number of particles in an elementary volume dnX of the phase space located at X is given by W(X,t)dnX for a single realization of the underlying carrier flow velocity field u(x,t) and temperature field T(x,t), where W(X,t) is the phase space density, i.e. H. the number of particles per unit volume in phase space. As a result, one must have the following to prove the conservation of particle number within this elementary volume at X with respect to W:

$$\frac{\partial W}{\partial t} + \frac{\partial}{\partial \mathbf{X}}[W\dot{\mathbf{X}}] = 0 \tag{3.12}$$

For the evaporating droplet example, one would have explicitly:

$$\dot{\mathbf{X}} = [\dot{m}, \dot{\Theta}, \dot{v}, \dot{\mathbf{x}}] \tag{3.13}$$

where the elements of X. arise from the mass, momentum, and energy conservation equations for a single particle droplet and reflect the particle equations of motion in the broadest sense. However, because of the turbulent nature of the underlying carrier flow field and the random nature of X, one can only ever properly refer to the PDF corresponding to a particular set of X values. The total average of W over all system realizations is used to symbolize this as W. The conservation equation (Liouville's equation) for W may be averaged out to find the equation for W (the PDF equation). In order to keep things simple, the instantaneous components of X are divided into their mean X and fluctuating components X.

$$\frac{\partial\langle W\rangle}{\partial t}+\left(\frac{\partial}{\partial m}\langle\dot{m}\rangle+\frac{\partial}{\partial\Theta}\langle\dot{\Theta}\rangle+\frac{\partial}{\partial\mathbf{x}}\cdot\mathbf{v}+\frac{\partial}{\partial\mathbf{v}}\cdot\langle\dot{\mathbf{v}}\rangle\right)\langle W\rangle$$
$$=-\frac{\partial}{\partial m}\langle\dot{m}'W\rangle-\frac{\partial}{\partial\Theta}\langle\dot{\Theta}'W\rangle-\frac{\partial}{\partial\mathbf{v}}\cdot\langle\dot{\mathbf{v}}'W\rangle \qquad \textbf{(3.14)}$$

When the convective component (transport without turbulence) is found on the LHS and the dispersive component (gradients of the net fluxes as a result of turbulence) is found on the RHS. The turbulent fluxes must be connected, either directly or indirectly, to W and its derivatives in order to solve the equation. The most crucial component of the PDF technique is hence the closure problem, which has to be solved.Consider the scenario of the evaporating droplet in more detail to show how the values of X. rely on the characteristics of the particle and the underlying carrier flow. The general connection is derived from the mass conservation of a spherical droplet of diameter dp evaporating in a gas of mass density g.

$$\dot{m}=\pi\rho_g d_p D_v Sh(Re_p, S_c)\ln\left[\frac{1-\alpha_v}{1-\alpha_{vs}}\right] \qquad \textbf{(3.15)}$$

Where m is the mass fraction of vapor emitted by the particle in the locally undisturbed gas flow in comparison to the (saturated) vapor mass fraction at the droplet (or particle) surface, which is assumed to be in equilibrium with the particle and thus directly depends on the temperature of the particle, Dv is the vapor's molecular diffusion coefficient, and Sh is the droplet's Sherwood number for the mass transfer of vapor into or out of the droplet, which is

$$Re_p=\frac{d_p|\mathbf{v}-\mathbf{u}|}{\nu_g},\quad Sc=\frac{D_v}{\nu_g} \qquad \textbf{(3.16)}$$

where vg is the gas's kinematic viscosity. The local particle Reynolds number also affects variations in particle-droplet velocity and temperature. The motion equations are all interdependent and dependent on the instantaneous particle Reynolds number, which is dependent on the relative velocity between the particle and the locally undisturbed gas.

3.6 Eulerian Approach

Euler's method treats the collection of particles or droplets as a continuous medium with characteristics similar to those of a liquid. One example of a continuous attribute is the bulk density, or the mass of the particles per unit volume of the mixture. The average velocity over an averaging volume is known as particle velocity. The development and presentation of the governing equations for Euler's method are the goals of this section. The application of Eulerian's technique to the scattered phase is sometimes referred to as the two-fluid or Eulerian Eulerian approach since the continuous phase is a fluid. Here, the phrases are used interchangeably. Since the equations for both phases have the same form in Euler's method, the same methods may be used to solve both.

Euler's method may be described on several levels. The particle and carrier liquid have the same velocity when the Stokes number is low enough (velocity equilibrium). A low Stokes number indicates that the particles are moving and dispersing at the same speed as the carrier flow if the characteristic time employed in the determination of the Stokes number is a time reflective of carrier phase turbulence. The two-phase mixture in this situation may be thought of as a single phase with modified attributes (density, heat capacity, etc.).

A lower Stokes number indicates that the particles are travelling with the mean velocity of the carrier flow but may not disperse at the same pace owing to turbulence if the Stokes number is based on a characteristic time of the flow field. The circumstance where the carrier fluid and particle velocities are not equal is of more practical importance. This could be brought on by body forces acting on the particles, turbulent fluctuations, and velocity gradients in the mean flow field. The mean particle velocity in an averaging volume is assumed to be the local particle velocity:

$$\{\mathrm{v}\} = \frac{\sum_k \mathrm{v}_k}{N} \qquad \textbf{(3.17)}$$

N is the volume's total number of particles, and the symbol for volume averaging is. Alternatively, the mass-averaged velocity is defined by:

$$\tilde{v} = \frac{\sum_k m_k v_k}{\sum_k m_k} \qquad (3.18)$$

Where, in the average volume, mk denotes the mass of particle k. Favreaveraging is the name given to this sort of averaging. The single particle (or droplet) conservation equations are added across all the particles in the control volume to get the equations for a particle cloud, from which Euler's dispersed phase equations are derived. depicts a cloud of atoms or droplets in a Cartesian control container. The property flow over all surfaces is taken into consideration while deriving the basic finite difference equations. The limit is then determined by dividing the finite difference equations by the control volume as the volume gets closer to the limit. Crowe et al. (1998) provide more details. The entire time, index notation is employed.

3.6.1 Equation of Continuity:

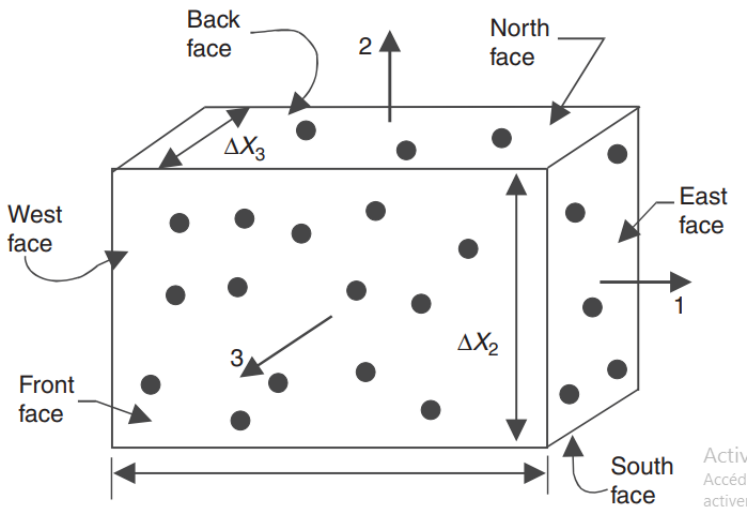

Fig3.4 : Dispersed-phase element regulate volume in three dimensions.

Any scattered phase element's fundamental continuity equation is dm/dtm. Calculating the net droplet mass outflow through the control surfaces while adding the rates of mass change of all the components in the calculation cell results in:

$$\frac{\partial}{\partial t}(\alpha_d \rho_d) + \frac{\partial}{\partial x_i}(\alpha_d \rho_d \tilde{v}_i) = \sum_k \dot{m}_k / V \qquad (3.19)$$

where d represents the dispersed phase's volume proportion, vi represents the mass average velocity of the dispersed phase, and vi represents the material density of the dispersed phase. All of the droplets in the control volume V are summed. The scattered phase's mass source term, also known as S-mass, is the final term in the equation. Smass, the mass swell term for the continuous phase, is negative for the dispersion phase, thus the minus sign. The continuity equation must be written differently if the mass-average speed is substituted for the basic mean speed. The velocity in the average volume is represented in this instance as:

$$v_i = \{v_i\} + v_i' \qquad \textbf{(3.20)}$$

Where vii is the velocity's divergence from the average. The bulk density ρ_d, is also written as

$$\overline{\rho}_{\mathrm{d}} = \overline{\rho}_{\mathrm{d},0} + \overline{\rho}'_{\mathrm{d}} \qquad \textbf{(3.21)}$$

The average mass flux is where d,0 is the bulk density at the center location and d is the variance in bulk density at neighboring places.

$$\langle \overline{\rho}_{\mathrm{d}} v_i \rangle = \langle \overline{\rho}_{\mathrm{d}} \rangle \langle v_i \rangle + \langle \overline{\rho}'_{\mathrm{d}} v_i' \rangle \qquad \textbf{(3.22)}$$

You may think of the extra phrase as a term for mass diffusion. This factor would be 0 in a flow with homogenous particle velocities or homogeneous bulk density. In inhomogeneous particle density fields, turbulence will produce a variety of particle velocities that will result in a net mass flux. The two-fluid formulation simulates the dispersion of particles in turbulent flows using the gradient transport model. Assumed in relation to Fick's law is that:

$$\langle \widetilde{\rho}_{\mathrm{d}} v_i' \rangle = -D_{\mathrm{d}} \frac{\partial \overline{\rho}_{\mathrm{d}}}{\partial x_i} \qquad \textbf{(3.23)}$$

where Dd is the phase's dispersion coefficient. It is necessary to conduct experiments or use auxiliary analysis to ascertain the dispersion coefficient's value. A dispersion coefficient was anticipated by Picard et al. (1986) using Tchen's (1949) early study of particle motion in turbulence as a basis. To take into consideration the consequences of crossing trajectories, adjustments are required. Semi-empirical correlation was proposed by Picard et al. and used by

Rizk and Elghobashi in 1989. Finding or decreasing a number from an experiment that is thought to be indicative of the flow field being simulated is necessary since, regrettably, there are no straightforward analyses or models that offer Dd as a function of particle characteristics and flow turbulence. Reeks has shown using the PDF strategy.

The boundary conditions provide another issue. It makes sense to set the bulk density gradient perpendicular to the wall to zero if the particles reflect specularly off the wall. Another estimate must be used if the impingement is non-specular. The zeroing of the bulk density at the wall does not reflect a realistic boundary condition for the bulk density field if drops happen on the wall and there is no re-entrainment. focuses on choosing appropriate boundary conditions for flawlessly reflecting and absorbing walls. The two-fluid continuity equation with volume-average velocity has the following final form:

$$\frac{\partial}{\partial t}(\alpha_d \rho_d) + \frac{\partial}{\partial x_i}(\alpha_d \rho_d \{v_i\}) = \frac{\partial}{\partial x_i}\left(D_d \frac{\partial \overline{\rho}_d}{\partial x_i}\right) - S_{mass} \qquad \textbf{(3.24)}$$

Use of F_{avre} (mass averaging) eliminates the diffusion term.

3.6.2 Equation of Momentum

An individual mass m dispersed-phase element's momentum equation is:

$$m\frac{dv_i}{dt} = F_i + mg_i \qquad \textbf{(3.25)}$$

The mass must be removed from the surface uniformly for this equation to apply to a responding droplet. In other words, it doesn't help the droplet's motion. M. vi is added to either side to produce

$$\frac{dmv_i}{dt} = \dot{m}v_i + F_i + mg_i \qquad \textbf{(3.26)}$$

The forces on the element are as follows:

$$F_i = -V_d\frac{\partial\{p_c\}}{\partial x_i} + V_d\frac{\partial\{\tau_{c,ij}\}}{\partial x_j} + L_i \qquad \textbf{(3.27)}$$

where pc and c,ij represent the continuous phase's average compressive and shear stresses, respectively. All additional forces, such as the buoyancy force, steady-state drag, virtual inertia force, and Basset force are included in the force Li. The only drag that may be significant in flows containing heavy particles is the steady-state drag. Another method for creating the momentum equation is to add up all of the dispersion phase elements in the computational cell. The differential equation that results is:

$$\frac{\partial}{\partial t}(\alpha_{\mathrm{d}}\rho_{\mathrm{d}}\widetilde{v}_i) + \frac{\partial}{\partial x_j}(\alpha_{\mathrm{d}}\rho_{\mathrm{d}}\widetilde{v}_i\widetilde{v}_j) = \sum_k \dot{m}_k v_{i,k}/V - \alpha_{\mathrm{d}}\frac{\partial p}{\partial x_j}$$

$$\alpha_{\mathrm{d}}\frac{\partial}{\partial x_i}\tau_{ij} + \sum_k L_{i,k} + \alpha_{\mathrm{d}}\rho_{\mathrm{d}}g_i - \alpha_{\mathrm{d}}\frac{\partial}{\partial x_j}\left(\sum_k \overline{\rho}_{\mathrm{d},k}v'_i v'_{k,j}\right) \qquad \textbf{(3.28)}$$

where vi is both the fluctuation velocity and the mass-average velocity. vi,k is the difference between the mass-average velocity and the velocity of the kth particle. The momentum source through mass exchange across the phases is represented by the first component on the right side of Eq. (3.15). This phrase is written as:

$$-\sum_k \dot{m}_k v_{\mathrm{i},k}/V = -S_{\mathrm{mom},i} \qquad \textbf{(3.29)}$$

This phrase describes the momentum connected to the mass emitted by the droplet surfaces as they move at a velocity of Vi,k. In order to designate the momentum addition to the carrier phase as positive, the negative sign is selected. The last term, which is known as the scattered phase's Reynolds stress, is equivalent to a Reynolds stress.

$$\tau^{\mathrm{R}}_{\mathrm{d},ij} = -\sum_k \overline{\rho}_{\mathrm{d},k}v'_{k,i}v'_{k,j} \qquad \textbf{(3.30)}$$

Because mass-average velocity is not the same as momentum-average velocity, this word is necessary. Traditionally, the Boussinesq approach (stress proportional to strain rate) has been used to estimate the Reynolds stress in the dispersal phase:

$$\tau^{R}_{ij} = \mu_{\mathrm{s}}\left(\frac{\partial v_i}{\partial x_j} + \frac{\partial v_j}{\partial x_i}\right) - \frac{2}{3}\mu_{\mathrm{s}}\frac{\partial v_k}{\partial x_k}\delta_{ij} \qquad \textbf{(3.31)}$$

where the solid viscosity is s. Because particle velocity changes rely on particle characteristics and particle history in addition to local turbulence, selecting a solid viscosity is highly challenging. According to a Stokes number-dependent function based on the integral time scale

of the carrier phase turbulence, Chung et al. (1986) connected the solid viscosity to the eddy viscosity of the carrier liquid. Simply put, Rizk and Elghobashi (1989) employed a constant ratio for the relationship between the solid and liquid eddy viscosities.

Since turbulent particle fluctuations lead to a non-zero value for the Reynolds stress in the dispersed phase, the Boussinesq approximation has the drawback of allowing one to see a Reynolds stress without a gradient in the mean velocity field (no strain rate). In a bubble field, the momentum equation, Eq. (13.158), also holds true. The Reynolds stress term and changes in bubble velocity are connected in a similar manner. In Zhang and Prosperetti (1997), a comparable version of the distributed phase momentum equation is offered. The momentum equation gets simpler if the forces acting on the particles or droplets are merely the drag forces and the unsteady elements may be ignored.

$$\frac{\partial}{\partial t}(\alpha_{\mathrm{d}}\rho_{\mathrm{d}}\tilde{v}_i) + \frac{\partial}{\partial x_j}(\alpha_{\mathrm{d}}\rho_{\mathrm{d}}\tilde{v}_i\tilde{v}_j) = -\alpha_{\mathrm{d}}\frac{\partial p}{\partial x_i} - S_{mom,i} + \alpha_{\mathrm{d}}\frac{\partial}{\partial x_j}(\tau_{ij}) + \frac{3\pi\mu_c}{V}\sum_k d_k f_k (u_i - v_i)_k + \alpha_{\mathrm{d}}\rho_{\mathrm{d}}g_i + \alpha_{\mathrm{d}}\frac{\partial}{\partial x_j}\tau^{\mathrm{R}}_{\mathrm{d},ij} \tag{3.32}$$

Where k is the ratio of drag to Stokes drag, mk is the mass of the particle k, and V is the velocity response time. The momentum equation is reduced to if each droplet has the same mass and evaporates at the same pace.

$$\frac{\partial}{\partial t}(\alpha_{\mathrm{d}}\rho_{\mathrm{d}}v_i) + \frac{\partial}{\partial x_j}(\alpha_{\mathrm{d}}\rho_{\mathrm{d}}v_i v_j) = -\alpha_{\mathrm{d}}\frac{\partial p}{\partial x_i} + n\dot{m}v_i + \alpha_{\mathrm{d}}\frac{\partial}{\partial x_j}(\tau_{ij} + \tau^{\mathrm{R}}_{\mathrm{d},ij}) + n3\pi\mu_c df(u_i - v_i) + \alpha_{\mathrm{d}}\rho_{\mathrm{d}}g_i \tag{3.33}$$

Particle velocity variations caused by carrier phase turbulence and particle collisions are two causes of the dispersion phase's Reynolds stress. The Reynolds stress factor would still be there even in the absence of collisions or carrier phase turbulence because of differences in particle velocities brought on by the size distribution of the particles. Such a condition would arise in a flow of particles near the throat of a venturi, where the smaller particles would have a tendency to travel at a velocity that is similar to the local fluid velocity, while the bigger particles would have a significant velocity lag.

In this instance, the introduction of a momentum equation for each particle size category might be used to avoid the Reynolds stress brought on by velocity change. Relationships for solid viscosity and other parameters for dense phase flows were derived using kinetic theory models. For the kinetic energy of the particle phase's fluctuating motion, an extra equation is added. The ideas from kinetic theory may be applied to create the governing equations for dense-phase flows since particle-particle interactions and molecule interactions in a gas are comparable. Bagnold (1954), who obtained an equation for the repulsion pressure in a uniform shear flow, is nominally given credit for this strategy. Many others have added to this strategy, most notably Savage (1983).

The fundamental idea is that molecular interactions are responsible for pressure wave propagation and viscosity in a single-phase fluid, but particle-particle collisions are in charge of momentum and energy transfer in dense-phase flow. The term "granule temperature" refers to the kinetic energy connected to changes in particle velocity and is defined as

$$\Theta = \frac{1}{3}\langle C^2 \rangle \qquad \textbf{(3.34)}$$

where C represents the particle motion's fluctuating speed. Shearing in the granular flow and hydrodynamic forces can both result in granular temperature. Inelastic particle-particle and particle-wall collisions, as well as dissipation in the fluid, can cause dissipation. Similar to how heat diffuses, granular temperature may as well. According to Gidaspow (1994), the stress term in the momentum equation based on kinetic theory is as follows:

$$\tau_{d,ij} = \left[-p_s + \xi_s \frac{\partial v_k}{\partial x_k} \right] \delta_{ij} + \mu_s \left(\frac{\partial v_j}{\partial x_i} + \frac{\partial v_i}{\partial x_j} \right) - \frac{2}{3} \frac{\partial v_k}{\partial x_k} \delta_{ij} \qquad \textbf{(3.35)}$$

where ps is the solids pressure, s is the solids phase's bulk viscosity, and s is the solids' shear viscosity. These three variables depend on the granule temperature, particle reformation coefficient, particle diameter, material density, and volume fraction, among other factors. The force on solids is:

$$p_s = \rho_d \alpha_d \Theta [1 + 2(1 + e) g_o \alpha_d] \qquad \textbf{(3.36)}$$

where a radial distribution function is referred to as g_o.

$$g_o = \frac{3}{5}\left[1 - \left(\frac{\alpha_d}{\alpha_{d,max}}\right)^{1/3}\right]^{-1} \quad \textbf{(3.37)}$$

The form of the solids-phase bulk viscosity is

$$\xi_s = \frac{4}{3}\alpha_d^2 \rho_s d g_o (1+e)\left(\frac{\Theta}{\pi}\right)^{1/2} \quad \textbf{(3.38)}$$

The shear viscosity can be written as

$$\mu_s = \frac{2\mu_{s,dil}}{(1+e)g_o}\left[1 + \frac{4}{5}(1+e)g_o\alpha_d\right]^2 + \frac{4}{5}\alpha_d^2\rho_s d g_o (1+e)\left(\frac{\Theta}{\pi}\right)^{1/2} \quad \textbf{(3.39)}$$

Where $\mu_{s,dil}$ s,dil is the diluted solids-phase viscosity indicated by

$$\mu_{s,dil} = \frac{5\sqrt{\pi}}{96}\rho_d d\Theta^{1/2} \quad \textbf{(3.40)}$$

The relationship between the change in and the generation via velocity gradients, the dissipation through collisions, and the diffusion through gradients requires the use of an extra equation. The specifics may be found in Gidaspov (1994). The two-fluid models based on granular temperatures have been used to a number of numerical models for dense-phase flows. These consist of sedimentation, fluidized beds, and chute flow. The two-fluid model was used by Sinclair and Jackson (1989) to simulate dense flows in vertical pipes. gives an example of applying kinetic theory for the constitutive equations to forecast flow in a fluidized bed using two-fluid modeling. Using the two-fluid model for dense-phase flows provides a number of benefits.

The key benefit is that enormous systems may be described without having to account for the dynamics of individual particles. Additionally, the two-fluid equations for the solid phase may be solved using the numerical methods used for single-phase flows. However, while constructing the constitutive equations, a certain amount of empiricism must be included.

Additionally absent are features like particle sliding, rotation, and size distribution. Additionally, rarefied fluxes should be included in the granular temperature model. In this instance, it would be necessary to more accurately characterize the hydrodynamic effects on the particle oscillation in turbulence.

In order to account for flow dilution, Bolio and Sinclair (1996) presented extensions to the two-fluid model. Particle-particle interactions in dense flows provide more energy to particle fluctuation than local turbulence does in the continuous phase.

3.6.3 Mixture model:

The Mixture model is a substitute approach that is used in the traditional Eulerian theory. The continuum mechanics concepts for a single phase are generalized in this method to numerous interpenetrable continua. The fundamental premise is that all phases are present at every material site at every instant of time. For the conservation of mass and momentum, the equations of balance are proposed. To simulate the flow of a fluid including a dispersed phase at high Reynolds numbers, a mixture model technique based on the Euler-Euler method is utilized. The dispersed phase might consist of solid particles, liquid droplets, or bubbles.

The solid particle distribution in a stirred tank was simulated in order to calculate the particle concentration using a mixture model, which has been used extensively on particle-liquid mixtures in more complex flow geometries. The effects of the solid particles on the typical liquid flow were ignored, and the axial direction of the particle diffusion velocity was acknowledged. (**M. Lämmel, D. Rings, K. Kroy**) used the mixture model to simulate the flow of an intricate hydrocyclone classifier's mixture of air, liquid, and particles.

A two-dimensional axisymmetric grid was used to model the classifier. The centripetal and gravitational accelerations were used to compute the vertical and radial components of the relative velocity. stated in their validation research that the mixture model's limits are more in the modeling of turbulence and the behavior of particles close to solid barriers than in the mixture model itself.

3.6.3.1 Evolution of the Mixture approach :

The favre-averaged balancing equations have been provided by a number of writers. The form of the mixture model equations depends on the applications.

Deferential equation modeling is one of the most challenging aspects of multiphase flows in general. In order to account for the existence of the particles, the suitable single-phase turbulence model must be modified. Additionally, the diffusion coefficient's form in the continuity equation for the dispersed phase must be calculated.

A stationary model that is similar to the mixing model was developed by (**T. Pähtz, J.F. Kok, H.J. Herrmann**), An expanded k-model was used to model turbulence. Because the constitutive equation for the turbulent stress component was built up as a sum of contributions from several phases, the turbulent viscosity for each phase was determined independently. The k-model provided the turbulent viscosity of the gas. (**T. Pähtz, J.F. Kok, H.J. Herrmann**) has mathematically modeled the mixture model used to account for the tiny particles in airflow. According to the model's findings, the particles' relaxation durations in the carrier gas are brief. As a result, the particles are seen as motionless, settling particles in the area. The carrier gas's turbulent structure may be changed by the particles, who are allowed to interchange momentum with the fluid.

3.6.3.2 Mixture model equations :

In the study of multiphase flows, modeling differential equations is regarded as one of the major issues. Depending on particular applications, several writers "(Ishii, 1975)" such as "(Ahmadi and Ma, 1990)" "(Hwang, 1989)" and "(Gidaspow, 1994)" presented the Favre-averaged balance equations of the mixture model. Changing the single-phase turbulence model to account for the effects of the particles and figuring out the form of the diffusion coefficient that appears in the equation of continuity for the dispersed phase fluid are two examples of the practical problems with the mixture model. By creating a model based on stationary state that is similar to the model used in the mixture model, "(Johansen and Anderson, 1990)" utilized the k-model to represent the turbulence.

The mixture model was used to describe the tiny particles in the airflow. The turbulent stress term was provided as the total of contributions from the two phases, and the turbulent viscosity for the two phases was computed separately. It is concluded that the carrier gas's turbulent structure can be altered by the particles exchanging momentum with the fluid. When it comes to overall momentum and mass, the elements of distinct phases (whether numerical or actual)

in a mixture model behave as a single fluid flow. The mixture properties employ the fluid qualities such as density, viscosity, etc.

The equation for each phase, which is written to allow the transport of the species across the volume without following the typical convective and diffusive terms of the mixture, was presented using the species concentration. An extended flow term is used to incorporate this motion or drift, which was in charge of the phase slip, into the species equation. The force balance on each phase utilized to compute the normal flow term was modified by the change in velocity from mixture to phase. The mixture technique monitors the average phase concentration and uses a single momentum equation to compute the mixture velocity.

The continuous phase is related to the scattered phase slip velocity. Based on the balance of body and drag forces caused by the density difference, the slip velocity was determined. "(Pericleous and Drake, 1986)" wrote the governing equations for continuity and momentum for the scattered phase and continuous phase, using algebraic equations to approximate the momentum equations for the sand particles. The modeling is based on the assumptions that each phase's density is roughly constant and that both phases share the same pressure field. The momentum equation Eqs(1), the continuity equation Eqs(2), the viscous and turbulent stresses equation Eqs(3), and the transport equation for the dispersed phase equation Eqs(4) are the governing equations used for mixture models. (Johansen and Anderson, 1990)":

$$\boldsymbol{\rho \mathbf{u}_t + \rho(\mathbf{u}\,.\,\nabla)\mathbf{u} = -\nabla p - \nabla.\tau_{Gm} - \nabla.\left[\rho c_d(1-c_d)\left(\mathbf{u}_{slip} - \frac{D_{md}\ \nabla \emptyset_d}{(1-c_d)\ \emptyset_d}\right)\left(\mathbf{u}_{slip} - \frac{D_{md}\ \nabla \emptyset_d}{(1-c_d)\ \emptyset_d}\right)^T\right] + \rho g} \qquad \textbf{(3.41)}$$

$$\boldsymbol{\rho + \nabla.(\rho \mathbf{u}) = 0} \qquad \textbf{(3.42)}$$

$$\boldsymbol{\tau_{Gm} = (\mu + \mu_T)\left[\left(\nabla \mathbf{u} + (\nabla \mathbf{u})^T - \frac{2}{3}(\nabla\,.\,\mathbf{u})\mathbf{I}\right)\right]} \qquad \textbf{(3.43)}$$

$$\boldsymbol{\frac{\partial}{\partial t}(\emptyset_d \rho_d) + \nabla.(\emptyset_d \rho_d \mathbf{u}_d) = -\mathbf{m}_{dc}} \qquad \textbf{(3.44)}$$

Where ρ is the mixture density, it is as:

$$\boldsymbol{\rho = \emptyset_c \rho_c + \emptyset_d \rho_d \quad And \quad \emptyset_c = 1 - \emptyset_d} \qquad \textbf{(3.45)}$$

The velocity u (m/s) used in **(1)** is the mass-averaged mixture velocity, it defined as:

$$\boldsymbol{\mathbf{u} = \frac{\emptyset_c \rho_c \mathbf{u}_c + \emptyset_d \rho_d \mathbf{u}_d}{\rho}} \qquad \textbf{(3.46)}$$

The relation between the velocities of the two phases $\mathbf{u_c}$ and $\mathbf{u_d}$ is defined by:

$$\mathbf{u_d - u_c = u_{slip} - \frac{D_{md}}{\emptyset_d(1-c_d)} \nabla \emptyset_d} \qquad \textbf{(3.47)}$$

u_{slip}(m/s) represent the relative velocity between the two phases. The relation gives it as:

$$\mathbf{\frac{3\,C_d}{4\,d_d} \rho_c \left|u_{slip}\right| u_{slip} = -\frac{(\rho-\rho_d)}{\rho}(-u_t - (u.\nabla)u + g)} \qquad \textbf{(3.48)}$$

C_d (Dimensionless) is the particle drag coefficient, Essentially explain as a balance between buoyancy force acting on the dispersed phase and viscous drag, for the Schiller – Naumann drag model,$C_d = 0.44$.

In the Mixture model, it is assumed that the densities of both phases, ρ_c and ρ_d are constant, consequently the following alternative form of the continuity equation for the mixture is become as :

$$\mathbf{(\rho_c - \rho_d)\left\{\nabla . \left[\emptyset_d(1 - c_d)u_{slip} - D_{md} \nabla \emptyset_d\right] + \frac{m_{dc}}{\rho_d}\right\} + \rho_c (\nabla . u) = 0} \qquad \textbf{(3.49)}$$

The Eqs(9) is derived from Eqs(4) and Eqs(2). D_{md}(m^2/s) is a turbulent dispersion coefficient accounting for extra diffusion required to turbulent eddies, it defined by:

$$\mathbf{D_{md} = \frac{\mu_T}{\rho\,\sigma_T}} \qquad \textbf{(3.50)}$$

σ_T (dimensionless) is the turbulent particle Schmidt number. The particle Schmidt number is usually suggested a value ranging from 0.2 to 0.5. In the physics applications the default value is 0.35[5]. If there is not a turbulence, the D_{md} is taken as zero. If the solid concentration is not high, the *k*-ε model can be applied in dispersed multiphase flows. Corrections due to the dispersed phase to the standard single-fluid model have been developed [40][2][3][23]. The equations for the turbulent kinetic energy and turbulent dissipation have to be solved as [42][8] :

$$\mathbf{\rho \frac{\partial k}{\partial t} + \rho u . \nabla k = \nabla . \left[\left(\mu + \frac{\mu_T}{\sigma_k}\right)\nabla k\right] + P_k - \rho\epsilon} \qquad \textbf{(3.51)}$$

$$\mathbf{\rho \frac{\partial \epsilon}{\partial t} + \rho u . \nabla \epsilon = \nabla . \left[\left(\mu + \frac{\mu_T}{\sigma_\epsilon}\right)\nabla \epsilon\right] + c_{\epsilon 1} \frac{\epsilon}{k} P_k - c_{\epsilon 2}\, \rho \frac{\epsilon^2}{k}} \qquad \textbf{(3.52)}$$

Where P_k and μ_T are the production term and the mixture viscosity respectively, they given as :

$$\mathbf{\mu_T = \rho\, c_\mu \frac{k^2}{\epsilon}} \qquad \textbf{(3.53)}$$

$$\mathbf{P_k = \mu_T \left[\nabla u : (\nabla u + (\nabla u)^T)\right]} \qquad \textbf{(3.54)}$$

The so-called drift velocity is included in Eqs(4) as a diffusion term:

$$\mathbf{\frac{\partial}{\partial t}(\emptyset_d) + \nabla.(\emptyset_d\, \beta) = \nabla.(D_{md}\, \nabla \emptyset_d) - \frac{m_{dc}}{\rho_d}} \qquad \textbf{(3.55)}$$

$$\mathbf{\beta_d = u + u_{slip}\,(1 - c_d)} \qquad \textbf{(3.56)}$$

Correspondingly, the number density equation for turbulent flow corresponds to:

$$\frac{\partial n}{\partial t} + \nabla.(n\,\beta_d) = \nabla.(D_{md}\,\nabla n) \qquad (3.57)$$

Using the k-ε turbulence model, the viscous stress tensor contains an extra contribution, the Eq(3) is replaced by:

$$\tau_{Gm}=(\mu + \mu_T)\left[\left(\nabla u + (\nabla u)^T - \frac{2}{3}(\nabla .\ u)I\right)\right] - \frac{2}{3}\rho k I \qquad (3.58)$$

Despite having greater theoretical sophistication than the mixture model, the entire multiphase equations may be less accurate due to the final relationships' inherent uncertainties. This provides more evidence in favor of utilizing mixing models and the less complex homogenous flow models wherever possible. When compared to complete multiphase models, the mixture model has a substantially lower number of variables that must be solved.

3.7 Benefits and Drawbacks of the Euler Approach

The two-fluid model can be computationally more efficient because:

1. The numerical technique employed for the carrier phase can be applied for the scattered phase.

2. The model is constrained by the difficulty of simulating many particles or droplets.

One drawback is that the constitutive equations covering the effects of particle-particle collisions, carrier phase turbulence, and size distribution are not well established.

2. Mass, momentum, and energy have complex boundary constraints.

3. Due to the flow being progressively diluted, the equations are not relevant. The drawbacks will be reduced when PDF techniques and equivalent analyses emerge.

Chapter 4: Implementation and Applications

4.1 Numerical parameters

4.1.1 Computational domain

The domain for numerical simulation described here is as a 37.8 m long rectangular wind tunnel has 1m and 0.6m cross-section area

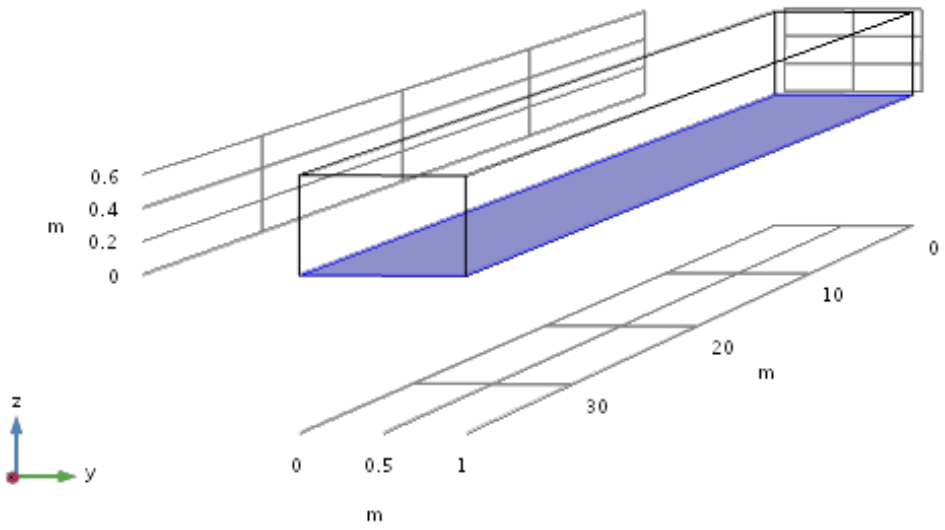

Figure 4.1: The geometry of the computational domain

4.1.2 Boundary conditions and meshing

The velocity of air u (m/s) in the inlet of the tunnel varied between 10 and 14 m/s. Depending on the bed configuration examined (erodible bed), the tunnel floor is covered with sand of a uniform height. We used sand with mean diameters of those size groups from experimental work in "(Liu and Dong, 2004)": 0.15 mm, 0.25 mm, and 0.35 mm with the same density ρ=2650 kg/m^3. Since the Mach number is less than 0.05, the continuous phase presented by air is treated as an incompressible gas. The values of turbulence intensity and the turbulence length scale are given 0.05 and 0.01m respectively without concentration of sand particles; In the outlet, the pressure value takes as referential P_{ref} = 1 atm. The boundary conditions are given as symmetrical for both air and sand phases. The meshing was chosen as tetraeders shape, it was 769097 domain elements, 63192 boundary elements and 2218 edge elements.

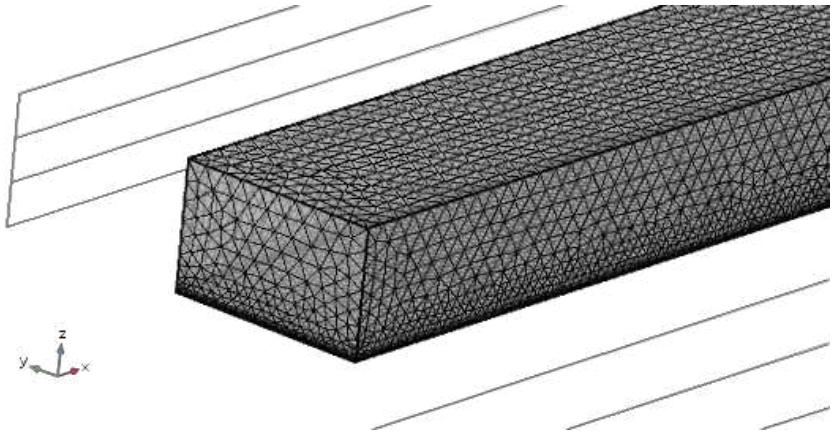

Fig4.2: meshing of the computational domain

4.2 Results

The numerical solution of partial differential equations is discretized by the finite-element method (FEM) using the discontinuous Galerkin formulation to implement the boundary conditions. The algorithm of second order was used for velocity-pressure coupling.

4.2.1 The velocity with validation (comparison with previous works) :

The variation of the mixture velocity profile with height within the saltation layer and similar experimental data for comparison"(Liu and Dong, 2004)" are shown in Figure4.4

Figure 4.3: A spatial sand velocity u (m/s) (on the *Y-Z* plane at *u=10* m/s and *dp* = 0.15 mm).

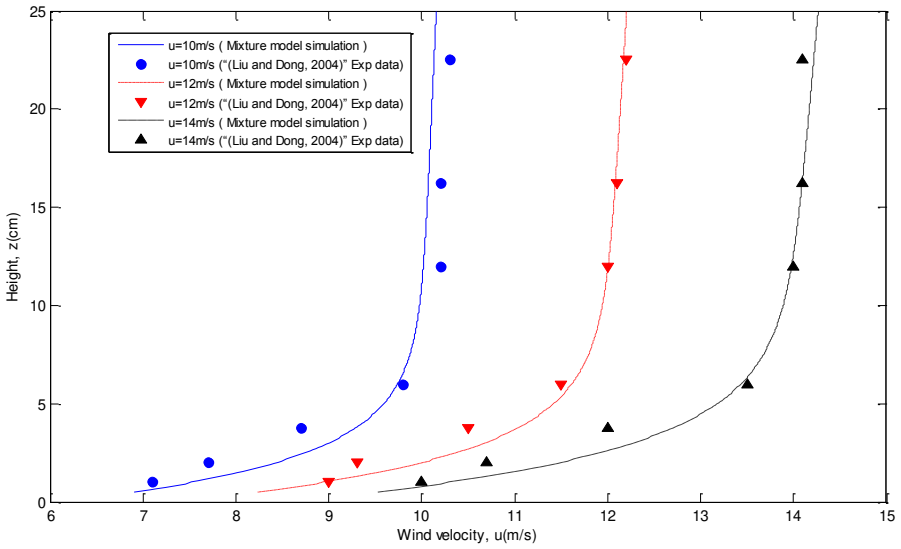

Fig4.4 : Comparison with experimental data "(Liu and Dong, 2004)" for different wind velocities

4.2.2 The concentration with validation (comparison with previous works)

Here again, to validate the reliability of our simulation results based on mixture theory, the published data of concentration profile of sand particles at similar experimental conditions were used in this study "(Liu and Dong, 2004)" Figure 4.6

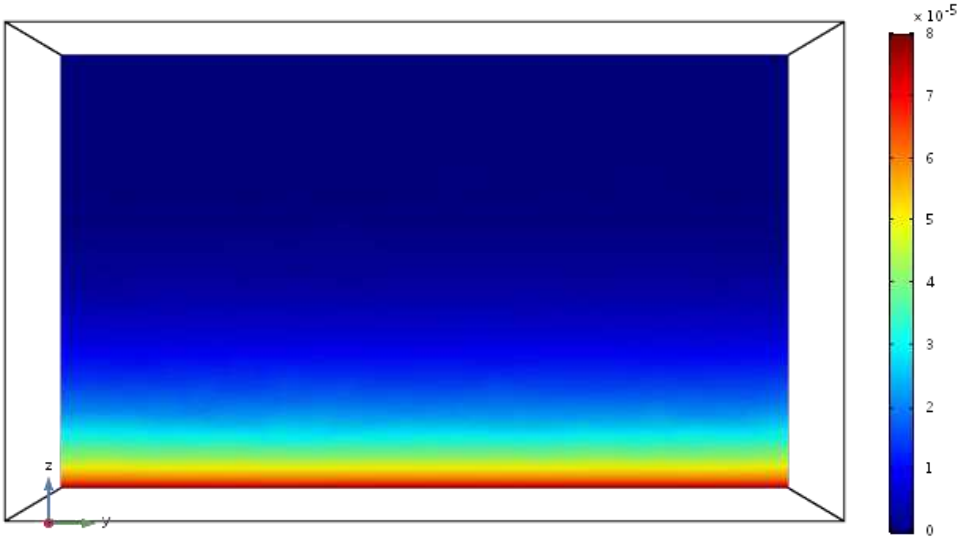

Figure 4.5: A spatial sand concentration distribution ($\emptyset_d$) on the *Y-Z* plane at *u=10* m/s and *dp* = 0.15 mm.

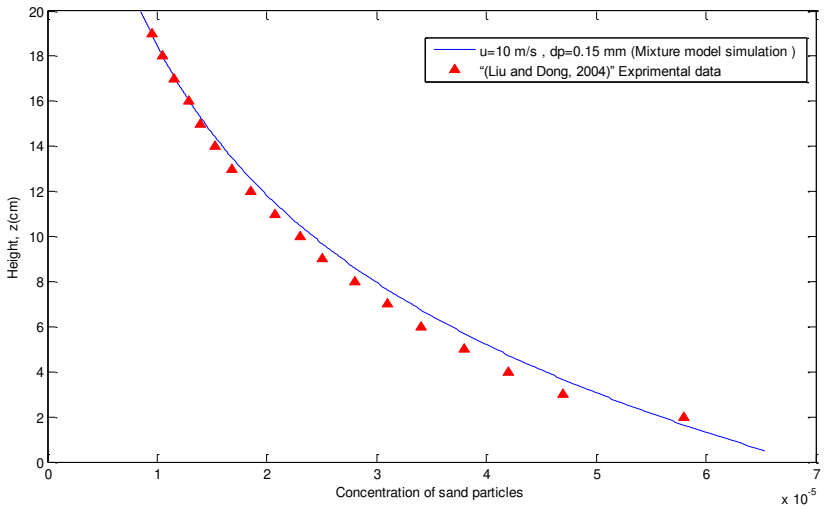

Figure 4.6: Comparison of concentration profile with experimental data of "(Liu and Dong, 2004)"

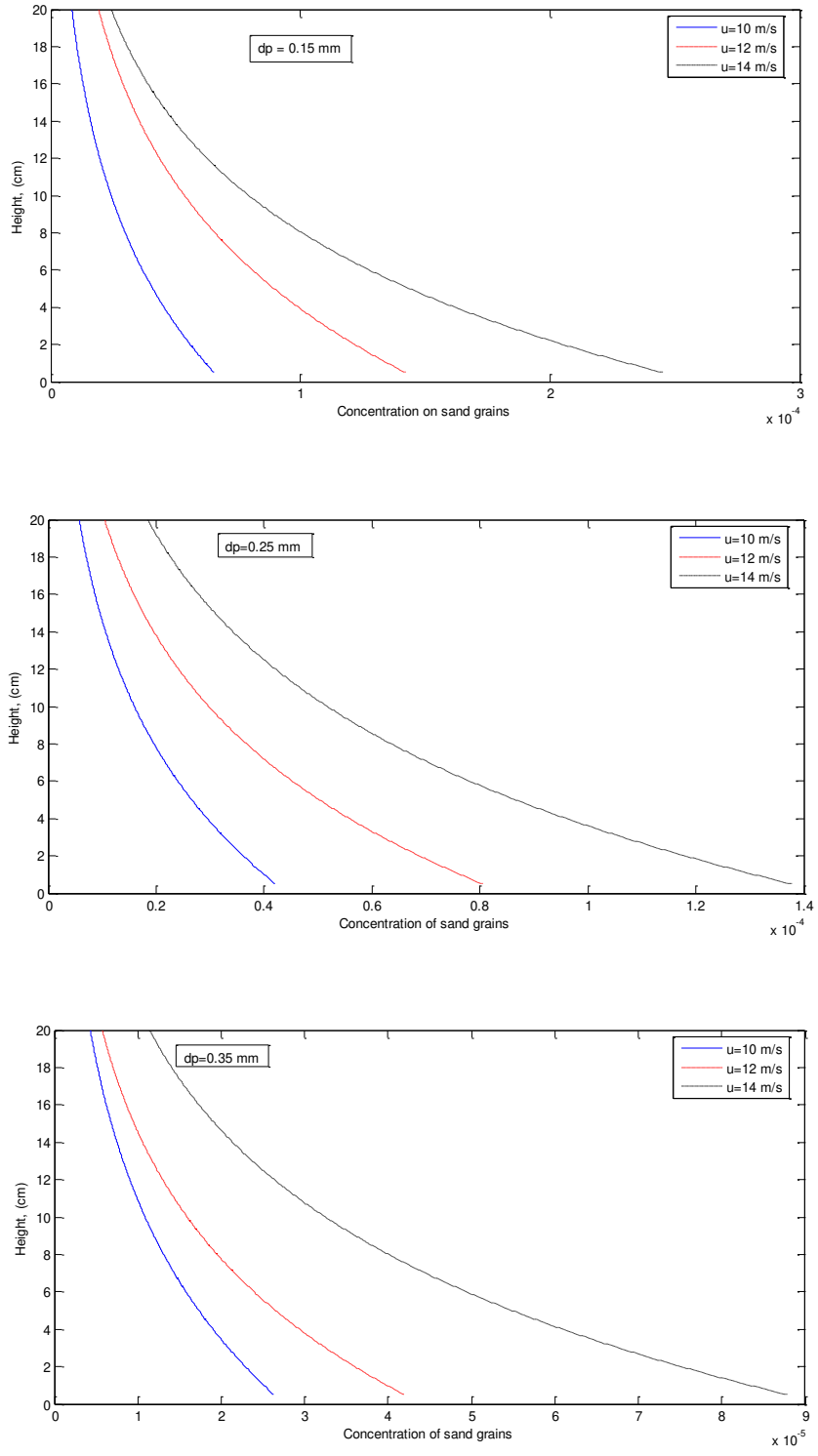

Fig4.7 : Vertical variation of the concentration of sand particles with height

- **Table 1: Results of regression between sand density and height**

dp (mm)	u (m/s)	a	b	R^2
0.15 mm	10	6.887e-05	0.1045	0.9852
	12	1.495e-04	0.1027	0.9737
	14	2.601e-04	0.1187	0.9865
0.25 mm	10	4.43e-05	0.1019	0.9921
	12	8.48e-05	0.1047	0.9805
	14	1.45e-04	0.1031	0.9722
0.35 mm	10	2.756e-05	0.09288	0.9966
	12	4.416e-05	0.102	0.9913
	14	9.26e-05	0.1047	0.978

Fitted function: $\emptyset_d = a.\ e^{-bz}$, where $\emptyset_d$ is sand particle concentration and z(cm) is height. dp(mm) is the sand particles diameter, u (m/s) is wind velocity and R^2 is the squared correlation coefficient

4.2.3 Kinetic energy

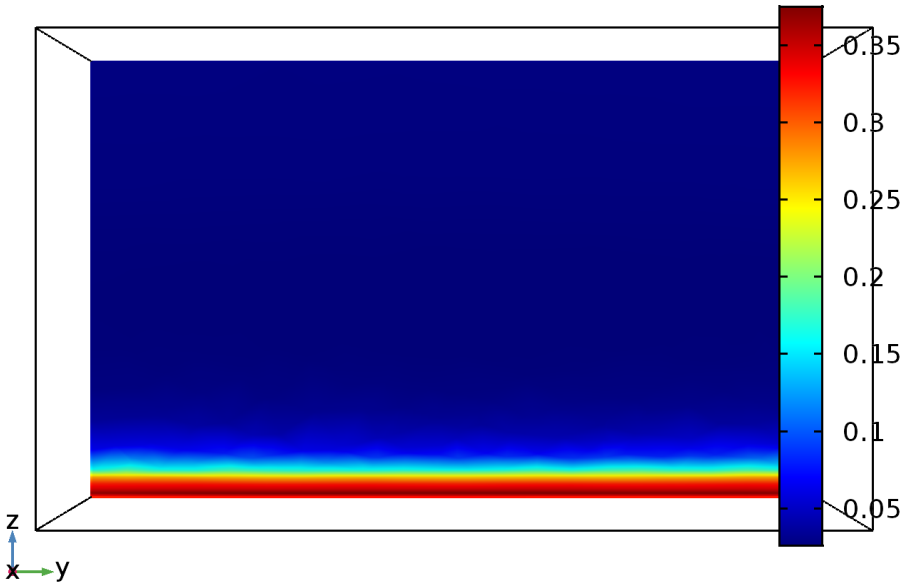

Fig4.8 : A spatial sand kinetic energy k (m^2/s^2) (on the *Y-Z* plane at *u=10* m/s and *dp* = 0.15 mm).

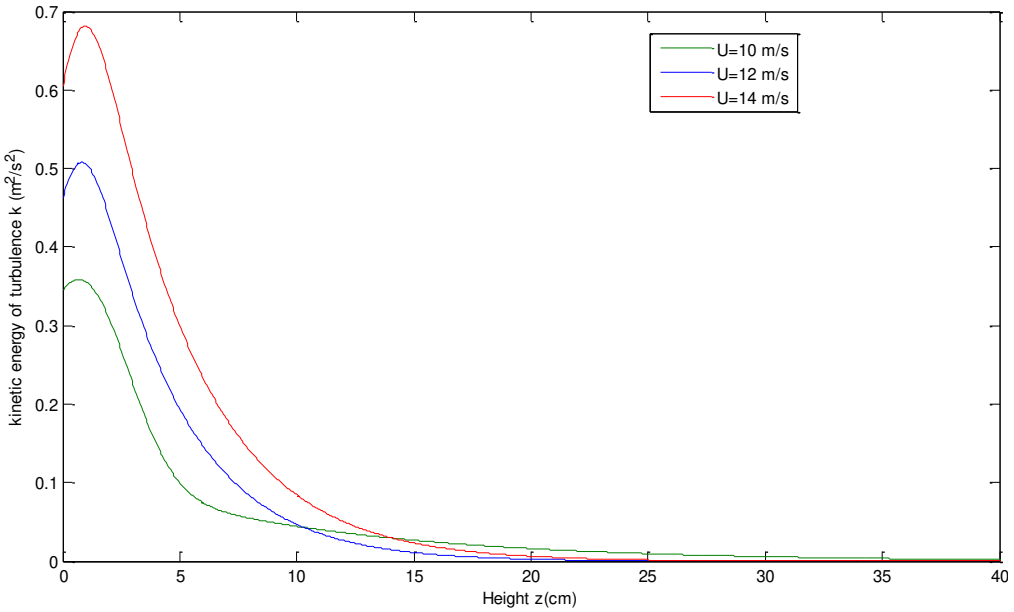

Figure 4.9 : Variation of the kinetic energy of turbulence k (m^2/s^2) of sand particles with height z(cm) for sand diameter dp=0.15mm and wind velocities: 10m/s, 12m/s and 14m/s.

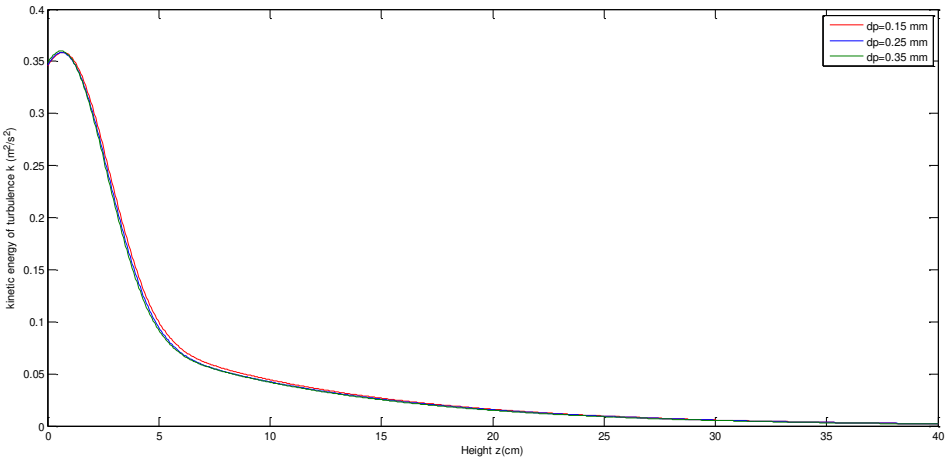

Fig 4.10 : Variation of the kinetic energy of turbulence k (m^2/s^2) of sand particles with height z(cm) for wind velocity u=10m/s and sand diameters dp=0.15mm, dp=0.25mm and dp=0.35mm

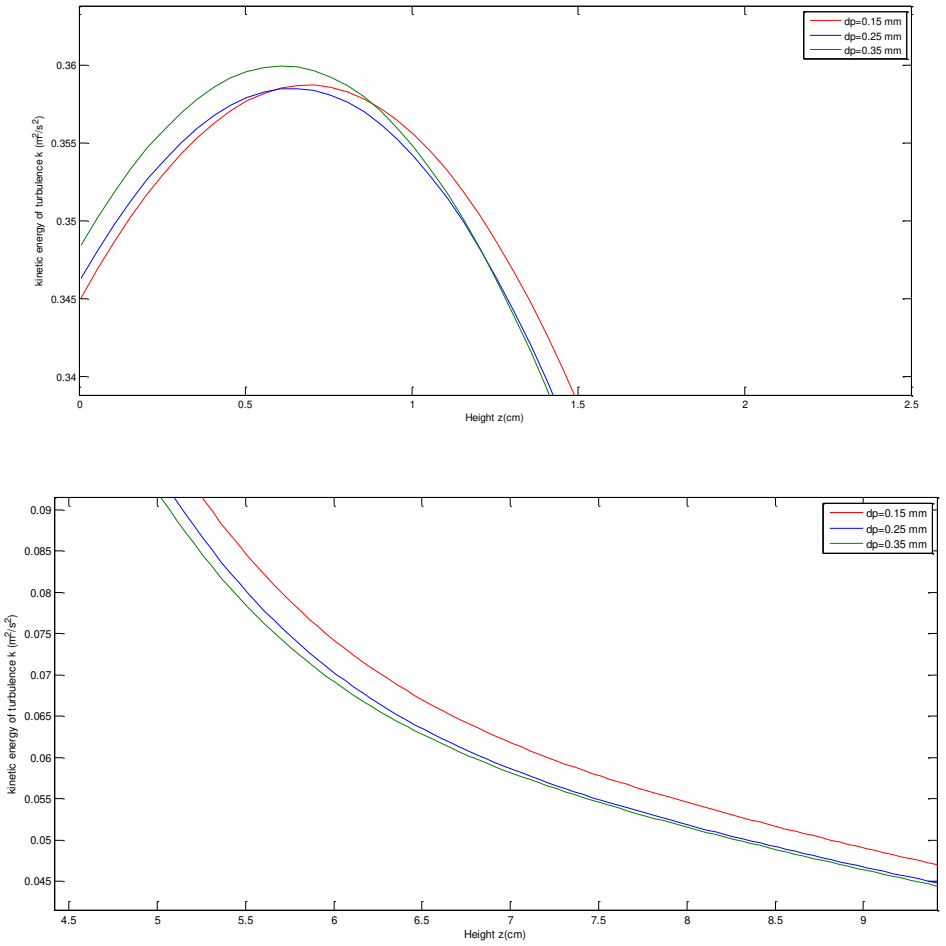

Fig 4.11 : Variation of the kinetic energy of turbulence k (m^2/s^2) of sand particles with height z(cm) for wind velocity u=10m/s and sand diameters dp=0.15mm, dp=0.25mm and dp=0.35mm

4.2.4 Turbulent diffusion coefficient of sand particles :

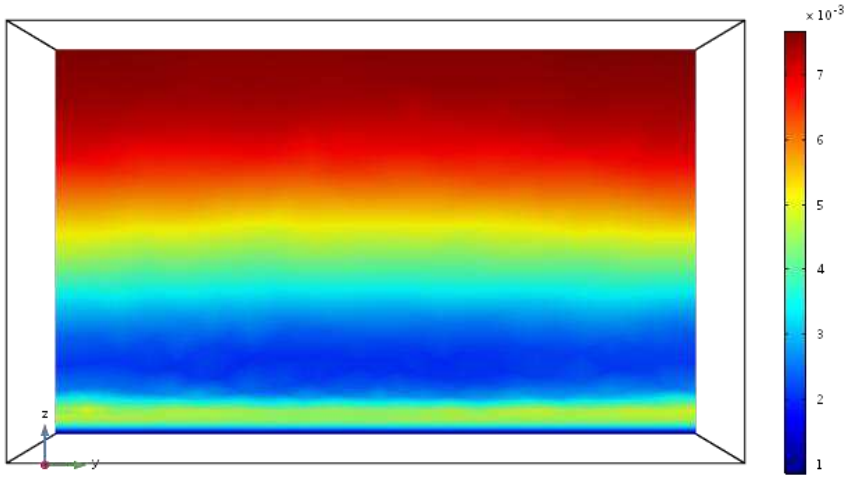

Figure 4.12:Spatial distribution of the turbulent diffusion coefficient of particles in the Z–Y plane at u=10 m/s and dp = 0.15 mm.

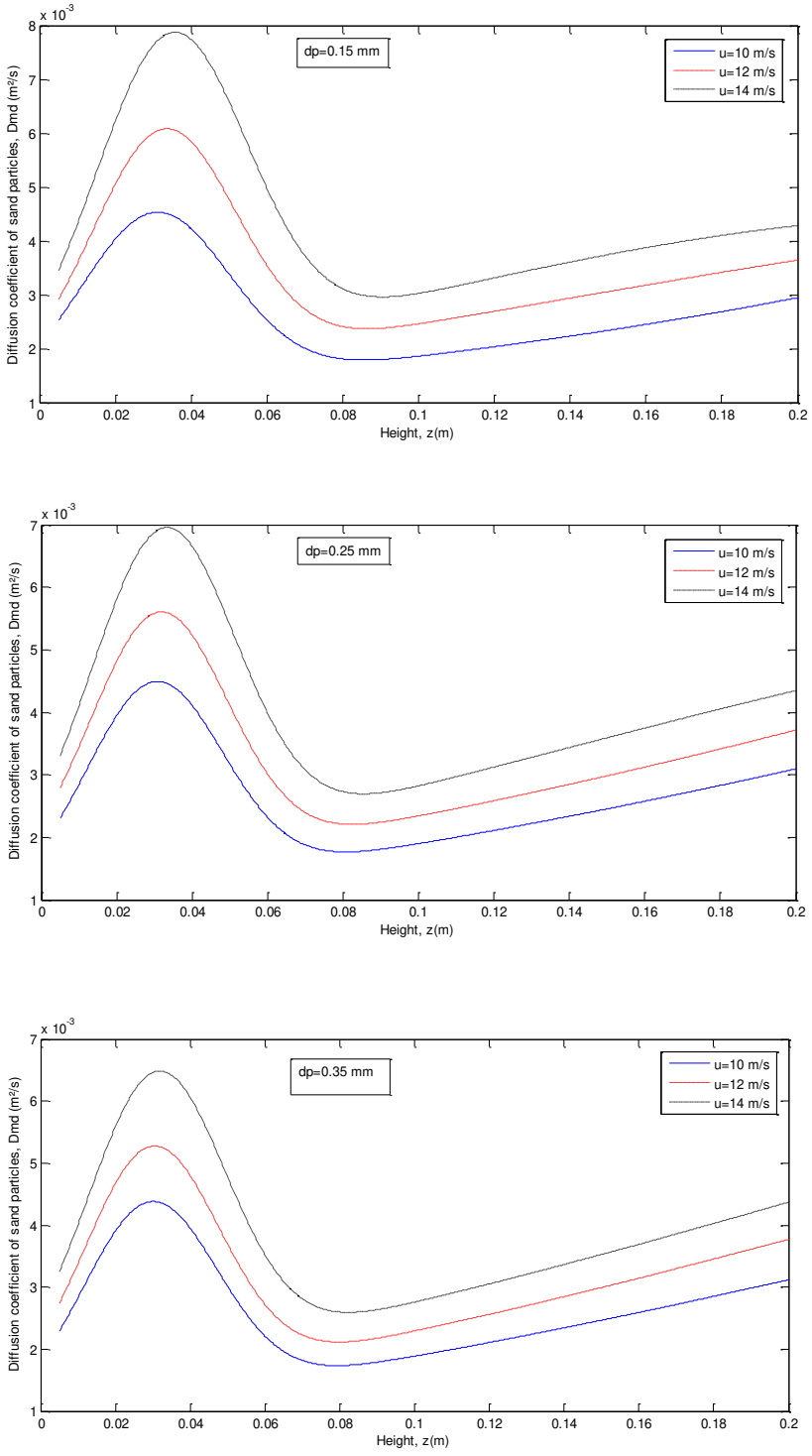

Figure 4.13 : Vertical values of particles diffusion coefficient for different particle sizes: 0.15mm, 0.25mm and 0.35mm

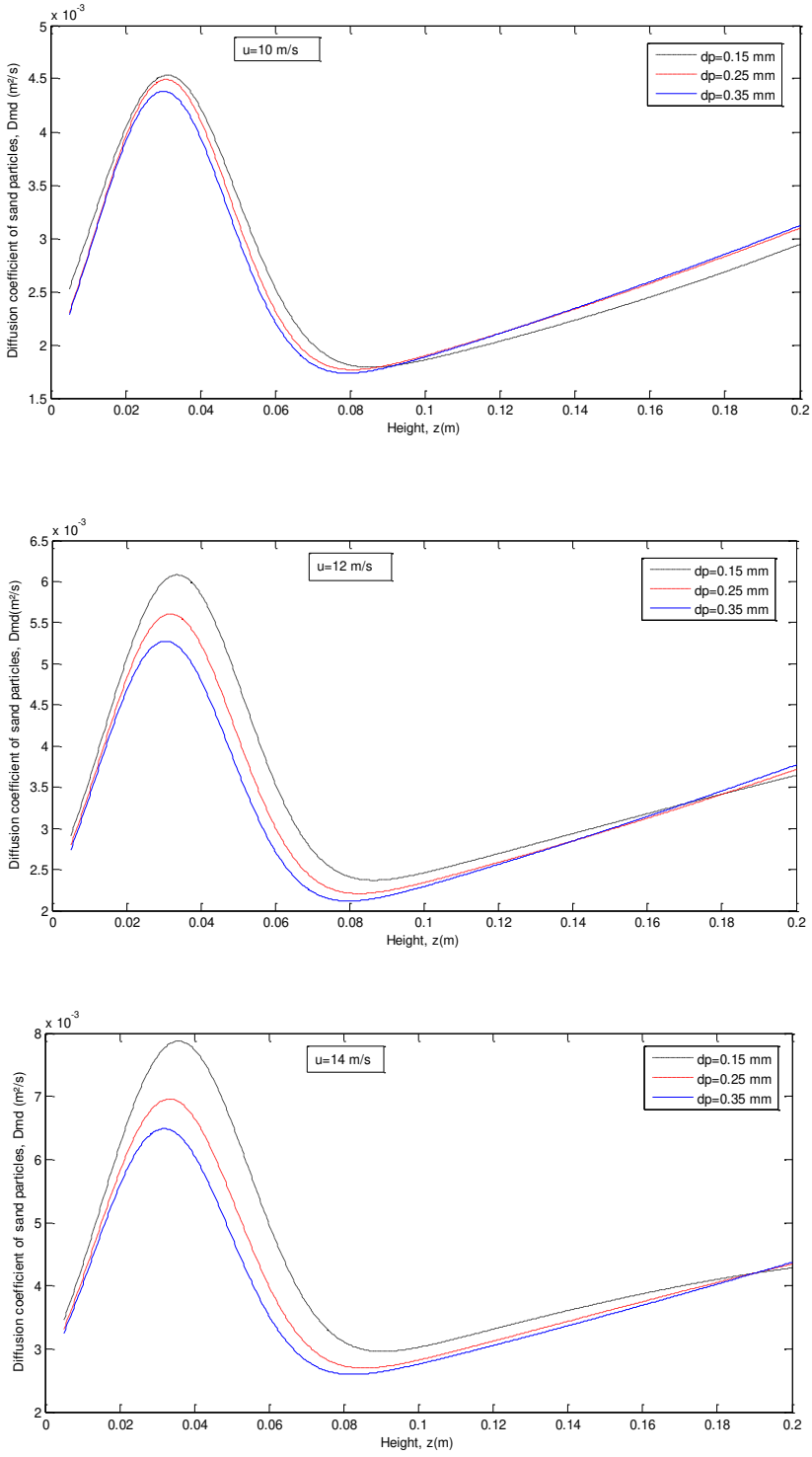

Figure 4.14 : Vertical values of particles diffusion coefficient for different wind velocities: 10m/s, 12m/s and 14m/s.

- **Table 2: Results of regression between particles diffusion coefficient and height**

dp (mm)	u (m/s)	a	b	c	a_1	b_1	c_1	R^2
0.15	10	0.00318	0.0304	0.0273	5.3e+10	13.45	2.398	0.899
	12	0.00438	0.0327	0.0267	0.00470	0.367	0.331	0.906
	14	0.00589	0.0347	0.0280	0.00448	0.251	0.238	0.913
0.25	10	0.00322	0.0300	0.0254	0.00757	0.610	0.434	0.898
	12	0.00399	0.0311	0.0256	0.00912	0.633	0.457	0.897
	14	0.00509	0.0324	0.0267	0.00556	0.351	0.304	0.903
0.35	10	0.00316	0.0293	0.0253	0.00625	0.519	0.383	0.897
	12	0.00379	0.0296	0.0254	0.00705	0.494	0.371	0.895
	14	0.00462	0.0310	0.0258	0.00800	0.505	0.392	0.897

Fitted function: $D_{md} = a \cdot e^{\left(-\left(\frac{z-b}{c}\right)^2 + a_1 e^{-\left(\frac{z-b_1}{c_1}\right)^2}\right)}$ **, where D_{md} is the diffusion coefficient of sand particles and z(m) is height. dp(mm) is the sand particles diameter, u(m/s) is a wind velocity and R^2 is the squared correlation coefficient**

4.2.5 Pression of Mixture flow P (Pa) :

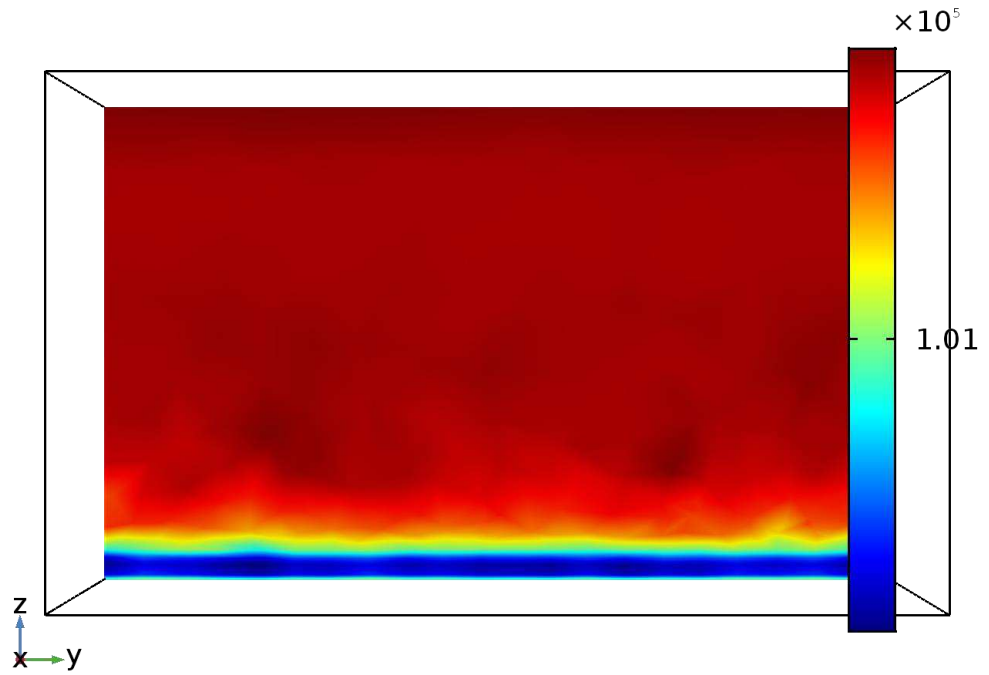

Figure 4.15 : A spatial pression of mixture flow P (Pa) (on the *Y-Z* plane at *u=10* m/s and *dp* = 0.15 mm).

4.3 Discussion

- The velocity :

It can be observed that the mixture velocity profile increases with the increasing height. At the same height, It is also seen that the logarithmic law profile is generally fit the variation of velocity with height, which can be accorded with previous studies of "(Liu and Dong, 2004)" "(Liu and Zhu, 1998)" "(Liu and Zou, 1994)". Velocity profiles for wind velocities of 10 m/s, 12 m/s, and 14 m/s in the wind tunnel indicate that the thickness of the mixture boundary layer is about 05cm to 06 cm (Fig4.4).

- The concentration:

It may indicate that the shape and type of particles of sand used in this simulation were spherical quartz, whereas the shape and type used in the experimental was natural sand, moreover the experimental conditions were not the same as the work of this study. Vertical profiles of particle densities for different velocities are shown in Fig4.7. The height (z*)* is measured from the surface of the sand bed. For different values of velocities, the particle density decays rapidly with height. The regression of particle volume fraction shows that the concentration of all grain sizes of sand particles and wind velocities decreases exponentially with height "(Liu and Dong, 2004)" "(Liu and Zhu, 1998)" as:

$$\emptyset_{\mathbf{d}} = \mathbf{a}.\, e^{-bz} \qquad \mathbf{(4.1)}$$

$\emptyset_{\mathbf{d}}$: Denote the particle density at height z. a and b are coefficients of fitted function regression. the Eqs(4.1) fits well to the simulation results data As shown in Table.1, with $R^2 = 0.97$ to 0.99. The suspension effect is negligible while the diameters of grain sand used are greater than 0.1mm. The findings show that the sand concentration in the saltation layer can be characterized by the natural of the exponential function. Denote that the particle density close to the sand bed is in the order of 10^{-5} to 10^{-4}. The coefficient (a) in Eqs(4.1) represents the density at the sand bed, it decreases with grain diameter size but increases with wind velocity (Table.1). The coefficient (b) correlates with the slope of the straight line. The variability of coefficient b in Table.1 shows that more sand is moved to higher height level as both wind velocity and sand grain diameter size increase.

- **Turbulent diffusion coefficient of sand particles :**

Among the parameters that influence particle dispersion are particle size, density, fluid scales, and turbulence structure. It can be indicated that the parameter that characterizes the particle dispersion is the relative mean velocity between the particle and the surrounding fluid, form inversely proportional to it "(Mustafa, 1992)". The diffusion coefficient can be calculated using the definition of the turbulent Schmidt number (Eqs4.2); It can be also defined as the ratio between the kinematic air viscosity *v* and the diffusivity D_{md} of sand particles:

$$\boldsymbol{\sigma_T} = \frac{\boldsymbol{\nu}}{\boldsymbol{D_{md}}} \qquad \mathbf{(4.2)}$$

Fig4.12 illustrates an example of the spatial distribution of the diffusion of the turbulent particle in the Z–Y plane at u=10 m/s and dp = 0.15 mm. From this Figure, it can be seen that within

the boundary layer (z<6cm) the diffusivity of sand particles increases and decrease rapidly with height. Outside the boundary layer, the diffusion coefficient increases slowly with increasing height.

Physically, σ_T represents the ratio between the viscous diffusion rate (linked to *v*) and the mass diffusion rate or diffusion coefficient (D_{md}). It can also describe the relationship between the rates of turbulent momentum transport and turbulent mass transport "(Tchen, 1947)", from the CFD simulations and experimental data, σ_T ranges from 0.2 to 0.5 "(Colli and Bisang, 2018)". In our simulation, we take the turbulent Schmidt number as 0.35. Fig.4.13 represents the impact of wind velocity on the diffusivity of sand particles for different particle diameters, indicating that the mixture kinetic energy affects the particles diffusion coefficient, which can be seen in Eqs(4.2), the viscosity of mixture flow increase with increasing the kinetic energy (k). The variation of diffusion coefficient with height can be written as a Gaussian distribution with the squared correlation coefficient R^2=0.90, it can be written as:

$$\mathbf{D_{md}} = \boldsymbol{a} \,.\, \boldsymbol{e}^{\left(-\left(\frac{z-b}{c}\right)^2 + a_1 e^{-\left(\frac{z-b_1}{c_1}\right)^2}\right)} \qquad \textbf{(4.3)}$$

The regression results of terms (a b c), (a_1 b_1 c_1) are shown in table.2. Fig4.14 proves that the particles with smaller particle sizes possessed a larger diffusion coefficient than those with larger ones. We see also out the boundary layer (z>>6cm) when the density of air is a major dominant the mixture density, the impact of the size of the sand particle is negligible on their diffusivity, that can be explicated the inversely proportional relationship between the concentration of particle and their diffusivity.

- Kinetic energy :

Figures 4.9 and 4.10 represent the variation of the kinetic energy of turbulence k (m^2/s^2) of sand particles with height z(cm) for sand diameter dp=0.15mm and wind velocities: 10m/s, 12m/s and 14m/s. and the second for sand diameters dp=0.15mm, dp=0.25mm and dp=0.35mm

An increase in kinetic energy can be seen in the field of height in contact with the floor. This energy is required to lift of sand particles from the bed. After that it is lost in kinetic energy exponentially due to the weight of particles

we can also point out that for the heights between 0 and 10 mm, the largest particles have more kinetic energy than the smallest ones (see figure 4.11a), but outside of the field, at heights greater than 10 mm, the opposite is true (Figure 4.11b).

- Pression of Mixture flow P (Pa) :

Figure 4.14 represent a spatial pression of the mixture flow P (Pa) (on the *Y-Z* plane at *u=10* m/s and *dp* = 0.15 mm). Although the pressure in the domain does not vary significantly, the variation in density with height can be seen to cause some depression fields in the plane Y-Z.

General Conclusion :

Large sand and dust storms can be harmful to people's health, agricultural land, infrastructure, and transportation when they develop in arid and semiarid regions due to a combination of strong winds and loose, dry soil surfaces. An estimated 2,000 million tons of dust are released into the atmosphere each year. While particularly unsustainable land and water management produce a large portion of this naturally by the Earth’s biogeochemical cycles a sizable portion is caused by human activity.

Since we work in engineering, the study of the numerical tool to analyze the physical characteristics of the Aeolian sand transport, particularly the Mixture method, was the most important part of our effort to throw light on the phenomenon in this thesis.

The concept of the mixture model was illustrated. It involves adding the diffusion stress in the momentum equation of the mixture flow, the algebraic equilibrium equation were used to solve the relative velocity, and implementing a scalar equation for the dispersed phase concentration. The results have been obtained by a numerical solution based on mixture theory when the wind tunnel configuration for different sand particle sizes and different wind speeds was performed.

The sand concentration profiles were in good agreement with previous experimental works. It confirms that the volume fraction of sand particles decreases in an exponential-decay function as the height increase and its value increases as the wind kinetic energy increases.

The diffusion coefficient of sand particles on Aeolian sand transport works has not been mentioned before, the results have indicated the D_{md} is varying with height as a Gaussian distribution; the constant terms of fitted function are established. The diffusion coefficient of sand particles was related to the form of the dispersed phase (sand grain sizes) and the kinetic energy of surrounding gas. Founding that the smaller particle's size is possessed a larger diffusion coefficient than those with the larger ones. The higher wind velocities allowed the sand particles to disperse on the air more than compared with the lower wind velocities.

The kinetic energy of sand particles was found decreases exponentially with height z, and for heights between 0 and 10 mm, the largest particles have more kinetic energy than the smallest ones, but outside of the field, at heights greater than 10 mm, the opposite is true.

General Conclusion

The most important benefit of the mixture model approach is the reduction of needed computational resources. It is a considerable alternative when the simulation time is a critical factor in modeling complex multiphase problems.

References

Adeniji, A. and Chen, C., Modeling of confined turbulent fluid-particle flows using Eulerian and Lagrangian schemes, Int. J. Heat Mass Transfer, Vol. 33, No. 4, pp. 691 – 701, 1990.

Ahmadi, G. and Ma, D., A thermodynamical formulation for dispersed multiphase turbulent flows Basic theory, Int. J. Multiphase Flow, Vol. 16, No. 2, pp. 323 – 340, 1990.

Abuduwaili, J., Gabchenko, M.V. and Junrong, X. (2008). Eolian transport of salts—A case study in the area of Lake Ebinur (Xinjiang, northwest China). Journal of Arid Environments 72, 1843–1852

ADHS (2012). Arizona Valley Fever Report, 2007–2011. Arizona Department of Health Services, Phoenix, AZ, USA

Agier, L., Deroubaix, A., Martiny, N., Yaka, P., Djibo, A. and Broutin, H. (2013). Seasonality of meningitis in Africa and climate forcing: aerosols stand out. Journal of the Royal Society Interface 10, 20120814

Al-Awadhi, J.M. and Misak, R. (2000). Field assessment of aeolian sand processes and sand control measures in Kuwait. Kuwait Journal of Science and Engineering 27, 159–176

Al–Dabbas, M.A., Abbas, M.A., Al–Khafaji, R.M. (2010). Dust storms loads analysis—iraq. Arab Journal of Geosciences 5, 121–131

Al-Dousari, A.M. and Al-Awadhi, J. (2012). Dust fallout in norther Kuwait: majour sources and characteristics. Kuwait Journal of Science 39, 171–187

Bakker, A. and Fasano, J., and Myers, K., Effects of Flow pattern on the solids distribution in a stirred tank Mixing, ICheme Symposium series No. 136, pp. 1 – 8, 1994.

Barker, B.M., Tabor, J.A., Shubitz, L.F., Perrill, R. and Orbach, M.J. (2012). Detection and phylogenetic analysis of Coccidioides posadasii in Arizona soil samples. Fungal Ecology 5, 163–176 BDFC (2016). Barcelona Dust Forecast Centre. http://dust.aemet.es

Bell, M.L., Levy, J.K. and Lin, Z. (2008). The Effect of Sandstorms and Air Pollution on Cause–Specific Hospital Admissions in Taipei, Taiwan. Occupational and Environmental Medicine.

Belnap, J. and Gillette, D.A. (1997). Disturbance of biological soil crusts: impacts on potential erodibility of sandy desert soils in southeastern Utah. Land Degradation and Development 8, 355–362

References

Bowen R., Theory of Mixtures, Part I. In: Eringen, Continuum Physics, Vol. III. New York: Academic Press, 1976.

Chen, C. and Wood P., A turbulence closure model for dilute gas-particle flows, Canadian J. of Chem. Eng., Volume 63, 349, 1985.

Colli, A. and Bisang, J., A CFD Study with Analytical and Experimental Validation of Laminar and Turbulent Mass-Transfer in Electrochemical Reactors, Journal of The Electrochemical Society, Volume 165, Number 2, 2018.

Creyssels, M. and Dupont, P. and Ould El Moctar, A., Saltating particles in a turbulent boundary layer: experiment and theory, J. Fluid Mech. 625 47–74, 2009.

Cadelis, G., Tourres, R. and Molinie, J. (2014). Short–term effects of the particulate pollutants contained in Saharan dust on the visits of children to the emergency department due to asthmatic conditions in Guadeloupe (French Archipelago of the Caribbean). PloS one 9, e91136 Cahill, T.A., Gill, T.E., Reid, J. Gearhart, E.A. and Gillette, D.A. (1996). Saltating particles, playa crusts and dust aerosols at Owens (dry) lake, California. Earth Surface Processes and Landforms 21, 621–639

Camino, C., Cuevas, E., Basart, S., Alonso–Pérez, S., Baldasano, J.M., Terradellas, E. and berjón, A. (2015). An empirical equation to estimate mineral dust concentrations from visibility observations in Northern Africa. Aeolian Research 16, 55–68 Cattle, S.R. (2016). The case for a southeastern Australian Dust Bowl, 1895–1945. Aeolian Research 21, 1-20 Cattle, S.R., McTainsh, G.H. and Wagner, S. (2002). Aeolian dust contribution to soil of the Namoi Valley, northern NSW, Australia. Catena 47, 245–264

Dong, Z. and Liu, X. and Wang H., The flux profile of a blowing sand cloud: A wind tunnel investigation, J. Geomorphology, vol. 49, no. 3– 4, pp. 219–230, 2003.

Dong, Z. and Qian, G., Analysis of the mass flux profiles of an aeolian saltating cloud, J. Geophys. Res. Atmos. 111 D16111, 2006.

Dong, Z. and Wang, H. and Zhang, X., Height profile of particle concentration in an aeolian saltating cloud: A wind tunnel investigation by PIVMSD, J.Geophys. Res. Lett. 30, 2004.

Elghobashi, S. and Abou-Arab, T., A two-equation turbulence model for two-phase flows. The Physics of Fluids, Vol. 26, pp. 931 – 938, 1983.

Fonty, T. and Ferrand, M., Mixture model for two-phase flows with high density ratios: A conservative and realizable SPH formulation, International Journal of Multiphase Flow, Pages 158-174, 2019.

References

Gidaspow, D., Multiphase flow and fluidization. Continuum and kinetic theory descriptions. Academic Press, 1994. https://doi.org/10.1016/C2009-0-21244-X.

Greeley, R. and Iversen, J., Wind as a Geological Process: On Earth, Mars, Venus and Titan, Cambridge, UK: Cambridge University Press, 1987.

Hwang, G. and Shen H., Modeling the phase interaction in the momentum equations of a fluid-solid mixture, Int. J. Multiphase Flow, Vol. 17, No. 1, pp. 45 – 57, 1991.

Hwang, G., Modelling two-phase flows of fluid and solid mixture, PhD dissertation. Ann Arbor, MI: Clarkson University. p 163, 1989.

Ishii, M., Thermo-fluid Dynamic Theory of Two-phase Flow, Springer New York, NY, 2010.

Jenkins, J. and Cantat, I. and Valance, A., Continuum model for steady, fully developed saltation above a horizontal particle bed, Phys. Rev. E82 020301R, 2009. https://doi.org/10.1103/PhysRevE.82.020301

Joseph, D. and Lundgren, T. and Jackson, R. and Saville, D., Ensemble averaged and mixture theory equations for incompressible fluid particle suspensions, Int. J. Multiphase Flow, Vol. 16, No. 1, pp. 35 – 42, 1990.

Johansen, S. and Anderson, N. and De Silva, S., A two-phase model for particle local equilibrium applied to air classification of powers, Power Technology, Vol. 63, pp. 121 – 132, 1990.

Johnson, G. and Massoudi, M. and Rajagopal, K., Flow of a fluid-solid mixture between flat plates, Chem. Eng. Sci., Vol. 46, No. 7, pp. 1713 – 1723, 1991.

Kang, L. and Liu, D., Numerical investigation of particle velocity distributions in aeolian sand transport, J.Geomorphology, Volume 115, Issues 1–2, , Pages 156-171, 2010.

Kang, L. and Zhao, G., An improved particle counting method for particle volume concentration in aeolian sand transport , J.Powder Technology Volume 280, Pages 191-200, 2015.

Kim, K. and Verlag, and Doster, J., Application of mixture drift flux equations to vertical separating flows, Nuclear Technology, Vol. 95, pp. 103 – 115, 1991.

Kocaefe, D. and Bui, R. and Provencher, R., One-phase model for stirring solid-liquid mixtures Toronto, Press Ontario, 1994.

Lämmel, M. and Rings, D. and Kroy, K., A two-species continuum model for Aeolian sand transport, New J. Phys. V14 093037, 2012.

Liu, X. and Dong, Z., Experimental investigation of the concentration profile of a blowing sand cloud, J.Geomorphology 60 . 371–381,2004.

References

Liu, Z. and Zou, J. and Dong X., Tentative calculation of wind–sand current energy, Chin. Sci. Bull. 39, 1016–1020, 1994.

Liu, Z. and Zhu, J. and Kuang, Z., Saltation in windblown sand, Sci. China Ser. A-Math. 41, 629–637, 1998 https://doi.org/10.1007/BF02876233

Lu, H. and Gidaspow, D., Hydrodynamics of binary fluidization in a riser: CFD simulation using two granular temperatures, Chem. Eng. Sci., Volume58, 3777–3792, 2003

Manninen, M. and Taivassalo, V. and Kallio, S., On the mixture model for multiphase flow, Espoo 1996, Technical Research Centre of Finland, VTT Publications 288. 67 p, 1996

Mathiesen, V. and Solberg, T. and Hjertager, B., An experimental and computational study of multiphase flow behavior in a circulating fluidized bed, Int. J. Multiph. Flow, 26, 387–419, 2000.

Mostafa, A. and Mongia, C., On the interaction of particles and turbulent fluid flow, Int. J. Heat Mass Transfer, Vol. 31, No. 10, pp. 2063 – 2075, 1988.

Mustafa, A., Turbulent Diffusion of Heavy Particles in Turbulent Jets, Faculty of Engineering, Journal of Fluids Engineering,Vol. 114 / p 669, 1992.

Neuman, M. and Maljaars, M., Wind tunnel measurement of boundary-layer response to sediment transport, J. Boundary-Layer Meteorology, V84, 67–83. 1997.

Pähtz, T. and Kok, J. and Herrmann, H., The apparent roughness of a sand surface blown by wind from an analytical model of saltation, New J. Phys. V14 .043035, 2012.

Passman, S. and Nunziato, J. and Walsh, K., A theory of multiphase mixtures. Rational Thermodynamics. New York: Springer-Verlag, 1984.

Pericleous, K. and Drake, S., An Algebraic Slip Model of PHOENICS for Multi-phase Applications, Numerical Simulation of Fluid Flow and Heat/Mass Transfer Processes Lecture Notes in Engineering vol 18. Springer, Berlin, Heidelberg, 1986. https://doi.org/10.1007/978-3-642-82781-5-29.

Rasmussen, K. and Iversen, J. and Rautahemio, P., Saltation and wind-flow interaction in a variable slope wind tunnel, J.Geomorphology, Volume17, 19–28, 1996.

Rasmussen, K. and Mikkelsen, H., On the efficiency of vertical array aeolian field traps, Sedimentology, Volume45, 789–80, 1998.

Rasmussen, K. and Valance, A. and Merrison, J., Laboratory studies of aeolian sediment transport processes on planetary surfaces, J. Geomorphology Volume 244, Pages 74-94, 2015.

Sauermann, G. and Kroy, K. and Herrmann, H., Continuum saltation model for sand dunes, Phys. Rev. E64, 031305, 2001. https://doi.org/10.1103/PhysRevE.64.031305.

References

Simonin, O., Eulerian formulation for particle dispersion in turbulent two-phase flows, Proc. 5th Workshop on Two-Phase Flow Predictions, March 19 - 22, Erlangen, FRG. Jülich: Kernforschungsanlage Jülich. Pp. 156 – 166, 1990.

Tchen, C., Mean Value and Correlation Problems Connected with the Motion of Small Particle Suspended in a Turbulent Fluid, Springer science-Business Media, 2013. https://doi.org/10.1007/978-94-017-6101-7.

Tu, J. and Fletcher, C., An improved model for particulate turbulence modulation in confined two-phase flow, Int. Comm. in Heat and Mass Transfer, Vol 21, No. 6, pp. 775 – 783, 1994.

Valance, A. and Rømer, K. and Dupont P., The physics of Aeolian sand transport, C.R Physique., 2015. http://dx.doi.org/10.1016/j.crhy.2015.01.006.

Van Rijn, L. and Strypsteen, G., A Fully Predictive Model For Aeolian Sand Transport. J.Coastal Engineering Volume 156, 103600, 2010.

Wang, H. and Zhang, X. and Dong, Z. and Ayrault, M., Experimental determination of saltating glass particle dispersion in a turbulent boundary layer, Earth Surf. Processes Landforms Volume31 1746–1762, 2006.

Wang, X. and Zhang, C., Studying the spatial and temporal changes in aeolian sand transport in a wind tunnel using 3D terrestrial laser scanning, Journal of Soil Science Volume71, Issue5,Pages 898-908, 2020.

White, B. and Mounla, H., An experimental study of Froude number effect on wind-tunnel saltation, Acta Mechanica, Suppl.1, 145–157, 1991.

Yang, Z. and Changsong, W., A Numerical Study of Aeolian Sand Particle Flow Incorporating Granular Pseudofluid Optimization and Large Eddy Simulation, Special Issue: The Motion of Particles in Turbulence 11(5), 448, 2020. https://doi.org/10.3390/atmos11050448.

Yintang, L. and Yi, G., Numerical simulation of aeolian dusty sand transport in a marginal desert region at the early entrainment stage, J.Geomorphology Volume 100, Issues 3–4, Pages 335-344, 2008

Yuan, Z. and Michaelides, E., Turbulence modulation in particulate flows a theoretical approach, Int. J. Multiphase Flow, 18, 779, 1992.

Zongyan, C. and Fengjun X. and Zhibao D., Fetch effect on the developmental process of Aeolian sand transport in a wind tunnel, J.Arid Land Volum12(3): 436–446, 2020